Polarimetric radar images: from acquisition to inversion

Elise Koeniguer

MANUSCRIT

Présenté pour obtenir

L'HABILITATION A DIRIGER DES RECHERCHES DE L'UNIVERSITÉ PARIS-SUD XI

Spécialité: Imagerie Physique

par

Elise COLIN KOENIGUER

Polarimetric radar images: from acquisition to inversion

Soutenue le 26 Novembre 2014 devant la Commission d'examen:

M.	Emmanuel TROUVÉ	(Rapporteur)
M.	François GOUDAIL	(Rapporteur)
M.	Mihai DATCU	(Rapporteur)
M.	Razvigor OSSIKOVSKI	(Examinateur)
M.	Thuy LE TOAN	(Examinateur)

MANUSCRIT

Présenté pour obtenir

L'HABILITATION A DIRIGER DES RECHERCHES DE L'UNIVERSITÉ PARIS-SUD XI

Spécialité: Imagerie Physique

par

Elise Colin Koeniguer

Images polarimétriques radar: de l'acquisition à l'inversion

Soutenue le 26 Novembre 2014 devant la Commission d'examen:

M.	Emmanuel Trouvé	(Rapporteur)
M.	François Goudail	(Rapporteur)
M.	Mihai Datcu	(Rapporteur)
M.	Razvigor Ossikovski	(Examinateur)
M.	Thuy Le Toan	(Examinateur)

Dedicated to the loving memory of Antonello de Martino.

1954 – 2014

San Francisco itself is art, above all literary art. Every block is a short story, every hill a novel. Every home a poem, every dweller within immortal.

— William Saroyan

CONTENTS

List of Acronyms

RAR	Real Aperture Radar
SAR	Synthetic Aperture Radar
PolSAR	Polarimetric SAR
InSAR	Interferometric SAR
DInSAR	Differential Interferometric SAR
PolInSAR	Polarimetric Interferometric SAR
PolTomSAR	Polarimetric Tomographic SAR
RVoG	Random Volume over Ground
SSIM	Similarity Structural Invariant Measurement
PSF	Point Spread Function
RDA	Range Doppler Algorithm
PFA	Polar Format Algorithm
CSA	Chirp Scaling Algorithm
RMA	Range Migration Algorithm
FOPEN	Foliage Penetration
GAF	Generalized Ambiguity Function
RCS	Radar Cross Section
SIRV	Spherically Invariant Random Vectors
DEM	Digital Elevation Model
HR	High Resolution
SOMA	South of Market, a large neighborhood in San Francisco, California
ROC	Receiver Operating Characteristic
BaBi	An indoor coherent bistatic RCS measurement in Onera
PEC	Perfect Electric Conductor
POA	Polarization Orientation Angle
LOS	Line of Sight
NLOS	Non Line of Sight

SONDRA	Supélec Onera NUS DSO Research Alliance
LPICM	Laboratoire de Physique des Interfaces et Couches Minces, CNRS-Ecole Polytechnique
FOI	Swedish Research Defence Agency
SATIE	Laboratoire des Systémes et Applications des Technologies de l'Information et de l'Energie
NTU	Nanyang Technological University, Singapore

INTRODUCTION

Remote Sensing is the science of acquiring information about the Earth's surface without actually being in contact with it. This is done by sensing and recording reflected or emitted energy and processing, analyzing and applying that information. The microwave portion or radar portion of the spectrum covers the range from approximately one centimeter to one meter in wavelength. There are two primary advantages of radar: all-weather and day or night imaging. Moreover, radar images are quite different from images acquired in the visible and infrared portions of the spectrum and have special properties. Due to these differences, radar offers different perspectives of the Earth's surface.

One of the main differences from conventional images comes from the processing that enables the final image to be produced. Radar imaging deals with a coherent processing, which means that the image is produced from the transformation of a complex variable: the Electrical Field. This image processing explains the speckle and the particular statistical distributions encountered in radar images.

The difficulty of interpreting radar images is also their greatest asset: the fact that the phase of the wave is controlled offers new possibilities in terms of so-called advanced techniques such as polarimetry and interferometry. For a plane electromagnetic (EM) wave, polarization refers to the locus of the electric field vector in the plane perpendicular to the direction of propagation. Many radars are designed to transmit microwave radiation that is either horizontally polarized (H) or vertically polarized (V). A transmitted wave with a given polarization can generate a backscattered wave with a variety of polarizations. It is the analysis of these transmitted and received polarization combinations that constitutes the science of radar polarimetry.

Although polarimetry has a long history that reaches back to the 18th century, the earliest work related to radar dates back to the 1940s. G.W. Sinclair introduced the concept of the scattering matrix to describe the radar cross section of a coherent scatterer in 1945. In the late 1940s and the early 1950s major pioneering work was carried out by E.M. Kennaugh. Polarimetry continued after Kennaugh, but only a few notable contributions were made until Huynen's studies in 1970s. The beginning of a new age began with the doctoral thesis of Huynen in 1970 which renewed interest in radar polarimetry. However, the full potential of radar polarimetry was never fully realized until the early 1980s, due in no small part to the advanced radar device technology. Technological problems led to a series of negative conclusions in the 1960s and 1970s about the practical use of radar systems with polarimetric capability. Among the major contributions of the 1970s and 1980s are those of W-M Boerner who pointed out the importance of polarization in addressing vector electromagnetic inverse scattering.

Together with these theoretical advances, sensors were developed, both for civilian and military purposes. First, polarimetric sensors were airborne sensors. The first polarimetric image distributed by NASA was acquired by the AIRSAR system, a practical fully polarimetric airborne system implemented by JPL in 1985. The well-known corresponding polarimetric image of Fig.1 was taken over San Francisco.

Figure 1: A well-known polarimetric image taken over San Francisco by the airborne system AIRSAR

Why did this image over San Francisco raise enthusiasm? Certainly because in this image we can distinguish different types of land covers that are very well discriminated by polarimetric false colors: ocean, built-up areas, and vegetation.

Then, NASA also launched the first fully polarimetric space-borne SAR in 1994 with the space shuttle SIR-C. This system was flown as a science experiment on the Space Shuttle Endeavor in April (SRL-1) and October 1994 (SRL-2). At the same time, many polarimetric airborne systems flourished in the early 1990s. The interferometric mode was also developing. Interferometry is another key technique of imaging radar, which can be used in differential mode, or for three-dimensional imaging. The POLINSAR mode, which combines polarimetry and interferometry was proposed in a 1997 paper Cloude and Papathanassiou (1997), and in Cloude and Papathanassiou (1998). The first Onera SAR images were acquired in this mode in 1999 on the Beaugency and Brétigny sites. At the beginning of my thesis, this new discipline grew, with the creation of the POLINSAR workshop by ESA, the European Space Agency, in January 2003.

Studies are ongoing, supported by an earlier in-depth knowledge gained from more defense-oriented issues. This knowledge has developed historically in Onera through anechoic chamber measurements, where polarimetry was used for target recognition on military vehicles. As the contribution of polarimetry to remote sensing applications was being demonstrated around the world, it became possible to use this technology for satellites. The first polari-

metric satellite SAR sensor was the ALOS PALSAR satellite, launched in 2006, followed by TerraSAR-X and RADARSAT-2 launched in 2007.

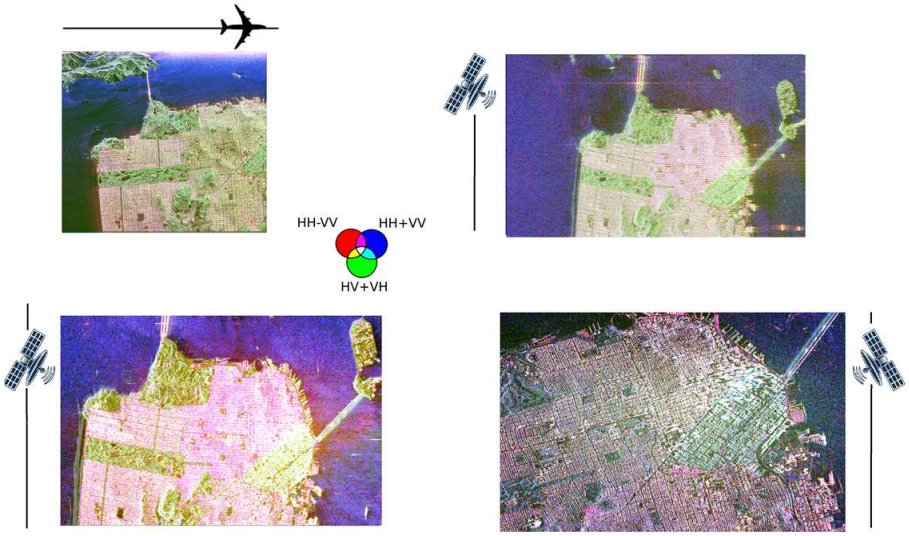

Figure 2: Different polarimetric images over San Francisco: AIRSAR (L-band), ALOS(L-band), RADARSAT-2(C-band), and TerraSAR-X (X-band)

These sensors each operate at different wavelengths, have different resolutions and different Signal-to-Noise ratio. For these reasons, the images in Fig. 2 differ greatly from one sensor to another. Indeed, in order to interpret them, we must take into account the specific sensor, since it soon becomes clear that the images obtained depend on the technological parameters. Thus, there is no optimal treatment for an image, but one treatment can only be considered as optimal according both to the environment considered and sensor dimensioning, such as wavelength, resolution and noise levels.

Due to the complexity of the environments considered and of the diversity of the sensors, in order to be able to propose the most appropriate treatment, it is also necessary to understand the underlying physical signals and the complex phenomenology involved between the wave and the environment. For this purpose, simulation is invaluable. Attempting to link together electromagnetic comprehension and information processing is at the heart of my research. This approach has been mainly applied both for applications concerning the forest and for applications in urban areas.

In order to present this approach in this paper, in the first part I discuss the intricate relationship between measurement and technological constraints. At this stage it is necessary to understand how the image is derived from the raw data acquired by the system, and also to know how measured quantities are defined exactly. This part of my research primarily involves the acquisition of knowledge on SAR imagery. I want to return to this point in a more general overview, especially to illustrate the diversity of possible approaches. I will illustrate how this knowledge was useful, especially for understanding the images acquired in new ways, circular SAR or bistatic SAR. This first part

was also an opportunity to file a patent for the calibration of polarimetric measurements, to suggest a more suitable spatial reference frame for data interpretation of bistatic polarimetric images, and, finally, to propose alternatives to conventional polarimetric parameters derived from statistical estimation.

Once SAR images are computed, we often have to process them, either to perform classification or detection. In order to do this, if several images are used, it is necessary to coregistrate them together. Then, according to the type of data, the statistical nature of the products provided may change. Our knowledge of statistics can be used to adjust the functions commonly encountered in imaging, such as detection and classification. The second chapter presents my contributions to coregistration, to statistical studies and their application to detection and classification functions.

The images thus processed are two-dimensional images. The scenes that contain terrain are projected onto the horizontal plane, unless dedicated techniques are used to restore their relief. Interferometry is one of these techniques, but polarimetry can also help to provide volumetric information. The third chapter will be devoted to the help of polarimetry for the transition from a two-dimensional image to a three-dimensional one.

Finally, the last chapter will cover the finer understanding and inversion methods of specific complex media, in close connection with the use of physical models, for two examples of environments: forest and urban areas.

To conclude, we will see how this general approach for developing processing, starting from the analysis of the raw measurements, improving our understanding of the physical interaction of the scene and the sensor, can be generalized to different imaging systems, both for co-design and processing of the data.

Part I

FROM RAW DATA TO THE IMAGE

SAR is an active imaging method based on microwaves that is used on mobile platforms such as airplanes or satellites. SAR is a form of radar that is used to create images of Earth's surface or of an object. The SAR algorithm enables an image of backscattering reflectivity to be obtained from the measurement of raw complex data. In this part, we first present studies that involve SAR image formation. Then we conduct a study about the way the different useful polarimetric parameters are obtained from this image. Finally, technological constraints concerning the polarimetric mode are discussed.

1

SAR IMAGE PROCESSING: HOW CAN AN IMAGE BE DERIVED FROM A RAW SAR SIGNAL?

Synthetic-aperture radar (SAR) is a form of radar tha is used to create images of an object, such as a landscape. In order to create a SAR image, successive radio wave pulses are transmitted to illuminate a target scene and the echo of each pulse is received and recorded. Signal processing of the recorded radar echoes, called raw data, enables the recordings from the multiple antenna locations to be combined to create the image.

The signal processing relating to this image formation is called the SAR algorithm. Different types of algorithms exist, and differ according to approximations that they make. However, in all cases, the SAR algorithm is able to transform the raw data into a reflectivity image, with physical resolutions that depend only on the mean frequency, the frequency bandwidth, the integration length which is the distance between the first pulse and the last pulse, and the geometrical configuration of acquisition.

In order to understand how we are able to achieve an image with these resolutions, several approaches are possible. While many books exist that detail SAR algorithms, there are very few that present different ways of understanding how, from an acquisition that returns a pulse of a certain frequency bandwidth, it is possible to obtain a reflectivity image with resolutions along two spatial axes.

Also, while an approach is generally sufficient to grasp the understanding of a SAR image under standard conditions (far- field, rectilinear path, monostatic configuration when sending and receiving antennas are co-located), it is quite different when this classic setting is left. During my years of research, innovative SAR imaging modalities have emerged: the bistatic SAR and the circular SAR.

Also, in first section we present all of the different approaches that enable the understanding of how a resolved image can be obtained from recording pulses along a trajectory. Then we will see which have been used to tackle more innovative modes, such as the circular mode or bistatic mode. These four approaches act in a complementary way to determine exactly how these new modes can affect the resulting image and have implications for the polarimetric mode.

1 THE MONOSTATIC MODE

For all approaches, we will use the same configuration and the same variables, described in Fig. 3. We will deal with the monostatic case, in which the radar receiver is at the same location as the transmitter.

A signal $s_0(t)$ is transmitted from each antenna position u, with a bandwidth B and a central wavelength λ. The signals collected are written $s(t,u)$ where t is called the short-time and u is a position of the antenna or long-time. The SAR image is synthesized from these acquisitions made during the path of the antenna, with a length L. L is also called the integration length.

The SAR image corresponds to a mapping of the ground reflectivity along two axes: the azimuth axis y, which corresponds to the axis of the trajectory, and the transverse axis x, or range axis.

SAR processing is the way in which we obtain this SAR image from the recording of the pulse echoes. At least four complementary approaches can explain how we are able to obtain a reflectivity image with resolutions according to two spatial axes x and y from the recorded pulses.

- An approach based on the generalization of classical radar, able to determine the range and the velocity of objects.
- A purely geometric approach dealing with iso-range lines and iso-Doppler lines. The density and orientation of the contours determine the image resolutions.
- A frequency approach, for which the signal is described in the two dimensional frequency domain, in terms of two variables k_x and k_y which are the dual variables of the space coordinates x and y of the image.
- A purely mathematical approach, which gives an analytical formulation of the problem of calculating a density reflectivity map $f(x,y)$ from the received signal $s(t,u)$ depending on time t and position u of the radar.

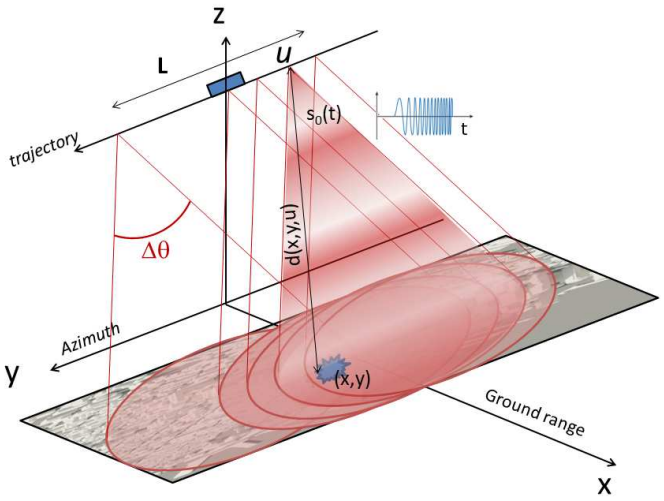

Figure 3: Geometrical parameters for a SAR acquisition

1.1 *A generalization of classical radar*

Classical radar is able to discriminate between separate echoes only if the difference between their delays is greater than the pulse width. Then the range resolution with a sinusoidal pulse is $\delta_x = \frac{\tau c}{2}$ where τ is the pulse duration and c is the celerity of the wave. Consequently, to increase the resolution, the pulse length must be reduced. Since SNR is proportional to the pulse duration, this introduces a trade-off between SNR and resolution. In order to still have a good SNR at the receiver, the pulse compression enables a large enough pulse: a signal is transmitted with frequency modulation, with a long enough length so that the energy budget is correct. This signal is designed in such a way that, after matched filtering, the width of the intercorrelated signals is smaller than the width obtained by the standard sinusoidal pulse. It is often a linear chirp, which is a signal whose instantaneous frequency increases linearlà y with time.

The range resolution attainable with a linear frequency modulation of a pulse on a bandwidth B is $\delta_x = \frac{c}{2B}$.

Thus, a range profile obtained by a classical radar can be considered as a one dimensional imaging process. In order to obtain a two-dimensional image, a first solution is to acquire several range profiles. This is what is done by Side-Looking Airborne Radar (SLAR) or Real Aperture Radar (RAR). In this case, the radar platform moves in the direction of the y-axis. The system uses an antenna that sends one pulse at a time and measures what is scattered back. The azimuthal resolution (better known as the cross-range resolution) depends on the beam width of the radar antenna. It is derived from the ratio of the physical size of the antenna (the real aperture) to the wavelength used. DUe to the spreading of the beam it is also dependent on the slant range. However, they are limited by the physical size of the antenna: a uniform aperture antenna has a lobe with an aperture angle $\phi = \frac{\lambda}{L}$ where L is the dimension of the antenna. One of the first RAR images acquired by an airborne system belonging to NASA is shown in Fig.4.

For satellite systems that are far away from Earth, the size of the footprint of one antenna measuring one meter in size would cover several kilometers. The azimuth resolution of an image improves as the aperture size increases. Unfortunately, increasing the aperture size (antenna length) may simply be impractical (antenna lengths of the order of kilometers). It is apparent that real aperture SLAR antennas sscould not be built large enough to achieve the desired azimuth resolution. In fact, it was never feasible to use SLAR in space because the antennas would be too large and their launch into space would be too expensive. In order to overcome this issue, Synthetic Aperture Radar refers to a method for improving the azimuth resolution. By using the entire set of recorded pulses for all antenna positions to synthesize the image, resolution depends on the integration length L. The distance that the SAR device travels over a target creates a large synthetic antenna aperture that plays the role of the size of the antenna. As a rule of thumb one can assume that the larger the aperture is, the higher the image resolution becomes, regardless of whether

Figure 4: A first Real Aperture Radar image acquired by a Side Looking Airborne System developed by Westinghouse, under sponsorship from the United States Air Force in 1954

physical aperture or synthetic aperture is used. This allows SAR to create high resolution images with comparatively small physical antennas.

1.2 *The geometrical approach*

In SAR imaging, the points of the scene to be imaged are separated according to two main physical parameters: their distance from the antenna and their Doppler frequency, due to the fact that the antenna velocity relative to the target changes. For an antenna position and its associated instantaneous velocity:

- The iso-range surfaces are spheres centered on the antenna. The intersections of these spheres with the horizontal ground are called iso-range lines. They are circles, as represented in Fig. 5. Far away from the radar, they can be approximated by segments.

- Physically, if the antenna emits a monochromatic wave, all points on the cone will be seen with the same Doppler frequency. If $\mathbf{R}$ is a unit vector from the platform to the target, and $\mathbf{v}$ is the platform velocity, the set of points $\mathbf{R}$ for which $\mathbf{R}.\mathbf{v}$ is constant is a cone whose axis is the vector $\mathbf{v}$. This cone intersects the horizontal plane in a hyperbola. Such a constant Doppler curve is an iso-Doppler curve. Note that in the general case where $\mathbf{v}$ is not necessarily horizontal, these intersections with a plane are quadrics: ellipses, parabolas or hyperbolas.

The intersection of a cone and a sphere is a circle. All points on the circle defined by the intersection of the *iso-range* sphere and *iso-Doppler* cone will be seen on the same pixel of the image. This means that if we consider only the points on the ground, there may be a possible ambiguity: the scene to the right

of the aircraft will be superimposed on the symmetrical scene on the left. In our configuration, it is not a problem because the antenna is quite directive and illuminates one side of the earth. The grid thus obtained on a flat surface is represented in Fig 5.

Away from the trajectory, the grid of resolution cells thus obtained can be regarded as rectangular. In this approach, we can summarize the SAR algorithm as follows: **The purpose of the SAR algorithm is to separate the contributions of the scatterers in the signal according to their distance and their Doppler relative to the antenna.**

1.3 *The frequency domain*

This approach considers the description of the signal in the two dimensional dual space plane from the one where we want to form our image plane. In each direction, the process may be viewed as a Fourier transform, as detailed in the following. The image-extraction process that we use can then be seen as another Fourier transform that is a reversal of the original natural one. In other words, acquiring an image involves recovering an amplitude or intensity function $s(x, y)$, according to two spatial dimensions x and y. Rather than physically acquiring this function directly, we try to obtain its Fourier transform, defined by $S(k_x, k_y)$. Once $S(k_x, k_y)$ is obtained, then the inverse Fourier transform recovers the desired signal.

Physically, the support of the function $S(k_x, k_y)$ is finite, which determines the resolution of its Fourier Transform $I(x, y)$. Thus, the study of the support shape of the registered signal immediately gives the resolutions that we can obtain. In practice, the radar system has limited frequency and angular support. This leads to incomplete filling of the signal support. The inverse Fourier transform of this finite support gives the point spread function (PSF) which describes the response of an imaging system to a point source. For a rectangular support, this PSF is the cardinal sine function. When the resolution increases, when the acquisition geometry changes, this support ceases to be the same and the study of this not perfectly rectangular shape allows the theoretical shape of the PSF to be found.

This approach can be illustrated for imaging in an anechoic chamber where the antenna is mounted on a circular railway. The antenna moves along an arc in the plane (x, y), whose center is the center of the scene to be imaged. The position of the antenna is described by a two dimensional vector $\mathbf{R_0}$ as shown in Fig.6. The position of each elementary target is given by a vector $\mathbf{r_i} = (x_i, y_i)^t$. For each antenna position, a wave with wave vector $\mathbf{k}$ is emitted towards the scene center. Thus, the signal returned by the whole scene considered as a set of elementary targets with reflectivity $\sigma(x_i, y_i)dx_i dy_i$ will be written as:

$$H(\mathbf{k}) = \int exp(j\mathbf{2kr})\sigma(x_i, y_i)dx_i dy_i = \int dx_i dy_i \sigma(x_i, y_i) exp(j2\mathbf{kr_i})\ exp(-j2\mathbf{kR_0}). \tag{1}$$

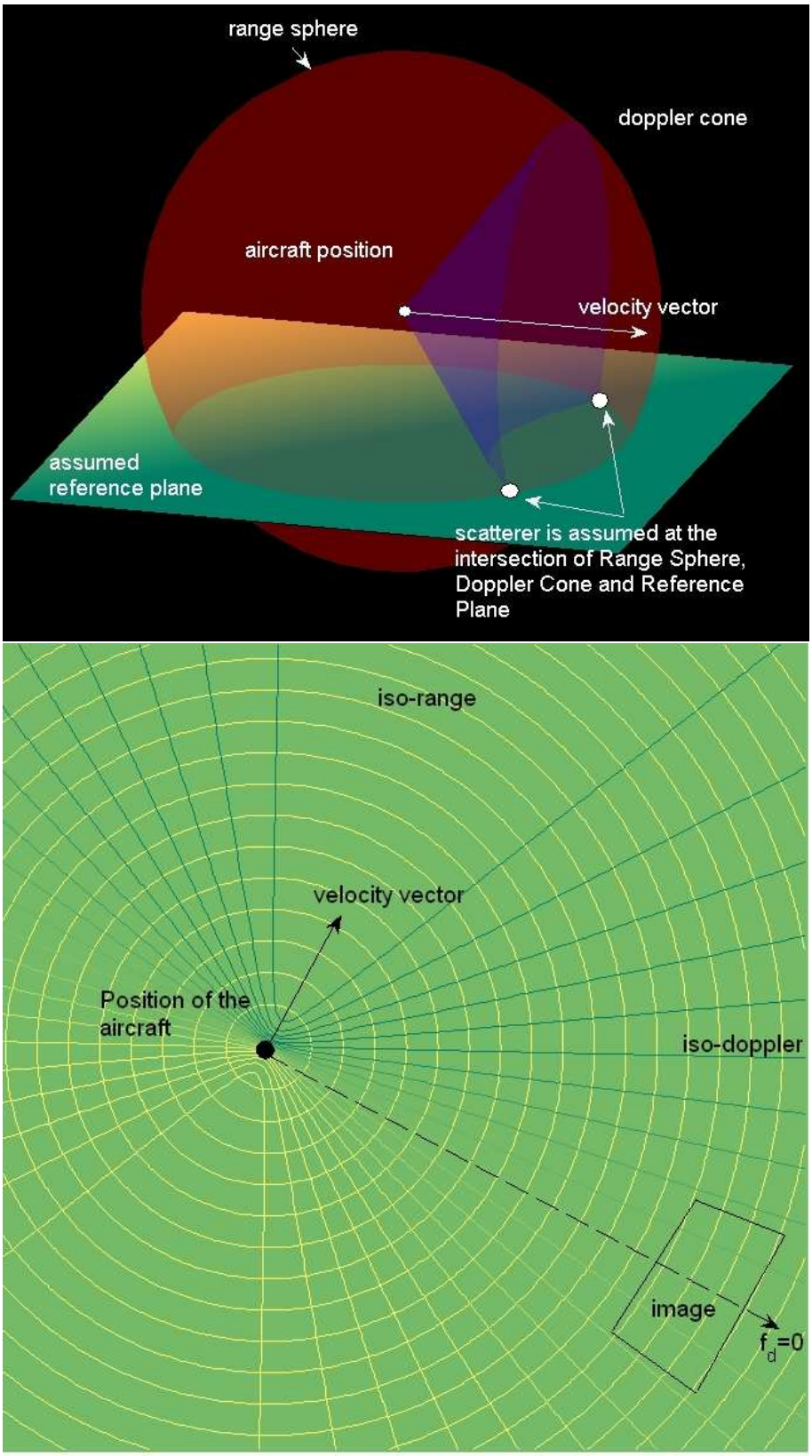

Figure 5: Resolution grid on the ground obtained by the intersection of the iso-range and iso-Doppler surfaces with a flat horizontal surface

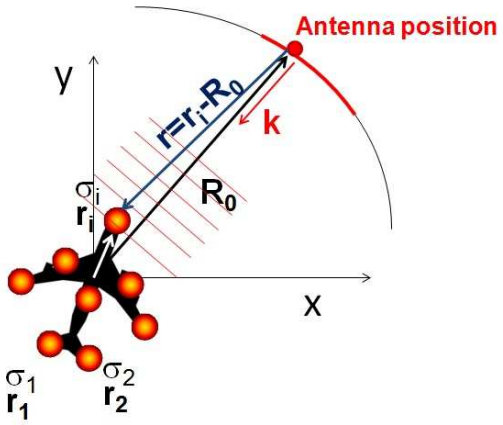

Figure 6: Geometrical parameter definition for illustrating the imaging of a target from an antenna mounted on a circular rail

The factor 2 comes from the consideration of the go-and-return path of the wave. Writing

$$exp(j2\mathbf{kR_0})H(\mathbf{k}) = \int dx_i dy_i \sigma(x_i, y_i) exp(j2(k_x x_i + k_y y_i)) \tag{2}$$

Let $K_x = 2k_x = 2k\cos\theta$ and $K_y = 2k_y = 2k\sin\theta$ one recognizes in the right term the two-dimensional inverse Fourier transform of the reflectivity function $\sigma(x, y)$:

$$\sigma(x, y) = TF^{-1}_{k_x \to x, k_y \to y}(exp(j2\mathbf{kR_0})H(\mathbf{k})) \tag{3}$$

However, the signal is not regularly sampled along the (x,y) coordinates of $\mathbf{K}_x$ and $\mathbf{K}_y$. Let us see how the signal is sampled. The angle of $\mathbf{k}$ corresponds to angle positions of the antenna on the circular rail. This angle lies between two values and we will choose the axis directed towards the mean value as the $x-axis$. The modulus of $\mathbf{k}$, $k = 2\pi f/c$ is proportional to the frequency. Thus, this modulus is also constrained by the minimum and maximum frequencies. The excursion domain of $\mathbf{K}_x$ and $\mathbf{K}_y$ represented on a plane in Fig.7 is the intersection of a circular crown, whose thickness is related to the frequency bandwidth and whose angular sector is linked to the opening excursion angle of the antenna positions:

If this area is approximated by a rectangular area, then the resolution along the x and y axis can be deduced as follows:

$$\Delta K_x = 2\Delta k = 4\pi\frac{\Delta f}{c}, \Delta K_y = 2k_0\Delta\theta \tag{4}$$

$$\delta_x = \frac{2\pi}{\Delta K_x} = \frac{c}{2\Delta f}, \delta y = \frac{2\pi}{\Delta K_y} = \frac{c}{2f_0}\frac{1}{\Delta\theta} \tag{5}$$

where dx and dy are the excursions along x and y. This allows us to make the following important observations:

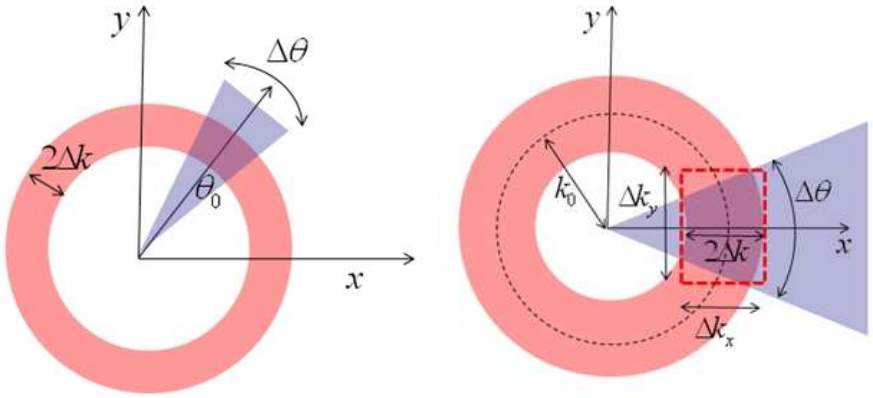

Figure 7: excursion representation of mathematical dual variables K_x and K_y

- Along an axis of the image, the resolution is inversely proportional to the frequency bandwidth.
- Along the other axis, the resolution is inversely proportional to the angular extent on which the scene is viewed.

Similarly, the maximum image size that can be achieved will be related to the sampling performed in the Fourier plane. For SAR acquisitions, the path is no longer circular; expressions between the conjugate variables, and data acquisition radar such as look angles and frequencies are more complex. However, the reasoning remains the same: the resolutions in x and y are related to the dual variables and their excursions; the maximum dimensions of the image will be related to the sampling of these variables.

1.4 *The mathematical approach*

The approach consists first in modeling the signal received by a radar according to the reflectivity of each pixel $f(x,y)$ signal. Then from the received signal, the aim is to isolate the reflectivity $f(x,y)$ which represents the desired image, by a series of treatments that may or may not involve approximations.

Generally, in a simplified two dimensional configuration, we can write the acquired signal $s(t,u)$ as:

$$s(t,u) = \iint dx dy f(x,y) s_0(t - \frac{2}{c} d(x,y,u)) \tag{6}$$

where $d(x,y,u)$ is the distance between an elementary target located at a position (x,y) and the antenna at a position u, and $s_0(t)$ is the transmitted signal in each pulse. $f(x,y)$ is the reflectivity of the elementary targets. The purpose of the SAR algorithm is to deduce the image reflectivity $f(x,y)$ from the recorded signal $s(t,u)$.

For this, we generally assume the scatterers to be white and isotropic, which means that $f(x, y)$ does not depend on the frequency or look angle used during acquisition. In addition, various algorithms exist according to a certain number of other approximations performed.

2 DIFFERENT ALGORITHM CLASS

The general mathematical problem has no simple solution. In practice, there are several algorithms to calculate $f(x, y)$ from $s(t, u)$. These algorithms can be divided into several large classes that vary mainly depending on the domain in which what is called *focusing* or *aperture synthesis* is performed. Depending on the choices made and the mathematical solutions, the algorithms differ in:

- The way in which the topography is taken into account. Since SAR imagery is 2D imaging, the scene is projected onto a flat horizontal surface, unless we want to take a numerical elevation model into account.
- The ability to take into account a large bandwidth or wide swaths. Some algorithms can lead to hypotheses that are not compatible with increasing resolutions.
- The complexity of implementation, with the number of interpolations to be produced, for example.
- The speed of execution.
- The flexibility to compensate for the motion so that it is not perfectly rectilinear. This is particularly an important concern for airborne imaging systems where deviations from a nominal path cannot be neglected. More generally, algorithms differ in terms of the capability to image with non-linear trajectories such as circular path.
- The validity in near field conditions, for example in an anechoic chamber.

The following is a list of the major types of SAR algorithms:

- **Spatio temporal methods: temporal correlation, backprojection.** They are called temporal because the focusing step is performed in the time domain. Unlike other algorithms, spatio-temporal methods easily take into account the exact geometry between the antenna and the imaged scene. The SAR image can be synthesized directly in any reference frame. The so-called temporal correlation method is intuitive but very expensive. The backprojection method is identical to the previous mathematical formulation; it requires an interpolation that significantly improves the computation efficiency. The so-called fast backprojection method is an improved version that divides the synthetic aperture into several subapertures. The final image is obtained by coherently summing all sub aperture images computed with a degraded azimuth resolution.

- **Polar format.** The RDA (Range Doppler Algorithm) algorithm, also called PFA (Polar Format Algorithm), is used on most satellite platforms. It makes use of the polar type of data in the frequency domain. An interpolation is required before the Fourier transform. The curvature of the wavefront is not totally compensated for. The CSA (Chirp Scaling Algorithm) avoids interpolation by making use of chirp structure in the azimuth processing.

- **RMA (Range Migration Algorithm) or (Ω, K) algorithm.** Focusing is done in the two dimensional frequency domain. Motion compensation is done with respect to a line. The algorithm is not suitable for a circular path. It fully compensates the curvature of the wavefront, and is therefore suitable for wide bandwidths. I have used it for most new SAR configurations, especially for high resolution, and for simulation purposes. This algorithm is also the one chosen to propose the multidimensional continuous wavelet transform (CWT) in radar imaging, initially developed to highlight the image degradations due to the assumption of anisotropic and white behavior of scatterers. In (**Colin**, Tria, Titin-Schnaider, Tabbara, and Benidir, 2004b) and (**Colin**, C.Titin-Schnaider, and Tabbara, 2005a), the wavelet transform method has been extended to the polarimetry and interferometry fields, to improve the results of these techniques.

3 THE CIRCULAR TRAJECTORY CASE

As we have seen before, the best azimuthal resolution is achieved when the target is viewed under all aspect angles. This is one of the reasons why circular SAR has been investigated. We see at least three other interests in circular trajectories:

- we will see in Part 3 that it could enable 3D imaging.

- when the directionality of targets has been proven to be crucial for signal response, a circular trajectory ensures the achievement of the best configuration for detection.

- shadow effects can be avoided, as an overlay problem through the rotation of the slant range projecting direction. This has been emphized in (Cantalloube, Oriot, and **Colin-Koeniguer**, 2008).

Hence, in 2004 Onera performed airborne circular SAR acquisitions jointly with FOI, the Swedish defense agency, during the LORAM campaign in Sweden. The airborne radar system RAMSES collected data over the Swedish forest to investigate the detection capabilities in the P-band and influences of different SAR parameters like resolution, central frequencies and look angle. In this context, circular trajectories have been used in order to analyze the presence of anisotropic scattering from the targets in the P-band. This campaign was to our knowledge the first one that made it possible to experiment with the processing of such images in the P and L bands, in full polarimetric mode.

These data have also been for me the opportunity to explore the potential of the PolInSAR circular mode to yield a higher detection rate.

In 2006, a new series of circular acquisitions was performed in the RAMSES calibration test area and two industrial and airport areas in France and Germany. The processing of these signals has been described in (Cantalloube, **Colin**, and Oriot, 2007). At X-band, the tridimensional aspect of the circular SAR imaging has been addressed on man-made targets (buildings, vehicles).

Thus, the airborne radar system RAMSES collected data over the Swedish forest to investigate the detection capabilities in the P-band and circular trajectories were used again in order to analyze the presence of anisotropic scattering from targets in the P-band. A general description of the operating mode of *flashlight SAR images* in the interferometric mode and the use of this for FOPEN purposes has been given in (Cantalloube and **Colin**, 2007).

Research on this circular mode in which I participated mainly in collaboration with Hubert Cantalloube at Onera, led to progress in all of the following aspects:

- **The choice of the SAR processors to be used in such configurations.** A serious difficulty with real circular data is motion compensation, which requires an accurate trajectory to be recovered, and for this, a point scatterer with an isotropic return to be observed. Focusing is very sensitive to motion compensation, thus it requires the use of the same techniques as in the case of very high resolution images. Moreover, some traditional SAR processors have to be rejected, because in the particular case of the circular trajectory and imaging within the circle, the geometry is stationary and singular at the circle center: the target has a same Doppler whatever the position of the plane. Finally, the wider relative bandwidth also disqualifies simplified range/Doppler types of algorithms. For these reasons, the flashlight mode has been proposed.

- **The limitation in the best achievable physical resolution.** Using this new imaging possibility, we have clearly demonstrated the strong anisotropic behavior of the main scatterers in the X-band. This proves both the limitations of the autofocus techniques based on the tracking of isotropic strong echoes for very high resolution images, and the impossibility of recovering a three-dimensional content by this method in the X-band. This has been the subject of several papers: Cantalloube, Oriot, and **Colin-Koeniguer** (2008), Cantalloube and **Colin-Koeniguer** (2008).

- **The useful directions for 3D reconstruction.**

  When computing an image on a given horizontal plane, elevated targets with respect with this given plane are not well focused on, and the direction of the focusing error changes with the observer; consequently an elevated point is mapped onto a circle. The radius of this circle is equal to $\Delta H/i$ where ΔH is the elevation error and i is the incidence angle. This artifact could be used to deduce the elevation H of the target, from the detection of the arc segments, as shown in Fig. 8. Our studies have revealed

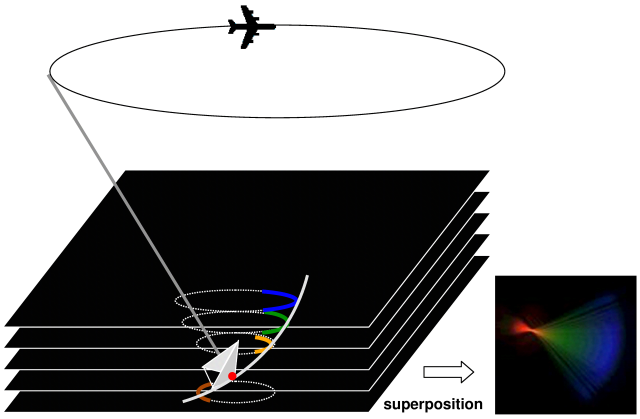

Figure 8: A trihedral corner illuminated by a circular flight: the different images obtained according by focusing on different elevation planes are surimperposed on a single image on the right using different colors

that unfortunately, the strong anisotropy of artificial targets illustrated in Fig. 9 at X-band makes this type of reconstruction impossible for vehicles. I have also proposed a new technique for DEM reconstruction from polarimetric circular images, which is presented in Part 3.

- **The link between the polarimetric return and the look angle.** These acquisitions have been an opportunity to demonstrate the importance of the look angle in the polarimetric behavior of artificial targets. The most emblematic example is the canonical trihedral corner. Seen laterally by a radar antenna, it becomes a dihedral effect, as illustrated in Fig. 10. These targets correspond to different canonical polarimetric returns.

- **The benefit of this configuration for FOliage PENetration (FOPEN) purposes.** A study has used the polarimetric content of the data in this unusual geometry to improve the detection rate of the targets hidden in the forest. During the campaign in Sweden, it was shown that using circular trajectories improves target detection. In this new campaign, detection appeared to be very difficult on classical SAR images because the forest was very dense. Since the targets were very sensitive to the orientation angle, the circular mode improved detection performances. Thus the full-polarimetric and interferometric information have been used in order to explore the potential of the POLINSAR circular mode to yield a higher detection rate. A polarimetric contrast enhancement algorithm has been tested successfully for all look images of the flight. Results have been presented in (**Colin**, Cantalloube, and Dupuis, 2006a).

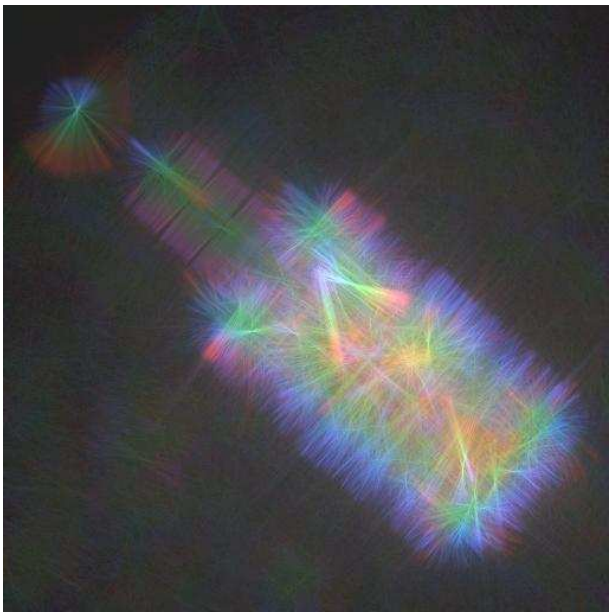

Figure 9: Representation of a military vehicle obtained by a circular trajectory: the different images obtained by focusing on different elevation planes are superimposed using different colors

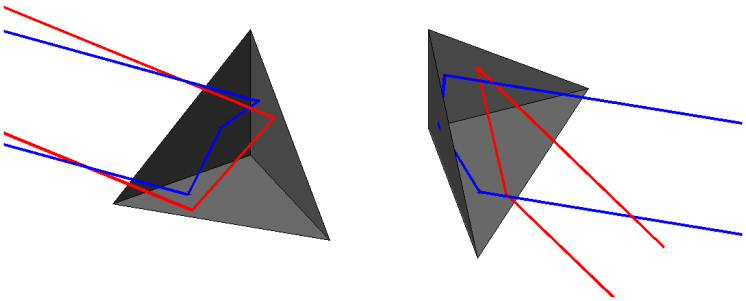

Figure 10: A trihedral corner viewed from a different look angle becomes a dihedral effect

4 BISTATIC SAR IMAGES

Bistatic image processing, with separated emitter and receiver, also opens promising applications. I have investigated algorithms for forming SAR images in a bistatic settings through several studies:

- In a stationary mode, where two aircraft systems acquire an image along parallel paths. This mode has been the one used for Onera bistatic experiments, with DLR, the German national aeronautics and space research centre, and with FOI. I have implemented a SAR simulator in this simplified configuration, coupled with a forest scene simulator, in order to be able to simulate the effects of bistatic imaging forest images.
- In a passive mode, with a receiver on the ground listening to a transmitter of opportunity, satellite or airborne system. This latter method has been investigated especially in the context of GPS transmitters, to see to extent a listening ground radar is able to use the signals of opportunity to form SAR images. It is also an interesting configuration for stealth technology. Anechoic measurements have been used in this context, on four spherical targets to investigate achievable resolutions in space. These measures have been used to highlight the effects of SAR integration on polarimetric bistatic images. In particular, we pointed out the effect of the change of polarimetric bases and polarimetric signatures during integration. This will be detailed in the next chapter.

During this last study, we have shown that an important feature of the radar image is the resolution. In any bistatic configuration, the calculation of the resolution becomes a topic in its own right, which has been treated in different ways:

- Following the frequency approach, the description of the extension of the signal frequency definition. It is an approach that we have developed at Onera.
- By studying the Generalized Ambiguity Function (GAF) of the radar system, obtained by the signal processing approach This ambiguity function corresponds to the result of the matched filter. The resolution calculation was obtained from the expression of this function. This approach was proposed by the team of Franck Daoult (University of Ville d'Avray, SATIE).

Both approaches were compared at Onera. In both cases, the theoretical formulas for range resolution and azimuth resolutions were established. The calculation of the ellipse resolution was then conducted. This allowed us to calculate the resolution for any direction, as well as for a set of preferred directions:

- The range axis is directed along the bisector of the bistatic angle, and is denoted by β. Along this axis, the distance resolution is equal to that of the monostatic case divided by the term $(\cos\beta)/2$. This term vanishes for

$\beta = \pi/2$. This result has an important consequence: it shows in particular that imaging cannot be performed with a mean bistatic angle of $\pi/2$

- The axis or Doppler azimuth corresponds to the direction of the derivative of the vector $\boldsymbol{\beta}$ over time.
- The axis orthogonal to the range axis or transverse axis.
- The minimum and maximum resolutions, respectively corresponding to the minor axis and major axis of the ellipse.

The characterization of this ellipse resolution was calculated. It provides important information on the features of the image that can be obtained. As an example, a bistatic image of four spheres obtained in an anechoic chamber shown in Fig. 13 highlights the elliptic shapes of the point spread function.

2

MEASUREMENT DATA

Now that I have shown how a radar image is processed, I present the content of the physical information carried by the value associated with each pixel of the image. This content is first analyzed for a typical SAR image, then for polarimetric and interferometric images.

Moreover, in order to understand the link between a polarimetric radar image and polarimetric images in other areas such as optics, we review all types of conventions that fall within the definition of polarimetric data.

Still with the aim of understanding the specifics of radar polarimetry, discussions are conducted on the relationship between the geometry of the acquisition and the polarimetric measurement.

Finally, the influence of the statistical estimation techniques necessary to obtain polarimetric parameters called second order parameters is presented.

1 GENERAL INFORMATION ON ADVANCED MODES

A conventional SAR image is a complex image, provided in modulus and phase. Generally, the phase information alone is not made use of. The modulus meanwhile, is relevant information, which is representative of the energy backscattered to the antenna. In this context, a calibration can quantify this modulus to give physical content to its value. Two types of variables can thus be provided:

- Radar Cross Section RCS which summarizes the ability of a target to reflect radar energy and has units of m^2. The RCS of an object is the cross-sectional area of a perfectly reflecting sphere that would produce the same strength reflection as the object in question would. Quantitatively, RCS is calculated from a ratio of Electric field intensities.
- The backscattering coefficient σ_0 or sigma naught, which is the average radar cross-section of a set of objects per unit area.

A polarimetric radar transmits with two orthogonal polarizations, often linear horizontal (H) and linear vertical (V), and receives the backscattered wave on the same two polarizations. This results in four received channels, i.e. HH, HV, VV and VH, where both the amplitude and relative phase are measured. The backscattering properties of the target in one pixel of the image can be completely described by a 2x2 complex scattering matrix $\mathbf{S}$. This matrix, called the Sinclair matrix in radars, is a coherent polarimetric representation relating the incident and scattered Jones vectors, describing the states of polarization of incident and scattered waves.

Interferometry processing is a method to analyze differences of phase information by combining two data observed from almost identical positions of a

satellite in orbit. This analysis method is devoted to either producing elevation data or measuring subsidence.

When the interferometric data are acquired in polarimetric mode, we have a PolInSAR mode which is currently an established remote sensing technique that allows the investigation of the 3D structure of natural volume scattering. When superimposing not only 2 but N images, we can make multibaseline interferometry or tomography. When multibaseline interferometric data are also polarimetric, we are speaking of PolTomSAR.

2 DEFINITION OF POLARIZATION BASIS, POLARIMETRIC MATRICES AND CONVENTIONS

Whether to set the polarization state of a wave, or to define the polarimetric behavior of a target, the choice of a base is dominant, and involves convention choice. Depending on the application field of polarimetry, optics or radar, we see that not only the measured quantities differ, but also the conventions used. Yet it is necessary to know these conventional choices precisely if we want to be able to transfer knowledge from one field to another. There are altogether three types of convention choices that it is necessary to bear in mind:

- The choice of a spatial reference, through the definition of three space vectors for each antenna of emission and reception antenna.
- The choice concerning the definition of the polarization state of a wave, usually through the definition of a vector, that can be either the complex 2-component Jones vector, or a real 4-component Stokes vector. Traditional bases use orthogonal linear polarizations, but circular polarizations are sometimes also useful.
- The choice concerning the polarimetric basis definition to define the polarimetric matrix representative of the target.

Since I have proposed new elements to better understand these different points, I will detail them hereafter.

2.1 *The spatial coordinates system*

The spatial coordinate system used to describe the polarimetric state of the incident and scattered wave is always perpendicular to the direction of the wave. However, in this perpendicular plane, the coordinate system is entirely arbitrary. This permits a degree of freedom, namely rotation about the propagation direction. This degree of freedom can be fixed by using a reference plane. Traditionally for remote sensing, we use the horizontal plane linked to the plane of Earth's surface, which is assumed to be locally plane. This leads to defining the horizontal axis as parallel to the surface of the Earth and the vertical axis as perpendicular to the latter and the wave vector. For the incident wave, the polarimetric vectors thus defined are denoted as $\mathbf{h}_i$ and $\mathbf{v}_i$, while for

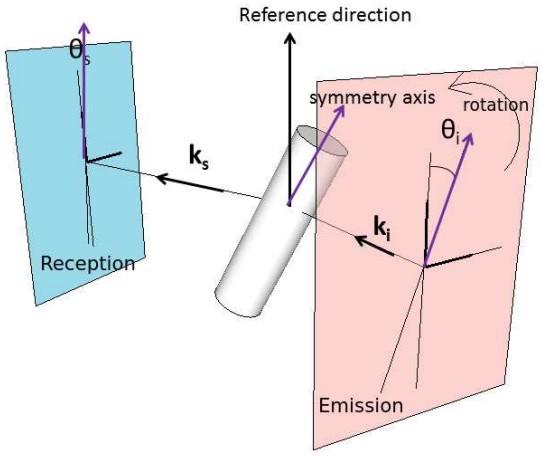

Figure 11: Orientation angles of a uniaxial object, in the incidence and scattered planes

the scattered wave they are denoted as $\mathbf{h}_s$ and $\mathbf{v}_s$. They are represented in Fig.12.

In optics, the reference plane can also be the transmitter-receiver-target plane. We will now explain why we prefer the use of this convention in the case of a bistatic radar acquisition.

Even in monostatic configurations, the exact definition of the geometry of the system has a major impact on the polarimetric information, due to its heavy dependence on the polarimetric basis used in the definition and measurement of the signals. In the bistatic case, we have shown that the geometry is much more difficult to handle.

To illustrate this, we have taken the example of a cylinder viewed in a bistatic setting, to illustrate three different geometrical effects:

1. The target orientation around the lines of sight in emission and reception. It can be described by two orientation angles θ_i and θ_s in the incident and scattered wave plane, defined with respect to a reference direction, as shown in Fig.11.

2. Emitting and Receiving antenna polarimetric orientations (or linear polarimetric basis). These can be described by two rotation angles in the incident wave plane and the scattered wave plane.

3. Emitting and Receiving antenna relative positions, described by a single angle β, the bistatic angle.

In a monostatic setting, the antenna polarimetric basis and target orientation effects (Points 1 and 2) are usually considered together because a target rotationabout the propagation axis is equivalent to an antenna rotation. The basis invariance of one target decomposition makes parameter roll invariant, i.e. the parameters are independent from the rotation of the target about the radar line of sight. It also means that the parameters can be computed regardless of the polarization basis. Thus, polarimetric basis issues are solved either by

roll-invariant parameters or appropriate rotations. In a bistatic setting, the first point and the second one are no longer equivalent:

- Physical target rotations around the line of sight (in the incident or scattered direction) are not only related to rotations in the scattering matrix. A change of the target orientation in the incident wave plane can change the mechanism viewed by the reception antenna, and not only the tilt angles.

- The term **disoriented target** means that the scattering matrix does not contain any more information about its tilt angles, as presented in (Huynen, 1970), and more recently in (Titin-Schnaider, 2010). When the tilt angles are estimated and removed or roll-invariant parameters are used, a rotation of the target in the incident wave plane or in the scattered wave plane (Point 1) can still affect the remaining parameters.

In order to perform a classical polarimetric study, eventually involving the usual tilt angle estimation, we have shown in (Trouvé, **Colin-Koeniguer**, Fargette, and De Martino, 2011) the importance of carefully defining our convention, which allows us to make a polarimetric analysis regardless of the orientation angles defined in Point 2. In this way the knowledge of the remaining tilt angles can improve the understanding of the remaining parameters.

If we want to focus on the influence of Emitting and Receiving Antenna relative positions (Point 3), using a single angle β, we have also shown that it is better to choose a convention linked to the scattering plane (emitter-target-receiver) to define the polarimetric bases, as illustrated in Fig. 12. This convention effectively removes the influence of Point 2 and reduces the analysis to a single variable: the bistatic angle. This point is detailed in (Trouvé and **Colin-Koeniguer**, 2009).

However, our recommendation is not the classical convention imposed by the classical radar measurement. For this reason, we have expressed, still in the same paper, the transition from the classical convention imposed by measurement, to the convention chosen here. We have proven that it is equivalent to two rotations.

We have also illustrated the importance of this choice for the polarimetric analysis performed, by bistatic measurement for isotropic targets, starting with a single metallic sphere, and gradually increasing the complexity by increasing the number of spheres, then finally considering a cloud of spheres.

As an example, in Fig. 13, two images of four spheres acquired in an anechoic chamber in a bistatic setting are represented using the different conventions: the classical convention in radar imaging on the left, and the one that we recommend for a bistatic analysis. In the image on the right, we see that the three spheres that are away from the center of the image appear in red, as is classically obtained for a canonical sphere in a monotatic setting, whereas the image on the left contains blue colors linked to cross-polarization, which are representative of the geometrical configuration of acquisition but not of the target itself.

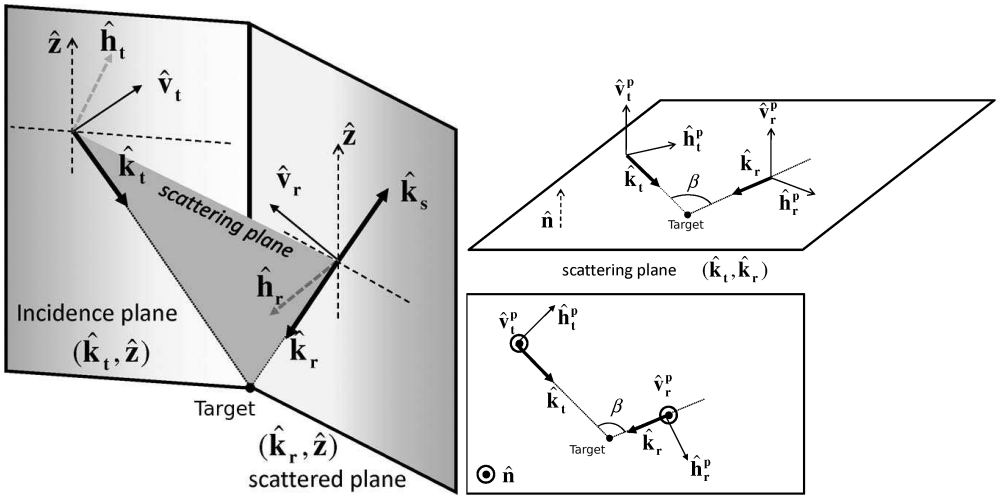

Figure 12: Convention of polarimetric spatial definitions based on the reference plane: $\mathbf{h}_i^p$ and $\mathbf{h}_s^p$ are in the scattering plane, $\mathbf{v}_i^p$ and $\mathbf{h}_s^p$ are orthogonal to this plane; $\mathbf{v}_i$ and $\mathbf{v}_s$ are in the incident and scattered planes, $\mathbf{h}_i$ and $\mathbf{h}_p$ are orthogonal to these planes.

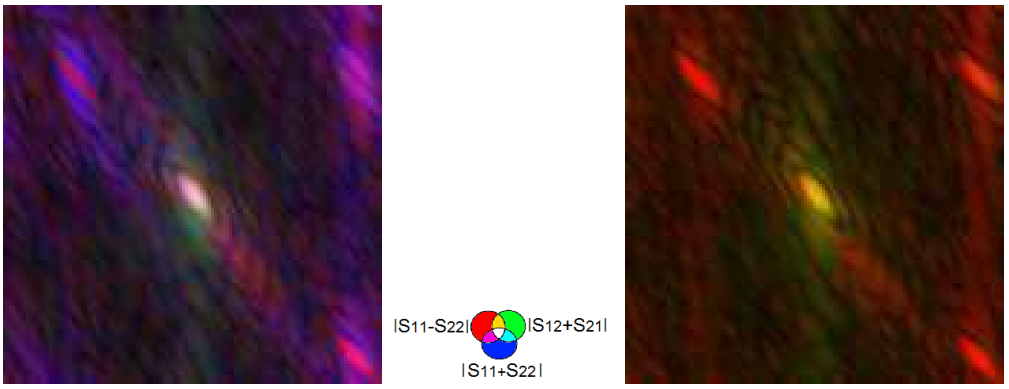

Figure 13: Bistatic polarimetric images of four spheres processed for two different spatial conventions: the radar classical convention on the left and those proposed in our studies on the right. The colors refer to combinations between the four elements of the Sinclair matrix S_{ij}

Moreover, in order to completely describe the coordinate systems, once the orientation of the two polarimetric vectors have been chosen in the wave planes, we also have to choose the convention about the directions of the unit vectors relative to the sense of propagation. This leads to two different conventions: *Forward Scatter Alignment* FSA and *BackScatter Alignment* BSA.

In the FSA convention, the $z-$axis is defined by the direction of propagation of the wave. In the BSA convention, the $z-$axis is positive when pointing towards the target both before and after the wave is scattered. This BSA convention is less intuitive, but is generally chosen in SAR polarimetric images because in the particular case of backscattering (monostatic case), the coordinate systems are the same for the cases of the EM wave propagating from the antenna to the target and for the wave scattered from the target back towards the antenna.

These conventions are important to express the relationships among polarimetric radar variables and optics variables. These relationships are explained in the following.

2.2 *The state of polarization of a wave*

The definition of the state of polarization of a wave is done either by using the Jones vector, which is a complex two-dimensional vector, or by using the Stokes vector, which is a four-dimensional real vector. The radar is able to perform a coherent measurement of the signals, and then deals with the measurement of a Jones vector, whereas optical devices refer to the definition of a Stokes vector. In both cases, the polarimetric basis used to define the Stokes vector or Jones vector must be composed of two orthogonal polarization states.

2.3 *The polarimetric measurement of a target*

The polarimetric measurement behavior of a target can be described by a polarimetric 2x2 scattering matrix that connects two complex Jones vectors. In optics, the scattering matrix is defined using the FSA convention and is called the Jones matrix, whereas in the radar field it is defined using the BSA convention and is called the Sinclair matrix. The Sinclair matrix $\mathbf{S}$ and the Jones matrix $\mathbf{J}$ are related by:

$$\mathbf{J} = \begin{pmatrix} 1 & 0 \\ 0 & -1 \end{pmatrix} \mathbf{S}^*. \tag{7}$$

The elements of the Sinclair matrix $\mathbf{S}$, often denoted as S_{HH}, S_{HV}, S_{VH} and S_{VV} can be arranged into a measurement vector by projection onto the Pauli matrix. This vector is called the scattering vector:

$$\mathbf{k} = \frac{1}{\sqrt{2}} [S_{HH} + S_{VV}, S_{HH} - S_{VV}, S_{HV} + S_{VH}, j(S_{HV} - S_{VH})]^T \tag{8}$$

The Sinclair matrix $\mathbf{S}$ and Jones matrix $\mathbf{J}$, as well as the scattering vector $\mathbf{k}$ are said to be *first order polarimetric parameters*. In a radar image, they are

contained in the information linked with a single pixel and do not require a statistical estimation.

In order to study the statistical behavior of polarimetric information in radar images, *second order polarimetric parameters* are considered. The coherence matrix is defined as an expected value of the product of the scattering vector $\mathbf{k}$ with its complex conjugate $\mathbf{k}^\dagger$:

$$\mathbf{T} = \left\langle \mathbf{k}\mathbf{k}^\dagger \right\rangle \tag{9}$$

The $\langle ... \rangle$ operator denotes the statistical averaging and † denotes the complex conjugate transpose. In SAR polarimetry the averaging is usually done spatially. The coherence matrix is always Hermitian matrix, i.e. a matrix that is equal to its conjugate transpose. Hermitian matrix diagonal elements are real and it has real eigenvalues, denoted by λ_1, λ_2 and λ_3. The eigenvectors form a unitary basis. A current set of parameters derived from an eigenvalue decomposition of the coherence matrix are the Cloude-Pottier parameters. Among these, the polarimetric entropy is defined in terms of the logarithmic sum of eigenvalues:

$$H = \sum_{i=1}^{3} = p_i \log_3 p_i, \quad p_i = \lambda_i / \sum \lambda_i, \tag{10}$$

where the p_i are the corresponding probabilities recovered from the eigenvalues λ_i. Cloude and Pottier also introduced a parameterization of the eigenvectors of matrix $\mathbf{T}$.

Mueller and Kennaugh matrices are alternative second order polarimetric matrices. They both link the Stokes vectors of the emitted and received wave. The Mueller matrix is expressed using the FSA convention whereas the Kennaugh matrix is expressed using the BSA convention.

The link between the classical Mueller matrix and the Kennaugh matrix is:

$$\mathbf{M} = \begin{pmatrix} 1 & 0 & 0 & 0 \\ 0 & 1 & 0 & 0 \\ 0 & 0 & -1 & 0 \\ 0 & 0 & 0 & 1 \end{pmatrix} \mathbf{K}, \quad \mathbf{K} = \begin{pmatrix} 1 & 0 & 0 & 0 \\ 0 & 1 & 0 & 0 \\ 0 & 0 & -1 & 0 \\ 0 & 0 & 0 & 1 \end{pmatrix} \mathbf{M} \tag{11}$$

Mueller polarimetry consists in the measurement of the Mueller matrix. Mueller polarimetry can be integrated into almost any active imaging or spectroscopic system, and can thus provide polarimetric information at any spatial scale, by adding a Polarization State Generator (PSG) in the illumination part, and a Polarization State Analyzer, or PSA, in the detection part.

In summary, optical imaging polarimeters measure second order parameters directly, while the radar imaging systems measure the first order parameters and estimate those of second order, usually from a spatial average.

3 SECOND MOMENTS IN POLARIMETRY: THE ORIGIN OF THE *depolarization* PHENOMENON

An essential concept of polarimetry lies in what we call here depolarization. By this term, we understand the ability of a target to transform a wave that is totally polarized, and that can be described in a deterministic way, into a random or partially polarized wave.

A deterministic target has a zero depolarization factor, whereas a so-called ideal depolarizer will have a depolarization factor equal to 1. Radar entropy contains the same kind of information on the randomness of the target.

However, one single measurement of the Sinclair matrix does not allow the randomness of the polarization of the received wave to be assessed. However, if the measurement is repeated many times with the same target, the statistical analysis of the matrices thus measured can tell us about the deterministic or random nature of the wave scattered by the target.

Thus in radar, we could quantify this random or deterministic behavior by considering statistical moments of order 2 of the scattering vector through the coherency matrix $\mathbf{T}$.

If all Sinclair matrices measured are identical, then the corresponding coherence matrix $\mathbf{T}$ is of rank 1, one of its eigenvalues is non-zero, and the polarimetric entropy or depolarization of this target is then zero. Conversely, if all eigenvalues are non-zero, then the corresponding target is non deterministic, and its entropy is strictly greater than zero.

Practically, the ergodic hypothesis states that the statistical estimation which should be made by using several samples of the measurement, can be made using the values of several adjacent pixels belonging to the same area.

The calculation of polarimetric parameters related to statistical properties trough spatial estimation in radar suffers from many drawbacks:

- First, it involves spatial averaging, which is performed at the expense of resolution.
- Up to now, radar parameters have been investigated mainly in a monostatic configuration.
- Polarimetric entropy has a high computational cost. This can be a handicap for the use of this parameter, including its use for polarimetric visualization of large images, as developed in (Praks, Hallikainen, and **Colin-Koeniguer**, 2010).
- The physical interpretation of polarimetric entropy is not obvious.
- Finally, whether or not the statistical estimation is equivalent to that which would be made on several pixels remains to be seen. It is likely that the sampling consequences and spatial resolutions are involved in this estimate, in a manner that is not necessarily controlled. Indeed, a non-trivial problem is to determine the physical phenomena that originate the depolarization.

In order to meet these different points, two parallel approaches were undertaken:

- The first is the proposed new alternative to entropy. This approach is the subject of the publication (Praks, **Colin-Koeniguer**, and Hallikainen, 2009). It has also led to propose an alternative for another polarimetric parameter: alpha. This approach meets the first four points as follows:
  - The resolution degradation is avoided for the alternative parameter to alpha.
  - The associated computational costs are greatly reduced.
  - New physical interpretations inspired by optics have been proposed for these alternative parameters
  - The extension of these parameters to the bistatic case is better understood.
- The second is to use an optical measurement device, which does not require spatial estimation to make measurements of depolarization or entropy, and conduct studies at the optical scale. This has allowed us to understand the physical origin of the depolarization in the particular case of nanotube forests, related to the integration of a variety of angular responses introduced by multipath. This progress is the result of the PhD thesis by Etienne Everaere, co-supervised by Laetitia Thirion-Lefevre from SONDRA and Antonello de Martino from the LPICM.

Both of our approaches are detailed below.

3.1 *An alternative parameter to entropy*

We describe here the first approach. It comes from the convergence of two completely different visions:

- Jaan Praks, from Aalto University in Finland, proposed alternative polarimetric parameters that can be calculated without eigendecomposition (Praks and Hallikainen, 2000b). He based the construction of these parameters on similarity invariants of Hermitian matrices, which are the determinant, the Frobenius norm and the trace (Praks and Hallikainen, 2000a).
- My own approach, presented first in (**Colin**, 2007), was to rise to the formulation of entropy, to understand the logarithmic form. As detailed below, by relaxing the additivity property that has little interest for radar, I came precisely to the same expression as that proposed by Jaan Praks. I also drew the link between this new parameter and those used in optics.

Following the conference paper (**Colin**, 2007), this alternative was studied in depth. The entropy parameter, either for thermodynamics, information theory

or polarimetry, is characterized by a certain number of mathematical properties, which originate from certain physical boundary conditions, each of these having a physical interpretation in the field of application:

- Continuity: entropy is a continuous measure. This means that a small change in the measurement produces a small change in entropy.
- Symmetry: the parameter value remains unchanged if the outcomes x_i are re-ordered.
- Maximum: if all outcomes are equiprobable, then entropy should be maximal.
- Additivity: the amount of entropy should be the same, even if the process is divided into parts.

Any definition of a parameter A satisfying these four assumptions has the form: $A \propto \sum_{i=1}^{n} p_i \log p_i$, where p_i is the probability of the output i. The necessity of the logarithm form is explained by the additivity property. Additivity property means that the entropy of a system composed by independent sub-systems is the sum of the entropies of its sub-systems. If sub-systems are not independent, the entropy of a system can still be calculated from the entropy of its sub-systems provided that we know how the sub-systems interact with each other. In the context of radar polarimetry, a sub-system would correspond to a partially polarimetric system. This property has a limited physical importance, since polarimetry operates in a space with less than three or four dimensions and moreover dividing the measurement of a fully polarimetric radar into several partially polarimetric radars does not decrease the total number of measurements nor the computation complexity, since it is the Sinclair matrix that is measured before computing the coherence matrix.

The parameter is called scattering diversity. It is similar to classical entropy but it does not have the additivity property. However, all of the other properties are verified. In order to achieve the same extreme points as for entropy, we have defined the following parameter in the monostatic case:

$$\hat{H} = \frac{3}{2}\left(1 - \|\mathbf{N}\|_F^2\right) \tag{12}$$

where $\|\|_F$ is the Frobenius norm and $\mathbf{N}$ is the coherence matrix normalized by the SPAN. In order to extend our scattering diversity parameter to the bistatic case, achieving 0 and 1 as extreme points, we define:

$$\hat{H}_{bistatic} = \frac{4}{3}(1 - \|\mathbf{N}\|_F^2 = \frac{8}{9}\hat{H}_{monostatic} \tag{13}$$

We have linked this parameter with at least two parameters that are used in optical polarimetry and have a physical interpretation. The first is called **degree of purity** (Gil, 2000) or **depolarization index** (Chipman, 2005). It is defined as the Euclidian distance of the normalized Mueller matrix $\mathbf{M}/M_{00}$ to the ideal depolarizer of the non-reciprocal case:

Optical polarimetry uses another parameter called the depolarization of the matrix:

$$\mathsf{dep}(\mathbf{M}) = 1 - \frac{\sqrt{\sum_{i,j} M_{ij}^2 - M_{00}^2}}{\sqrt{3} M_{00}} \tag{14}$$

This parameter indicates how far the matrix is from a set of Mueller matrices of non-depolarizing targets. It is connected to the average depolarization of the outgoing light. It is related to $\hat{H}_{bistatic}$ by:

$$\mathrm{dep}(\mathbf{M}) = 1 - \sqrt{1 - \hat{H}_{bistatic}} \tag{15}$$

To conclude with this, the scattering diversity that we propose as an alternative parameter to entropy is strongly related with the physical interpretation of average depolarization of the outgoing wave, and can be viewed as a distance of the target to an ideal depolarizer. Note that the ideal depolarizer has different Kennaugh matrices in the monostatic reciprocal case and in the bistatic case.

The proposed scattering diversity is also directly connected to the depolarization coefficient in optical polarimetry. Thus it quantifies the ability of the target to transform a perfectly polarized wave into a partially polarized one.

Finally during this study, we have also shown that the alpha angle can be replaced by the first element of the **N** matrix, called the **surface scattering fraction**.

Both proposed parameters have been proven to be suitable for image interpretation, classification and visualization in the same way as classical ones. For example, they are shown in a colored representation in Fig. 14 and compared to the classical ones, using the polarimetric AIRSAR image. In this figure, we see that the colored representations are very similar. However, the parameters used for the second one are easier to interpret and to calculate since they do not require calculation of eigenvalues or eigenvectors of the coherence matrix.

3.2 *An alternative measurement device to understand the origin of depolarization*

The physical origin of the depolarization is still poorly controlled in radar images. In all cases, entropy or depolarization comes from a coherent integration, which means a summation over intensities. This can be either:

- a temporal summation,
- a spatial summation,
- an angular summation,
- a frequency summation.

The classical estimation of entropy in radar images involves a spatial average. Indeed, the signal contained in a pixel is the coherent sum of contributions

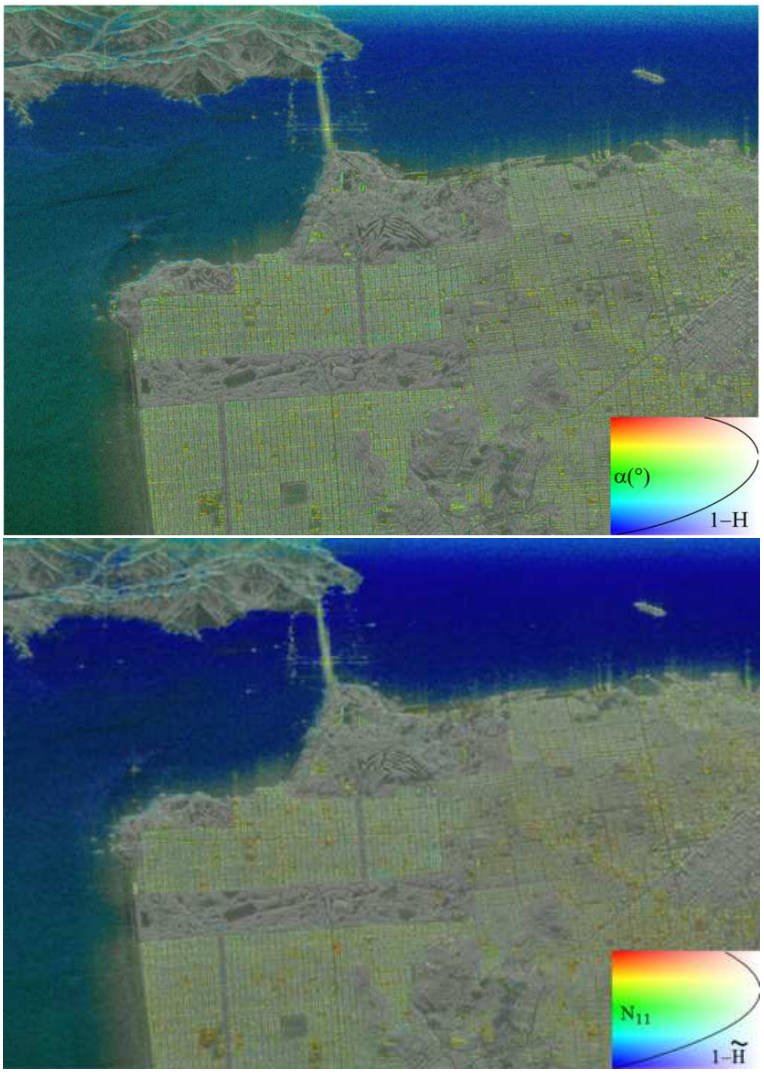

Figure 14: Polarimetric colored representation using first classical parameters Entropy and alpha, and then new proposed parameters scattering diversity and surface scattering fraction.

from all scatterers. However, it is difficult to predict the result of the interaction of all of these polarimetric phasors. Furthermore, it is unlikely that adjacent pixels contain exactly the same spatial distributions. The coherent sum of the contributions will be different, which can lead to the depolarization phenomenon that we will call spatial depolarization.

The frequency or angular summation is sometimes used to estimate coherence matrices from a radar indoor measurement. Usually, it is assumed that the target will have the same polarimetric behavior under different look angles. However, when an angular integration is done on a too large excursion, this assumption may not be true. Some targets such as dihedral corners have returns that are strongly dependent on the angle of orientation. Similarly, a variation of the frequency behavior can result in a depolarization effect.

The temporal integration, inherent to an optical device, can induce depolarization effects. A temporal incoherent average can also be applied in radar images by using successive acquisitions. In this case, the depolarization could be linked to the notion of temporal correlation. Indeed, it reflects movement or change in the polarimetric behavior of the scene during the integration period.

4 MONOSTATIC CASE AND BISTATIC CASE: CONSEQUENCES IN POLARIMETRY

SAR images have so far been acquired in the monostatic mode. In 2004, ONERA and the DLR conducted a first bistatic airborne campaign, dedicated to the feasibility of this imaging mode, at X-band. It was soon followed by other campaigns organized with FOI in Sweden, at lower frequencies, for the application of target detection under vegetative cover. These bistatic images of forest areas were not acquired in a polarimetric mode, because the technological constraints are numerous. However, we may thus wonder how a bistatic acquisition will affect the polarimetric analysis.

Until then, classical radar polarimetric theory made use from the beginning of the reciprocity property, which fails in a bistatic configuration. The first line of research to develop bistatic radar polarimetry has considered the theoretical development established so far in radar, and tried to extend it without using the simplifying assumption of symmetry. This approach was conducted in the same manner as for radar theory, first distinguishing deterministic targets and the Huynen theory and then addressing natural targets. This is the method that was first proposed in the dissertation of Anne Laure Germond (Germond, 1999), and later by Cécile Titin-Schnaider at Onera (Titin-Schnaider, 2008), (Titin-Schnaider, 2010).

I have proposed an alternative line of investigation to develop the bistatic polarimetry theory. It is to be guided by theories developed for optical polarimetry. First, a study was conducted on the physical origin of the reciprocity assumption, and any monostatic case that may be impaired. Then the available optics tools for analyzing a possible polarimetric bistatic acquisition were investigated. My approach was to see whether the arguments made so far on the optical scale have meaning on the radar scale, and therefore cross both

fields. This work was part of a more general approach that could be called *optical and radar convergence*. It was the subject of the PhD thesis of Nicolas Trouvé whose main results and perspectives have been presented in (**Colin-Koeniguer**, Trouvé, Everaere, and DeMartino, 2012). It is partly resumed in the dissertation of Etienne Everaere, and is developed in the last part of this book.

4.1 *Where can the reciprocity assumption fail in a monostatic configuration?*

The reciprocity assumption is a consequence of the Lorentz reciprocity theorem, which applies for targets composed of a linear isotropic, homogeneous material, and of finite dimensions. In this context, the theorem proves from Maxwell's equations, that we can exchange the roles of emission and reception antennas (Tsang and Li, 1985). Thus, it is trivial to show by applying the superposition theorem that the property extends to the superposition of several *Linear Homogeneous Isotropic* (LHI) targets without interactions between these. Let us view the first LHI hypothesis in more detail.

A material can be described by the most general relation $\mathbf{D} = f(\mathbf{E})$ where $\mathbf{D}$ is the electric displacement field and $\mathbf{E}$ is the electric field. When the material is linear, then this relation is linear too and the multiplicative coefficient linking $\mathbf{E}$ and $\mathbf{D}$ is a matrix called permittivity, and denoted by $\boldsymbol{\epsilon}$:

$$\mathbf{D} = \boldsymbol{\epsilon}(\mathbf{r}, \omega)\mathbf{E}. \tag{16}$$

The imaginary component of this permittivity is related to absorption loss, the rate at which energy is absorbed by the medium during the propagation, whereas the real component is linked to the phase velocity of the wave. The matrix contains the three dimensions of space. According to the different particular case of this tensor, we can then distinguish various material properties.

A medium is referred to as homogeneous when the permittivity does not depend on the spatial coordinates in the material. This concept defines the scale of the wavelength used. Thus, a medium may be regarded as quasi-static homogeneous in regimes where the correlation inhomogeneity length is much smaller than the wavelength of the incident electric field. The case of a target where a discontinuity occurs in the structure at the wavelength scale will therefore be more complex. It is thus necessary to generalize the reciprocity principle, to consider an equivalent effective dielectric permittivity, and consider its properties. Finally, a material will be isotropic if its permittivity does not depend on space coordinates and therefore is scalar.

Many media are not isotropic. However, there are some extensions of the Lorentz reciprocity theorem in the literature. For example, it has been shown that the principle is valid in the following cases:

- The target is anisotropic, but its permittivity matrix is symmetrical complex. This is the case encountered in most radar cases.
- The target consists of two contiguous LHI materials.

- The target is bianisotropic: it is constituted by a stack of horizontal layers of different permittivities (Tai, 1992).

On the contrary, it is possible to produce a number of cases where this property is no longer guaranteed, even in monostatic conditions:

- for the magneto optical media. The most common example is the radio waves passing through the Earth's ionosphere, which are likewise subject to the Faraday effect. The permittivity tensor is then Hermitian, but not symmetrical. Such materials are also known as gyromagnetic. The case of ferromagnetic materials is included.

- for nonlinear media, that is, media in which the dielectric polarization responds nonlinearly to the electric field of the light. This nonlinearity is typically only observed at very high light intensities when the electric field values are comparable to those of interatomic electric fields, such as those provided by lasers.

- for the active media whose permittivity varies over time, for example when permittivity is modulated in time by some external process.

4.2 *Can optical polarimetry be applied to radar polarimetry?*

Whatever the field of application, polarimetry refers to the measurement and interpretation of the polarization of transverse waves, most notably electromagnetic waves, that have traveled through or have been reflected, refracted, or diffracted by some material in order to characterize that object. The main difficulty encountered to provide an exchange between the optical polarimetry and radar polarimetry communities lies mainly in the vocabulary and convention differences. Practically, optical polarimetry and radar will differ by measurement types, and by the types of decompositions traditionally used for the notion of canonical targets, i.e whose behavior is representative of a given mechanism.

Originally for polarimetric radar, data were acquired in an anechoic chamber, by the way, as for optics, through obtaining Stokes matrices. The targets under study were deterministic targets. Also, the new capabilities offered by the coherent acquisition of a Sinclair matrix were a huge progress in reducing the number of measured observables. In the case of natural targets, theoretical developments have been proposed to estimate coherence matrices from several samples. At the optical scale with Mueller imaging systems, Mueller matrices are also measured. It is therefore possible to establish a bijective relationship between the optical measurements of Mueller matrices and the radar measurements of coherence matrices.

Once I highlighted when and how it is possible to draw the link between radar polarimetric acquisitions and optics polarimetric acquisitions, I also investigated the types of decompositions that are used in each field, in (**Colin-Koeniguer**, Trouvé, and Praks, 2010), and (**Colin-Koeniguer** and Trouvé, 2013).

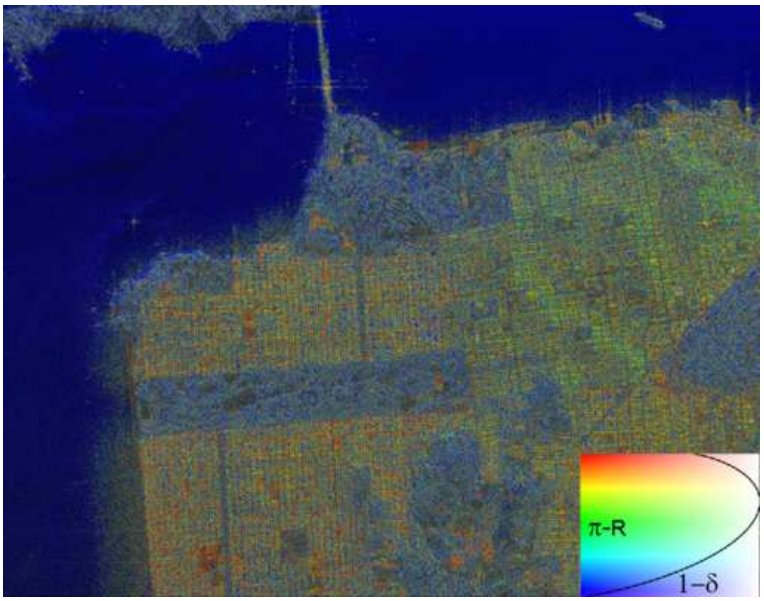

Figure 15: Colored representation of alternative optical parameters depolarization and retardance applied to the AIRSAR image

Traditionally, radar decompositions are additive decompositions, whereas optical decompositions are multiplicative. During my research, I was able to show that it was possible to use multiplicative polarimetric decompositions to SAR data. This work is largely in line with that proposed in (Souyris and Tison, 2007) on deterministic targets and their polar decomposition. This use of multiplicative optical decompositions is promising, especially for environments such as the forest, where a multiplicative description is particularly appropriate for stratified layers.

As an example, a colored representation of the AIRSAR image of San Francisco is proposed in Fig. 15, using the classical parameters of the Lu and Chipman decomposition, retardance and depolarization. Retardance is the difference in phase shift between two characteristic polarizations of light. It has been proven to be strongly related to alpha. The resulting image offers a good contrast between the different areas of the image: water and building areas, as for a classical radar colored representation.

3

DESIGN OF A POLARIMETRIC RADAR: TECHNOLOGICAL CONSTRAINTS

1 HIGH RESOLUTION OR POLARIMETRIC MODE?

To date, most polarimetric SAR have predominantly been implemented as experimental add-on modes to existing designs for single-pol or dual-pol systems. As a result, current and planned spaceborne SAR have full-polarimetric modes that are severely limited in swath width, are restricted in the range of look angles, suffer from low SNR and ambiguity problems, and are difficult to calibrate (Freeman, 2009). The consequence of this is that the high potential science return expected from polarimetric SAR data has not been realized.

In order to overcome this limitation, it is important to understand what the constraints that limit the polarimetric mode are.

If we want to alternate the emission of different polarizations, it will of course affect the pulse repetition frequency. The PRF is constrained by both the range ambiguities, and the azimuth ambiguities (McCandless and Jackson, 2004). The first condition imposes a maximum PRF to ensure a sufficient swath. The second imposes a minimum PRF to ensure an antenna small enough, and thus, consequently, a satisfactory azimuthal resolution. Let us express now these two kinds of requirement.

1.1 *The maximum PRF: avoid range ambiguities*

In order to avoid range ambiguity, the pulse repetition frequency must be smaller than the time it takes to collect returns from the entire illuminated swath. This condition can be written as:

$$\mathrm{PRF} < \frac{c}{2W'_x} \tag{17}$$

where W'_x is the maximum swath along the range axis, as shown in Fig.16 .

1.2 *The minimum PRF: avoiding azimuth ambiguities.*

In order to understand why a sufficiently rapid pulse rate is necessary, we must remember that targets along the azimuth axis are separated according their Doppler frequency, that is the apparent change in frequency between one target and the wave source, because of their relative motion. Then, the difference between the frequency of the transmitted signal and the returned signal must be less than the repetition frequency. The maximum Doppler shift is obtained for a point that is illuminated at a maximum distance ahead of the

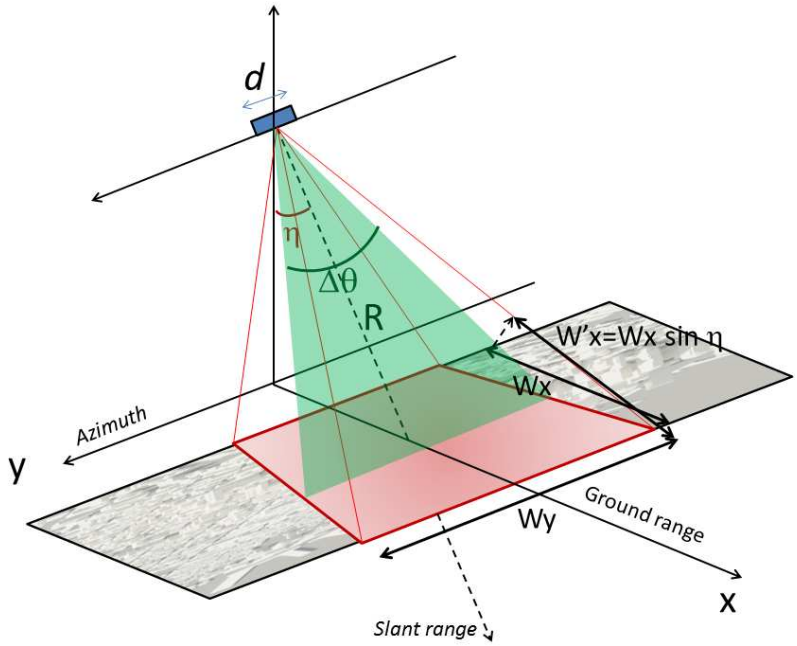

Figure 16: Geometrical representation of the SAR acquisition

radar, then at the farthest points of the illumination lobe. The shift Doppler frequency Δf_d obtained for a point with a relative radial velocity to the radar v_r is:

$$\Delta f_d = 2\frac{v_r}{\lambda} \tag{18}$$

where λ is the central wavelength. If $\Delta\theta$ is the angular aperture of the antenna, then the maximal value is obtained for $v_r = v \sin \Delta\theta/2$. With the condition $\Delta f_d max < PRF$ and $\sin \Delta\theta/2 \approx \Delta\theta/2 = \frac{\lambda}{2d}$, where d is the along-track dimension of the antenna aperture, we set the lower bound of the Pulse Repetition Frequency:

$PRF > \frac{2v}{d}$

This requirement necessitates the radar to send a pulse each time that the radar platform translates half of the along-track antenna length d. In other words, the maximum along-track distance between samples is $d/2$ (Freeman, 2006).

1.3 *Polarimetric mode: reducing swath or loss of spatial resolution?*

Azimuth resolution is also constrained by the antenna real dimension, and is thus related to the minimum PRF.

A RAR system achieves its resolution through the physical dimensions of its aperture, sometimes referred to as diffraction limited performance. As described previously, a SAR obtains a better azimuth resolution by using all

echoes acquired along an integration path, whose length is called the synthetic aperture length. However, the scene must be illuminated for all of the positions of the integration path. This means that the antenna must have a large angular extent, which is inversely proportional to the aperture dimension.

Let L be the integration length. Then

$$L < \Delta\theta R \tag{19}$$

where $\Delta\theta$ is the angular aperture of the antenna, and $\Delta\theta = \lambda/d$ where d is the dimension of the real antenna aperture. Let us recall that the azimuth resolution can be written as $\delta a = \frac{\lambda_0}{\Delta\theta} R$, obtaining

$$\delta a \geqslant \frac{d}{2}. \tag{20}$$

Thus, the best achievable for a focused SAR is approximately one half of the along-track real radar-antenna length.

Finally, we can express the conditions on PRF as a condition relation between the azimuth resolution and the range swath W'_x:

$$\delta_a > 2\frac{v}{c} W'_x. \tag{21}$$

Since this condition depends on the speed of the platform, it is more critical for spaceborne systems. This means that there is a trade-off between swath and azimuth resolution. Note that other parameters involve trade-off such as the transmitted powers. For example, in order to enable shorter pulses to be sent, the transmitted frequency bandwidth is often reduced, which is therefore at the expense of the range resolution.

Up to now, the polarimetric mode has been therefore designed at the expense of azimuth resolution. On all polarimetric satellites already sent, resolutions in the polarimetric mode are worse than those the single polarization modes. Conventional quad-pol SAR operate with interleaved transmission of alternate H-polarized and V-polarized pulses, receiving both H-polarizations and V-polarizations to build up a measurement of the full scattering matrix for each pixel on the ground. The SAR designer typically adopts an overall PRF that is twice as high as for conventional modes of operation. In the dual pol mode of TerraSAR-X for example, the radar toggles the transmit and/or receive polarization on a pulse-to-pulse basis. The effective PRF for each polarimetric channel is half of the total PRF, which means that the azimuth resolution is also reduced (Tomiyasu, 1978).

Therefore, it is very difficult to prove the benefit of polarimetric data, especially in the case of applications where the resolution is an essential criterion, such as in urban areas for the detection of buildings, or the identification of manufactured targets.

For this reason, urban studies were first made by using airborne data offering higher resolutions. Recently I have led polarimetric studies over urban scenes using satellite data, in particular after the launch of TerraSAR-X. TerraSAR-X polarimetric data have resolutions of the order of 2m x 6m, while

the single polarimetric modes have sub-metric resolutions. In addition, rather than abandoning the polarimetric mode when the resolution is insufficient, Nicolas Trouvé proposed in (Trouvé and **Colin-Koeniguer**, 2013) to combine it with high resolution images. This is the aim of the PhD thesis of Flora Weissgerber which began at the end of 2014. This thesis has led to two key contributions:

- The first concerns the statistical study of complex data used in polarimetry and interferometry, in particular through statistical studies about the coherence parameter. This will be explained in more detail in the next chapter. The underlying idea is to better understand the influence of the signal-to-noise ratio, which is sometimes different for the various polarimetric channels.

- The second relates to the reconstruction of the spectrum of a polarimetric image, using the spectrum of a single polarimetric image acquired at a higher resolution. This reconstruction would allow a polarimetric analysis while maintaining the maximum spatial resolution information.

The latter technique offers opportunities for a variety of applications, including the detection of urban buildings, and for changing detection between a polarimetric image and a High Resolution one. These works are developed in the next chapters.

It is clear that the future spaceborne SAR sensor and system parameters such as resolution, noise level, baseline, cross-talk isolation, revisit time, etc. can be optimized for the data acquisition with polarimetry for each group of applications (forestry, urban, agriculture). There is a need to make a first iteration between the PolInSAR community and the SAR system designers in order to consider the parameter specification in the design of future spaceborne SAR systems, the orbit selection and mission planning. Our recommendation is to promote resolution in polarimetric images for urban applications, and to maintain the swath for forestry

2 CALIBRATION

For polarimetric radar images, calibration is an essential step, to be able to rely on the physical values of intensity and phases that are measured.

The elements of the transmitter and receiver can introduce phase shifts and losses in signals. The attenuation and phase shifts are different for the horizontal and vertical antenna, and are the cause of calibration problems. Calibration consists in measuring these losses and phase shifts induced by the system, in order to eliminate them afterwards in the measured data. The relative calibration in phase and intensity between the two antennas is thus essential to consider working on polarimetric data.

Most polarimetric calibration techniques use signals from known sources, such as trihedral or dihedral corners, or active transponders. These targets are called *reference targets* or *canonical targets*. Consider, for example, the wave

backscattered by a trihedral corner. Its polarimetric signature with the BSA convention is the identity matrix. Practically, given that the antennas do not have exactly the same gains, and since no radar system has ideal characteristics, we do not measure this identity matrix. However, measuring these imbalances between polarimetric channels makes it possible to correct them during calibration. Most methods thus involve placing a number of these reference targets on the scene illuminated by the incident wave. Similarly, in an anechoic chamber, preliminary measurements are performed on calibration targets.

The calibration methods involve distortion matrices to characterize disturbances in emission and reception channels. They can be divided into two classes:

- general methods that make no assumptions about the distortion matrices to characterize disturbances and require three standard targets.
- simplified methods seeking to make the implementation easier, which make some assumptions about the distortion matrices.

We consider any bistatic configuration using two different antennas for transmission and reception. We model all disturbances induced in the transmission antenna by the Sinclair matrix $\mathbf{A}$, and all of the perturbations induced by the antenna reception by $\mathbf{W}$. The response of the target is $\mathbf{S}$.

Uncalibrated measured data mix information about the target and the disturbances induced by the system. The measured matrix $\mathbf{B}_0$ is as follows:

$$\mathbf{B_0} = \mathbf{A}.\mathbf{S}.\mathbf{W} \tag{22}$$

Calibration is aimed at estimating matrices $\mathbf{A}$ and $\mathbf{W}$, in order to finally obtain the matrix $\mathbf{S}$. In anechoic chamber, we can also consider the noise matrix $\mathbf{N}$:

$$\mathbf{B_0} = \mathbf{A}.\mathbf{S}.\mathbf{W} + \mathbf{N} \tag{23}$$

However, this matrix $\mathbf{N}$ is eliminated by subtracting a measurement of the empty chamber. In a SAR image, this matrix is neglected. Calibration thus consists in finding the eight complex coefficients of matrices $\mathbf{A}$ and $\mathbf{W}$. This principle is illustrated in Fig. 17.

There are several techniques to solve this problem. Limitations arise from the use of the canonical targets for all of the previous existing methods. In addition, all of the disadvantages are related to their installation: size, difficulty of deployment, sensitivity to the positioning angle, signal amplitude especially for bistatic settings, and the *a priori* knowledge of their polarimetric matrices. All related limitations can be avoided using the method proposed in the PhD thesis of Nicolas Trouvé, for which a patent has been filed.

If we consider any target, we know none of the three matrices $\mathbf{A}$ $\mathbf{W}$ and $\mathbf{S}$. Unlike previous conventional methods, the idea is not to use a canonical target and therefore the method does not make *a priori* make the matrix $\mathbf{S}$ considered.

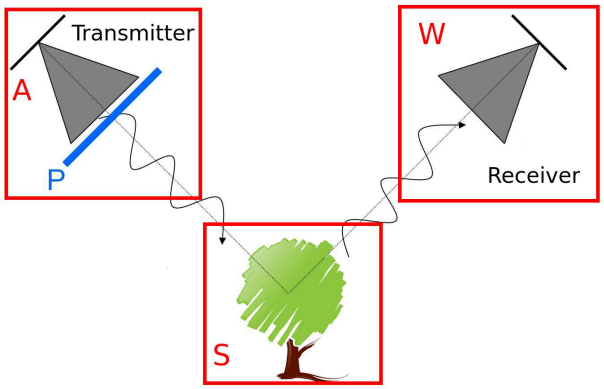

Figure 17: Principle of the new calibration method.

In any case, we will assume that the target matrix **S** is not singular and hence invertible.

We will now add a perturbation to the transmitting antenna. This disturbance **P** will affect the signal, so the final matrix measured is then:

$$\mathbf{B_1} = \mathbf{A}.\mathbf{P}.\mathbf{S}.\mathbf{W} \tag{24}$$

Assumptions about the disturbance are: two distinct and non-zero eigenvalues, and no eigenpolarization parallel to the polarization axes of the transmitting antenna. We suppose also that it is possible to turn the disturbance, in order to change the orientation of the eigenvectors relative to the polarization. Knowledge of the eigenvectors and eigenvalues is not necessary, all of the parameters will be estimated during calibration. The main property used here is the conservation of eigenvalues for similar matrices. This will allow us to find, first, the parameters of the disturbance and, as a second step, the calibration parameters of the antenna. One example of the simplest disturbance is the matrix **P** as follows:

$$\mathbf{P} = \begin{pmatrix} 1 & 0 \\ 0 & \lambda \end{pmatrix} \tag{25}$$

If we use Eq. 22 and 24 we find:

$$\mathbf{B_1}.\mathbf{B_0^{-1}} = \mathbf{A}.\mathbf{P}.\mathbf{S}.\mathbf{W}.\mathbf{W^{-1}}.\mathbf{S^{-1}}.\mathbf{A^{-1}} = \mathbf{A}.\mathbf{P}.\mathbf{A^{-1}} \tag{26}$$

Then we let:

$$\mathbf{C_1} = \mathbf{B_1}.\mathbf{B_0^{-1}} = \mathbf{A}.\mathbf{P}.\mathbf{A^{-1}} \tag{27}$$

$\mathbf{C}_1$ is known and measured twice; **A** is unknown. However, we know that **P** has two non-zeros eigenvalues, because $\mathbf{C}_1$ and **P** are similar, as can be seen from Equation 27. Thus, both matrices have the same eigenvalues.

Suppose that we carry out a rotation of our perturbation around the axis (it is desirable to depart from the limit angles 0 and 90 degrees, for example an angle θ =45 degrees is the best choice). We measure:

$$\mathbf{C_n} = \mathbf{B_n}.\mathbf{B_0^{-1}} = \mathbf{A}.\mathbf{R}(\theta_n).\mathbf{P}.\mathbf{R}(\theta_n)^{-1}.\mathbf{A^{-1}} \tag{28}$$

with

$$\mathbf{R}_\theta = \begin{pmatrix} \cos\theta & -\sin\theta \\ \sin\theta & \cos\theta \end{pmatrix} \tag{29}$$

For more simplicity we let:

$$\mathbf{P_n} = \mathbf{R}_{\theta_n}.\mathbf{P}.\mathbf{R}_{\theta_n}^{-1} \tag{30}$$

And we obtain:

$$\mathbf{C_n} = \mathbf{A}.\mathbf{P_n}.\mathbf{A^{-1}} \tag{31}$$

$\mathbf{A}$ is then the solution of the Sylvester equation:

$$\mathbf{C_n}.\mathbf{X} - \mathbf{X}.\mathbf{P_n} = 0 \tag{32}$$

Our knowledge of $\mathbf{P_n}$ is limited, but we can find the eigenvalues and eigenvectors from equations. Then for each new measurement n we obtain 4 different equations for each measured term, and 3 new unknown variables (λ_1, λ_2 and θ), and 4 common unknown variables for each measurement: the 4 components of $\mathbf{A}$. For each measurement, we add 4 new equations for only three new unknowns and then 4 measurements allow us to find *a priori* $\mathbf{A}$. If we ignore the phase and amplitude absolute value, we can consider that one eigenvalue is equal to one. Thus, two different angles are sufficient to find $\mathbf{A}$.

To summarize, the protocol is to perform:

- A measurement of any non-singular target. It may therefore be the target of interest, or a target of opportunity on the image.
- A measurement of the same target, adding a linear disturbance.
- A measurement of the same target, adding the same linear disturbance affected by a suitable rotation.

In general, the calibration consists in solving a system of 2 (or 4) Sylvester equations. For this resolution, one approach is to vectorize matrices and use Kroenecker products. Thus, the following convention is used:

$$\mathbf{X} = \begin{pmatrix} x_1 & x_2 \\ x_3 & x_4 \end{pmatrix} \qquad vec(\mathbf{X}) = \begin{pmatrix} x_1 \\ x_3 \\ x_2 \\ x_4 \end{pmatrix} \tag{33}$$

and the following properties:

$$vec(\mathbf{AB}) = (\mathbf{B^t} \otimes \mathbf{I})vec(\mathbf{A}) = (\mathbf{I} \otimes \mathbf{A})vec(\mathbf{B}). \tag{34}$$

We then find:

$$vec(\mathbf{C_n}.\mathbf{X} - \mathbf{X}.\mathbf{P_n}) = (\mathbf{I} \otimes \mathbf{C_n} - \mathbf{P_n^t} \otimes \mathbf{I})vec(\mathbf{X}) = 0 \tag{35}$$

We let:

$$\mathbf{H_n} = (\mathbf{I} \otimes \mathbf{C_n} - \mathbf{P_n^t} \otimes \mathbf{I}) \tag{36}$$

Since $\mathbf{A}$ is a solution of the system, by construction, we know that $\mathbf{A} \in Ker(\mathbf{H_n})$ but we know $\mathbf{H}_n$ to within a constant $theta_n$. We cannot ascribe a random value θ_n. However, we know that the system always has a solution. Thus, if we impose:

$$\dim(Ker(\mathbf{H_1}(\theta_1)) \cap Ker(\mathbf{H_2}(\theta_2)) \cap Ker(\mathbf{H_3}(\theta_3)) \cap Ker(\mathbf{H_4}(\theta_4))) \geqslant 1 \tag{37}$$

There is a vector $(\theta_1, \theta_2, \theta_3, \theta_4)$ that fulfills this, we have shown that this vector is unique to within a constant and we have proposed a method to estimate the vector. Given that the matrices and vectors are complex, it is impossible to use the method of least squares as the optical Mueller imaging systems do on Mueller matrices.

The main advantage of the invention proposed here is that during the entire calibration process the target $\mathbf{S}$ does not require to be known. Furthermore, no assumption about the position of the antennas has been made and thus this method works in a bistatic configuration.

In order to validate this approach, an experiment was set up. The proposed disturbance is a filter made in Alkard G produced by the Company Dedienne Multiplasturgie, whose main interest is to present a dielectric permittivity with non-zeros real and imaginary parts and well controlled throughout a certain range of radar frequencies. For a frequency of 10 GHz for example, ϵ= 11.7 +2.06i.

The filter was designed in collaboration with Tatiana Novikova from LPCIM to accurately model the performance of the network and to select the dimensions of slots, in order to achieve a network with two very different eigenvalues. Indeed, solving the resolution of the equation system assumes a simplification by $(\lambda_1 - \lambda_2)$. There will therefore be interest in having two distinct eigenvalues. In addition, the more the eigenvalues are different, the more accurate the numerical solution is. Once the perturbation had been designed, a first experiment was performed using it in the anechoic chamber BABI of ONERA. The filter and the experimental setup are depicted in Fig. 18.

This first experiment has validated the principle of analytical solution of the system proposed for a simple example, i.e., by fixing one of the eigenvalues of the perturbation at one. This is of course acceptable since we are not trying anyway to estimate the absolute phase and intensity anyway. After a measurement was made for the oriented and tilted filter, it was possible to find the angle of rotation, and thus demonstrate the feasibility of the method.

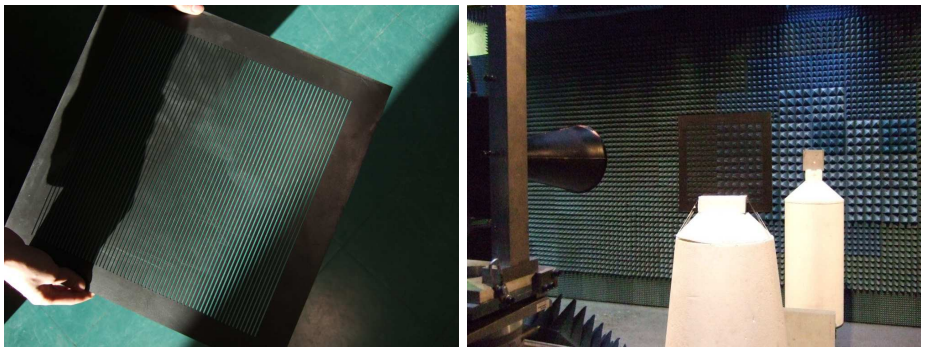

Figure 18: Pictures of the experimental setup to validate the new calibration method principle

3 DATA TRANSMISSION: COMPRESSION

All space-based SAR designs have an inherent limitation in regard to the amount of data that can be acquired. As in the case of range and Doppler ambiguities, the conflict between swath width and along-track resolution reoccurs in the data rate relationship. As the along-track resolution becomes smaller and the swath width growths, the swath width time and interpulse time approache one and time expansion buffering is no longer available to reduce data rates.

Again, the polarimetric channel multiplication is a problem, in regard to the transmission rate technologically feasible. Thus, to reduce data rates, compression techniques are often considered. The compression can be done before the image formation and is then called raw data compression. More recently, we have studied compression algorithms directly on the image itself.

One feature of polarimetric image compression is that it contains complex information. Part of my research concerned radar image compression whose phase is relevant: whether for interferometric or polarimetric techniques. The main conclusion of this study conducted with Gilles Vieillard at Onera has shown that it is preferable to perform the compression separately on the modulus and the phase, as on the real part and imaginary part. The solution that we have suggested consists in a vector quantization bloc compression for the modulus, and a linear quantization for the phase. I also performed other studies which showed that the wavelet compression was effective not only for the quality of the compressed image, but also for the speckle filtering.

The problem of image compression is involved in a more general problem called *big data*. Once the image sizes become large, and the number of temporal images increases, classic treatments become intractable. For this reason, it is necessary to consider alternatives, such as data compression, or segmentation, or speckle filtering for coherence estimation. This compression or segmentation can be made parallel to the treatment. In all cases, it is then necessary to keep in mind that the pretreatments such as compression, in essence, amend the statistical nature of the information contained in the image.

In the following, we present the statistical properties of the data, and all of the developments made on the raw images before any operation.

SUMMARY:

This section has described a number of advances in terms of image formation and associated variable descriptions, as well as technological aspects of the radar design.

- Regarding the formation of SAR images presented in the first chapter, my contribution was mostly conducted in collaboration with researchers at Onera in the DEMR. The related work enabled the understanding of the different approaches to SAR image formation, in order to better address innovative modes, such as circular and bistatic modes.
- The second chapter deals with radar measurable definitions, including polarimetric ones. This section includes the study of polarimetric second parameters. This work quickly led to a spontaneous collaboration with Jaan Praks in University of Helsinki. This collaboration has led to the proposal of alternative parameters to entropy and the alpha parameter. This line of research led me to the proposal of a first thesis on the comparison of polarimetric tools in optics and in radar. This thesis was conducted by Nicolas Trouvé, and directed by Antonello de Martino at LPICM. The optical device was proposed as an alternative to radar bistatic polarimetric measurement. The thesis of Nicolas Trouvé also allowed the theoretical development of bistatic polarimetry, boosting the use of multiplicative polarimetric decompositions. A study was conducted on the influence of the choice of polarimetric bases for bistatic settings and their consequences on the geometry. It led to the recommendation of using a new reference spatial basis for analyzing polarimetric bistatic images.
- The final chapter in this section concerns the radar design. An innovative method of calibration dedicated to polarimetric radars, both for bistatic and monostatic cases was proposed. This method differs from traditional calibration methods in that it does not require the deployment of reference targets on the ground. Also, a study of the technological constraints explains why the polarimetric mode leads to the degradation of the resolution. It is behind the latest proposed thesis, which focuses on the combination of high resolution single polarization images and polarimetric images acquired with degraded resolution. This thesis is being conducted by Flora Weissgerber in partnership with Telecom Paris Tech with the supervision of Nicolas Trouvé and Jean-Marie Nicolas.

Part II

POLARIMETRIC IMAGE PROCESSING

Once an image has been computed through a SAR algorithm, we can perform some operations on it, in order to obtain an enhanced image or to extract some useful information from it. These kinds of operations are part of image processing. Image pre-processing is the technique of enhancing data images prior to computational processing. The goal is to enhance the visual appearance of images and/or to improve the manipulation of datasets. It includes coregistration of several images, appropriate radiometric and geometric corrections and filtering. I begin this chapter by presenting an innovative method for the co-registration of images, which has been proven to be effective even in a challenging context. Then, I present my work on the statistical nature of the images, which is particularly important for the implementation of higher level processing. The features of the highest level, such as classification or detection, are finally addressed in this part.

4

CO-REGISTRATION

1 PROPOSITION OF AN INNOVATIVE METHOD FOR SAR IMAGES

Registration is a fundamental task in image processing used to match two or more images obtained, for example, at different times, from different sensors, or from different viewpoints. The precision required for this registration depends on the application (Li and Bethel, 2008), which may be:

- change detection
- interferometry, either for *Differential Interferometry*, DInSAR with velocity measurements, or for elevation estimations.
- information fusion between images from different sensors.

The methods can be divided into two different categories: spatial methods and frequency domain methods.

- Spatial methods operate in the image domain, matching intensity patterns or features in images. Intensity-based methods compare intensity patterns in images via correlation metrics, while feature-based methods find correspondences between image features such as points, lines, and contours.
- Frequency-domain methods find the transformation parameters while working in the transform domain.

Frequency domain methods work for simple transformations, such as translation, rotation and scaling. Phase correlation is a fast frequency-domain approach to estimate the relative translational offset between two similar images. Applying the phase correlation method to a pair of such images produces a third image which contains a single peak. The location of this peak corresponds to the relative translation between the images. Unlike many spatial domain algorithms, the phase correlation method is robust to noise, occlusions and other defects that are typical of satellite images. Additionally, phase correlation uses the fast Fourier transform to compute the cross-correlation between the two images, generally resulting in large performance gains.

These types of methods are traditionally the ones that are used for radar. Given that the transformation sought is not necessarily a rigid translation all over the image, we compute this method in order to estimate the translation for a grid of points, which is then fitted on a polynomial surface to evaluate the deformation all over the image.

However, these methods remain quite time consuming: it can take several hours for large images. Moreover, the applications encountered become increasingly challenging. This is the case, for example, for:

- close images in non-interferometric conditions, whose deformation between images depends on terrain elevation, and can vary by several pixels over the entire image.
- images with very big temporal decorrelation, for example images at X-band with several years of revisit time. Many geophysical data sets suffer from severe decorrelation problems due to a variety of reasons, making precise coregistration a non trivial task.
- images acquired in different SAR modes (stripmap, spotlight) with different resolutions and speckle patterns.

Part of my research has been devoted to investigating a registration method already developed and used at ONERA-DTIM, but within a different context: an optical flow method applied to stereovision and to real-time video processing applications. This method fits into spatial methods rather than frequency, which means that it takes into account the intensity and not the phase. This operation is also efficient for non-interferometric conditions. EFolki is a special implementation of the initial Folki optical flow (Champagnat, Plyer, Le Besnerais, Leclaire, Davoust, and Le Sant, 2011) on GPU, developed by Aurélien Plyer during his PhD thesis. This variant leads to performances unchallenged by previous techniques in terms of robustness and acceleration of its computation time (Plyer, Le Besnerais, and Champagnat, 2014). By adapting the method parameters such as the size of the search window and the scale level for radar images, subject to speckle noise, the result is more than conclusive:

- The robustness makes the registration method efficient under all conditions encountered. It has been, for example, used for change detection of images of Toulouse under non interferometric conditions, without the use of a Digital Elevation Model to correct the misregistration effects due to the relief.
- The execution time of the code was of the order of one minute, on our 4000x4000 pixel image. Comparatively, another available frequency method took several hours on the same image. Moreover, a GPU implementation of the method exists and would make it faster, less than a second.
- The accuracy of the estimated determined offset is of the order of one twentieth of the pixel. It is sufficient for all of the most demanding applications such as interferometry.

This is yet another example of a response to a problem, found by investigating methods for other application areas, i.e, optical video, analyzing the specifics of the radar in this context (here, speckle and the complex nature of the signals), and making the necessary adjustments to this method to fit these characteristics. This initiated work opens the door to many opportunities, including the application for registration algorithms in more complex situations

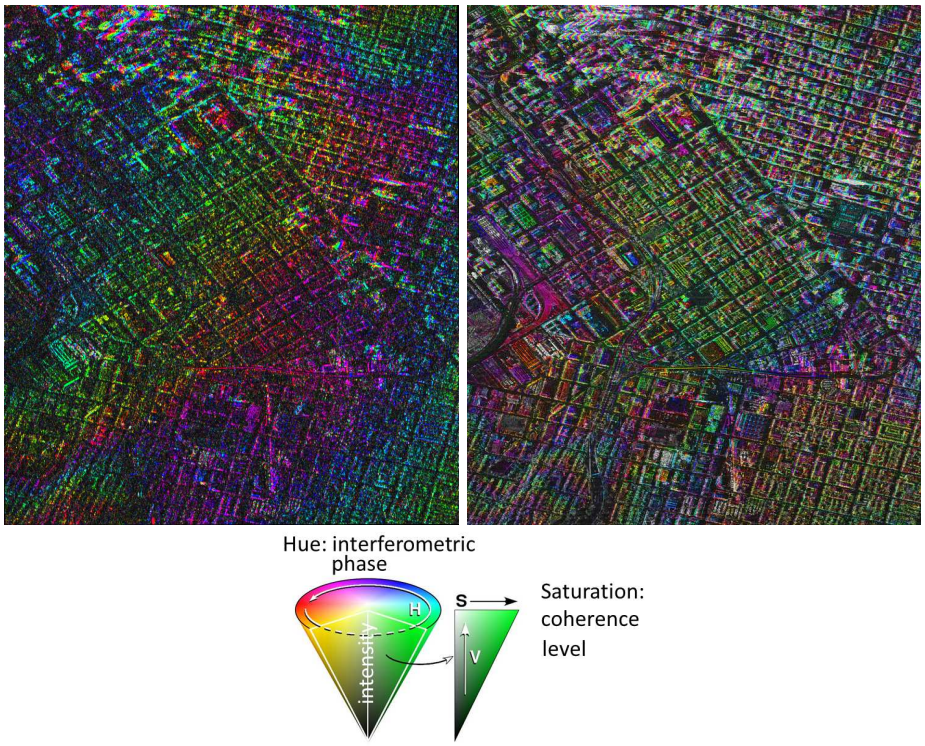

Figure 19: Different interferograms obtained after coregistration by eFolki: on the left, between two polarimetric images with an 11-day temporal baseline, on the right, at a high resolution and with an 11-day temporal baseline

and the feasibility of the joint registration and intended application, for example, change detection.

2 APPLICATION TO INTERFEROMETRY AND CHANGE DETECTION

This coregistration technique has been applied to various images under interferometric conditions. For example, the image in Fig. 19 on the left is the resulting interferogram obtained by combining two low resolution polarimetric images with an 11-day revisit time, whereas the figure on the right is the resulting interferogram obtained by combining two spotlight high resolution images with the same revisit time.

EFolki has also been proven to be effective for images with a long temporal baseline at X-band, in a situation of high temporal decorrelation. A special effort has been focused on the co-registration of data with different resolutions. In Fig.20, two images with two different resolutions and a revisit time of 18 months are combined.

eFolki has also been applied under non-interferometric conditions, still combining different resolutions, but with close incidence, in order to aid in change detection, on images of Toulouse (Weissgerber, **Colin-Koeniguer**, and Janez, 2014).

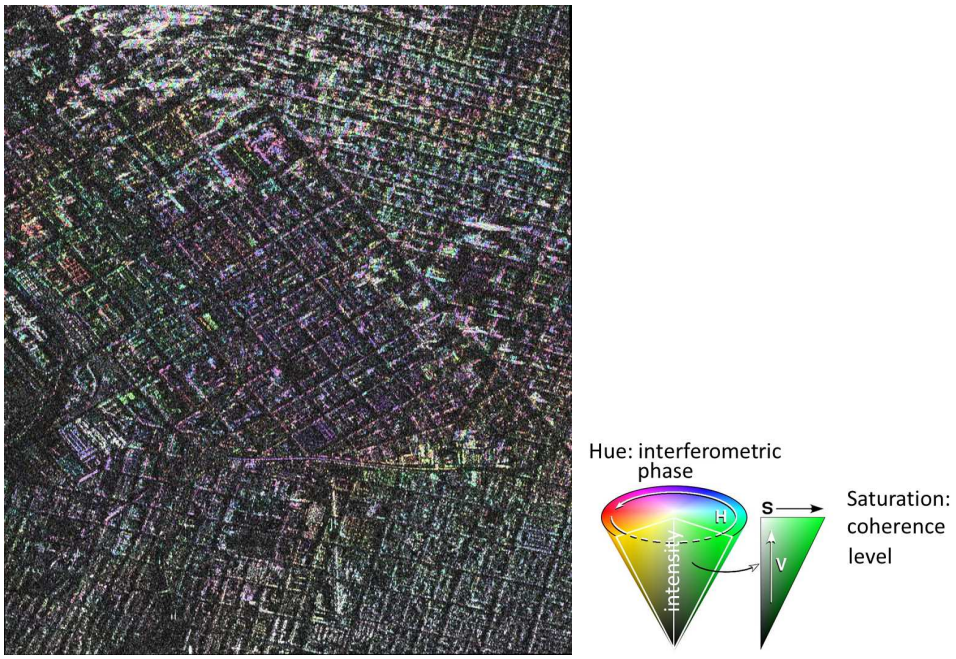

Figure 20: interferograms obtained after coregistration by eFolki, between two different resolutions and radar mode with a 18 month temporal baseline.

More challenging applications include coregistration also between optical and radar images, as is successfully demonstrated in Fig.21, on images of the Deepwater Horizon oil spill, collected in 2010 at an interval of one day. Coregistration is successful using the coast structure. It reveals the displacement of the extent of the spill.

Given these results, the question is: how far can we go in the coregistration of remote sensing images using eFolki?

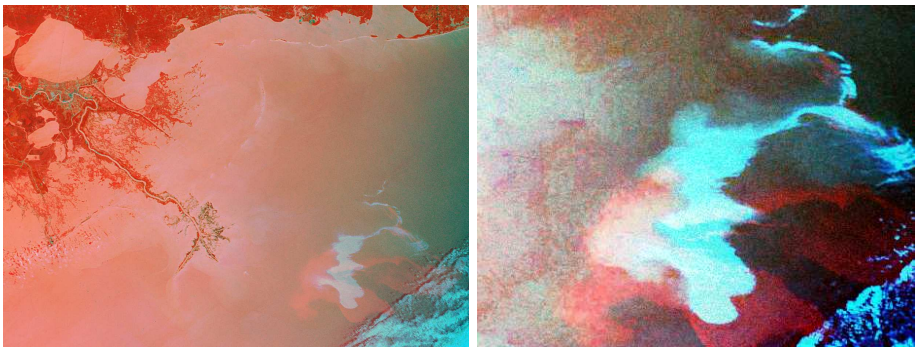

Figure 21: Coregistration between an optical image and a radar image of ENVISAT. Red: radar image, Green and Blue: MERIS optical channels. Zoom on the oil spill is given on the right.

5

STATISTICS MODELLING

Knowing the statistical laws of the measured quantities is essential for many treatments, involving in particular the concepts of estimation and the notion of distance. This is the case for:

- Speckle filtering
- Detection
- Classification or Segmentation
- Coherence estimation

First, I recall the state of the art knowledge on the statistical variables for SAR images, then for polarimetric SAR and PolInSAR images, and I show what theoretical advances were made during my research about the perspectives raised by statistical tool advances.

1 AMPLITUDE AND INTENSITY STATISTICS

1.1 *State of the Art about classical distributions for Intensity and Amplitude*

Goodman developed a speckle modeling in 1975 for a resolution cell containing a large number of scatterers, under the following assumptions:

- the amplitude and phase of the signal transmitted by each scatterer are independent,
- the phase of a scatterer is uniformly distributed between $[-\pi, \pi]$,
- scatterers are independent.

Under these assumptions, it is possible to show that the complex signal received Z, which is the sum of contributions from all scatterers, follows a circular complex Gaussian centered distribution. The real and imaginary parts Z_R and Z_I of this signal follow a standard normal distribution with variance σ^2.

The amplitude follows a Rayleigh-phase Nakagami distribution and a uniform distribution between $[0, 2\pi]$. Finally, the intensity $I = A^2$ signal follows an exponential law.

1.2 *Speckle is not an electronic noise*

Here, care must be taken with regard to the meaning of the word *speckle* for radar, and the definition of what we call noise. Speckle is often considered or

treated as a granular *noise* because it degrades the quality of SAR images and causes difficulties for image interpretation. In that sense, speckle is often regarded as a multiplicative noise. However, speckle is explained by the physics of the measurement. It inherently exists due to the coherent image process, and must not be considered the same as the classic thermal additive noise that affects the measurement.

Thermal noise is the background energy that the radar receiver channel generates and is another additive noise.

In order to obtain the statistical representation of the signal including both speckle and noise influence, a scattering vector $\mathbf{k}$ of an image measured on a multichannel SAR system can be modeled by the following equation:

$$\mathbf{k} = \mathbf{s} + \mathbf{b} = \boldsymbol{\tau} \circ \mathbf{x} + \mathbf{b} \tag{38}$$

where $\circ$ is the Hadamard term-to-term product. The signal $\mathbf{x}$ is the signal backscattered by the target and the vector $\boldsymbol{\tau}$ is called the texture, whereas $\mathbf{b}$ is the thermal noise.

In agreement with the speckle theory modeled by Goodman, $\mathbf{x}$ follows a zero-mean Gaussian circular statistics of covariance matrix $\boldsymbol{\Upsilon}$. Contrariwise, $\boldsymbol{\tau}$ is deterministic and due to the material from which various parts of the scene are made.

The thermal noise $\mathbf{b}$ also follows a zero-mean Gaussian circular statistics of covariance matrix $\boldsymbol{\Gamma}$.

In statistics studies, we must differentiate the statistical influence of the speckle from studies that deal with thermal noise and finally from those that consider clutter as a signal that comes from the scene (for example vegetation, ground) but is not the target of interest.

1.3 *Multilook and mechanism mixture*

Let I_1 I_2 ... I_L be L independent and identically distributed intensity measures. Then, it is already known that the average of these measures follows a gamma law of order L. This result is useful when dealing with multilook data, when intensities are averaged together, to reduce the speckle for example.

However, there is another case where we must consider the summation of different intensity samples: this is the case of layover. The previous Goodman signal model is that of a resolution cell containing a single type of scatterer or electromagnetic mechanism. However, sometimes in resolution cells, there can be an overlap of several different mechanisms. For example, this is the case for roofs of buildings that are projected in the same range resolution cell. During the PhD thesis of Azza Mokadem, the problem of the superposition of several mechanisms of different types within the same resolution cell was discussed. Within this framework, an apparently simple result whose proof is counter-intuitive has been raised: it has been shown that the intensity distribution of an overlap always follows an exponential law, and not a gamma of order 2, which one expects to find in the case of the sum of two exponential laws.

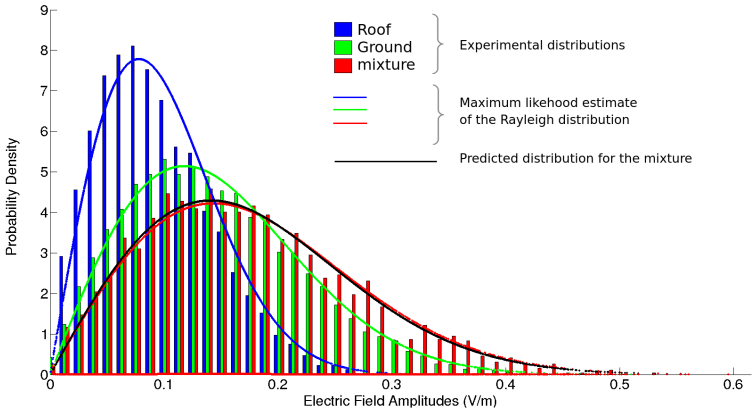

Figure 22: Example of validations of statistical behavior of a layover area.

An experimental validation of this result has been conducted and is represented in Fig.22. This validation also concerns the interferometric coherence modeling.

2 POLARIMETRIC STATISTICS

When dealing with polarimetry, we must describe the law of multivariate data. Taking again the expression of the signal:

$$\mathbf{k} = \mathbf{s} + \mathbf{b} = \boldsymbol{\tau} \circ \mathbf{x} + \mathbf{b} \tag{39}$$

Polarimetric Synthetic Aperture Radar (PolSAR) data are usually modeled by a multivariate circular Gaussian probability density function for $\mathbf{s} = \tau\mathbf{x}$, which is completely determined by the multilook polarimetric covariance matrix that follows a complex Wishart distribution. In this case, texture τ can be considered as a deterministic scalar and $\mathbf{x}$ describes the polarimetric information.

For high resolution textured areas, the Gaussian clutter model may no longer be valid and is commonly replaced by the compound Gaussian model: In this case the clutter is modeled as a product between the square root of a scalar random variable t that corresponds to the texture and an independent complex circular Gaussian random vector.

$$\mathbf{k} = \sqrt{t} \circ \mathbf{x} + \mathbf{b} \tag{40}$$

Many texture models have been studied and applied to classification and segmentation. The Gamma texture distribution leads to the classical K distributed covariance matrix and more recently the Fisher distribution has been studied in Bombrun et al. (2011) and leads to the KummerU distribution. Good results have been demonstrated using a more accurate texture distribution but require a prior knowledge. These distribution parameters also need a large

amount of samples to be estimated, which is not possible at the early stage of a segmentation process, when each segment contains very few pixels.

The SIRV model (*Spherically Invariant Random Vectors*) is based on the same traditional product where $\mathbf{x}$ is an independent complex circular Gaussian random m-vector. The SIRV model includes most texture distributions and does not require estimation of the texture parameters. This model is very convenient for PolSAR segmentation when we need a more accurate result than the Gaussian model, and allows us to use the full resolution available while maintaining reduced computing times (Trouvé, Sangnier, and **Colin-Koeniguer**, 2012).

3 COHERENT SIGNAL STATISTICS

For most advanced applications that use coherent signals whose relative phase is meaningful, we use the complex correlation. Practically, this correlation $C(s_1, s_2) = \gamma e^{i\Phi_{1,2}}$ is defined for two signals s_1 et s_2 by:

$$\tilde{C}(s_1, s_2) = \frac{\sum_{k=1}^{L} s_{1,k} s_{2,k}^*}{\sqrt{[\sum_{k=1}^{L} s_{1,k} s_{1,k}^*][\sum_{k=1}^{L} s_{2,k} s_{2,k}^*]}} = \tilde{\gamma} e^{i\tilde{\phi_{1,2}}} \tag{41}$$

If averaging is not needed, i.e. with $L = 1$, the modulus of this correlation is 1 and the resulting interferometric phase is very noisy.

Without taking into consideration the noise for such signals, and still under the Goodman hypothesis, it is possible to derive the PDF of the estimated coherence modulus $\tilde{\gamma}$ and the estimated phase $\tilde{\phi_{1,2}}$, in terms of L, the number of samples used in the estimation. These expressions reveal that the higher γ is, the more precise the estimation of the phase is. However, the number of samples L has a more important effect than γ on the shape of the phase distribution. The higher L is, the more precise the phase estimation is, even with a low coherence level.

To go further in the statistical analysis of the coherence behavior, including the link between the coherence level and the accuracy of its phase, we need statistical tools that are able to describe complex quantities. Generally, this problem is reduced to the joint statistical study of its real and imaginary parts. These last two terms can be written as the complex variable of its complex conjugate.

In her thesis, Flora Weissgerber addressed the problem in an original way by considering the statistics of coherence in amplitude and phase. For phase statistics, she used the directional statistics.

The signal phase φ is an angular variable defined as modulo 2π. Hence linear statistics cannot be used because any angular φ and $\varphi + 2\pi$ correspond to the same phase. For directional random variables such as the phase, the probability density $P(\phi)$ is defined in (Mardia, 1999) as follows:

- $P(\phi) \geqslant 0$ on $(-\infty .. + \infty)$
- $P(\phi + 2\pi) = P(\phi)$ on $(-\infty .. + \infty)$

- $\int_0^{2\pi} P(\phi)d\phi = 1$

We can define the moment of order p of the probability density by the following formula:

$$\Phi_p = E[e^{jp\phi}] = \int_0^{2\pi} e^{jp\phi} P(\phi)d\phi \tag{42}$$

We can show that $\Phi_0 = 1$. The first moment $\Phi_1 = Re^{i\theta}$ is particularly useful since θ gives the preferred direction of the distribution $P(\varphi)$ and the mean resultant length R gives information about the concentration of the distribution $P(\varphi)$. If the distribution is really narrow and centered around its preferred direction, R will be close to 1. In the case of a less concentrated distribution $P(\varphi)$ or a multimodal distribution, R will decrease. It will be really close to 0 when the distribution is uniform around the circle or bimodal with the two modes separated by π.

By leading different simulations, it has been shown that in the presence of thermal noise, the distribution of the estimated phase is a better way of gathering the information of similarity between the two images as compared to the degree of coherence or the mean resultant length.

Flora Weissgerber investigated R and γ, which yield information regarding the level of cross information of images. They evolve as with the covariance of speckle or the SNR. Both are overestimated when only few samples are used in their empirical estimator. They differ substantially when the SAR images have a strong texture. Indeed, Φ_1 does not take into account the amplitude of the scatterer, whereas the texture has an influence on C computation. It can artificially increase the C value. The estimated phase depends on the relative amplitude of the scatterer. A strong scatterer will impose its phases in the correlation computation to any window that it is part of. Thus the choice between the use of the correlation or first moment will depend on the importance of the texture. If only strong scatterers must be taken into account, the correlation should be used. This can be the case in polarimetry if only the behavior of some target is needed. However, when the response of all scatterers is important, the first moment should be used. This is the case in interferometry when the height of both streets and buildings must be retrieved.

When using these estimators, one must keep in mind that both γ and R qualify the phase distribution that they use for estimation and not the estimated phase distribution. The coherence γ or the mean resultant length R will be high when the pixel-to-pixel phase difference distribution is really narrow. Even for distributions with low γ or R, the distribution of the estimated phase can be narrow. This averaging reduces the phase noise.

In order to estimate the interferometric phase, Flora Weissgerber has proposed a double averaging as a good alternative to obtain a good estimation of the phase difference in the presence of thermal noise. This promising estimation method is illustrated in Fig. 23 and 24 on a simulated image highlighting the effects of resolution. For the double estimation, first a classical spatial estimation is computed and then the circular moments are estimated.

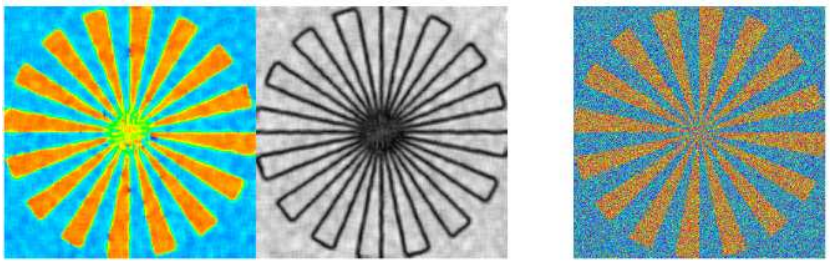

Figure 23: A classical estimation of interferometric coherence in phase and modulus, with an 18x18 window on the left, interferometric coherence without averaging on the right.

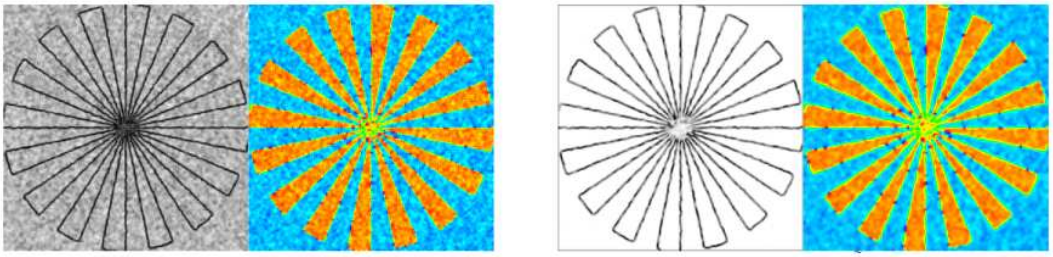

Figure 24: A classical estimation of interferometric coherence in modulus and phase, with a 9x9 window on the left, followed by a circular moment estimation on the right

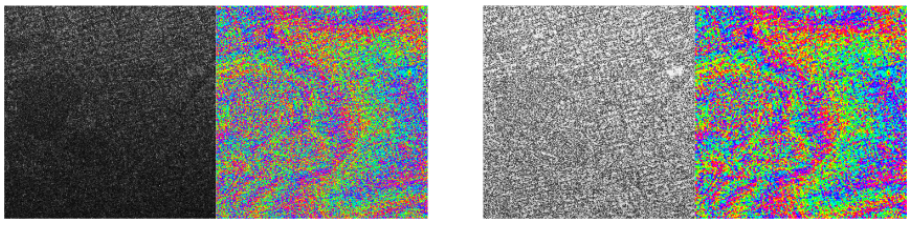

Figure 25: Different kinds of averaging to estimate interferometric coherence, with a 9x9 window on the left, followed by a circular moment estimation on the right

These simulated results prove the efficiency of this averaging: the quality of the phase seems to have improved, the coherence level is better contrasted. Coherence is higher in homogeneous in large areas, and lower in the transitions. The interferometric phase is homogeneous in large areas but takes on median values in the transitions. These simulations are assessed by coherence estimation on real data in Fig. 25. The figure on the right, corresponding to the double estimation, clearly shows an estimation of the phase with lower noise. The corresponding coherence level offers a better contrast and a higher coherence level.

This is on-going work and several parametric studies are still under investigation. In addition, in this thesis several questions are raised about the relationship between some polarimetric parameters and the noise, including:

- How the entropy of depolarization estimation is affected by the noise level.
- What the exact relationship between the quality of a polarimetric phase and the quality of the correlation module is.

6

APPLICATIONS TO SEGMENTATION, DETECTION

The previous sections cover preliminary steps that are essential to be able to then propose processing algorithms, such as segmentation, detection and classification. I present here some of the processing that I have investigated in SAR images, and the potential benefits of polarimetry.

1 SEGMENTATION

Image segmentation is aimed at gathering pixels into regions. Segmentation can have several goals. It may for example separate objects from the background. The segmentation can also be a method of compressing the information: by keeping a value for the segment found. Finally, the segmentation allows a better estimation of the coherence matrices by using pixels belonging to a homogeneous region. In this context it can therefore be seen as a speckle filter.

During his PhD thesis, Nicolas Trouvé proposed a segmentation method for POLSAR images over urban areas (Trouvé and **Colin-Koeniguer**, 2011). For this segmentation, he investigated:

- The definition of a POLSAR statistical distance, adapted to different metrics. For example, using a SIRV based distance, adapted to any kind of texture (Trouvé and **Colin-Koeniguer**, 2010).
- The sensibility of Polarimetric information vs Intensity (SPAN) in these different methods.

While it is the regular choice for most classification and segmentation algorithms, the Wishart distance has multiple issues regarding the impact of the SPAN. If this distance is applied to the non-normalized matrix (dividing by the span) then the polarimetric information becomes negligible compared to the SPAN information. However, on the other hand the SPAN remains a very reliable information, that must be used in the segmentation process.

The main interest of SIRV is that we do not need to know the modeling of the said texture, which can be particularly interesting for very high resolution data. The SIRV coherency estimator is also much better at estimating the boundaries between two areas since there is no "mixed" zone between both. The Fixed Point estimator has been shown to be very robust in the presence of strong singular targets that may have been included in the averaging windows. The SIRV distance is power invariant since the covariance matrices are normalized. SPAN information remains useful to improve segmentation but the Wishart distance used on non-normalized covariance matrices had the major issue of drastically favoring the power information over the polarimetric information.

In order to provide segmentation mostly focused on the polarimetric information, Nicolas Trouvé included the SPAN information but pondered to a level comparable to the polarimetric information.

- Sample Covariance Matrix, even though it is optimal in the Gaussian case is very sensitive to noise pixels (hence the "box" effects even in uniform areas). Spatial variations such as the transition from the top to the bottom area are very noise sensitive: a virtual area is even created by mixed effects from the two areas and is located at the boundary. Singular small targets are blurred, their size is overestimated and their real location is lost.
- SIRV Fixed Point Covariance Matrix is much more accurate for each area, the edges, and the singular target.
- Wishart Segmentation based on the Sample Covariance Matrix suffers from the same side effects, which is not the case for the SIRV distance Segmentation.
- Colors, and hence the covariance matrix, for each segment are much brighter in the SIRV Segmentation, since the Fixed Point Covariance Matrix is unaffected by noise pixels that are included as the segments grow.

Shape parameters are also used to:

- encourage the segmentation of very small pixels once the number of segments have been reduced to 20% of the initial segmentation.
- encourage linear edges according to the maps that highlight them as shown in Fig. 26.

This type of algorithm can be useful:

- Coupled with a classification algorithm, as proposed in (Formont, Trouvé, Ovarlez, Pascal, Vasile, and **Colin-Koeniguer**, 2011).
- For 3D rendering, as presented in (Trouvé and **Colin-Koeniguer**, 2011) and (**Colin-Koeniguer** and Trouvé, 2011). A 3D reconstruction has been obtained over Toulouse (France), using only the PolInSAR data in single pass mode, required for this types of algorithm, and with an adequate ambiguity height. The result will be detailed in the following part.
- For data compression.

2 DETECTION: BUILDING, SUPERSTRUCTURES

Localization of lines and pylons is part of the important information for mapping the territory:

- For communities that need to develop their urban plan or agricultural development.

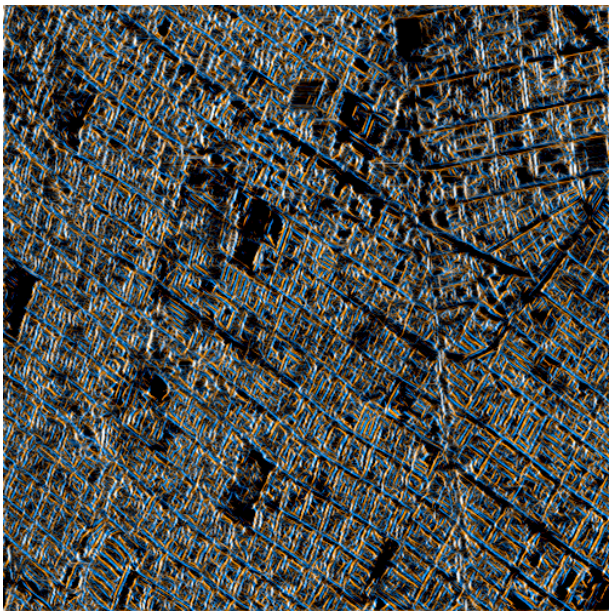

Figure 26: Map used for shape criteria in the segmentation software, emphasizing linear elements of positive contrast in orange, and negative contrast in blue, over a UAVSAR image of San Francisco

- For tourist organizations. A pylon tower is an excellent marker on the map and in the landscape to locate.
- The aeronautical Information Services: identifying obstacles at great heights (including pylons and lines) to regulate air navigation.

Regarding this last point regarding low altitude navigation, electrical cables are in fact a very common source of accidents. Many collision accidents with pylons or cables by helicopters have been identified, making it the highest risk of fatal accident. The most recognized causes are poor pilot vision and poor appreciation of the environment, taking off, landing or during phases of flight at low altitude Goy (2012).

In order to define tools for the automatic detection of superstructures such as pylons, power cables, wind turbines, etc., a phenomenological study was first conducted. It was shown that among the advanced modes, the most reliable to detect such superstructures were interferometric methods, which make it possible both to detect a bright object, and to provide an interesting contrast level with the interferometric coherence.

Polarimetry also allows a more reliable signature of objects such as pylons or wind turbines, in which we invariably find a strong double-bounce mechanism at the structure bottom.

Finally, the intensity spatial signature for such a structure has been shown to be relatively stable for a given structure and given image parameters. For this reason we have developed a method of correlation between pixels of the most significant intensity, with the pixels obtained on a reference image intensity. This method gave the most successful results, analyzed in terms of ROC

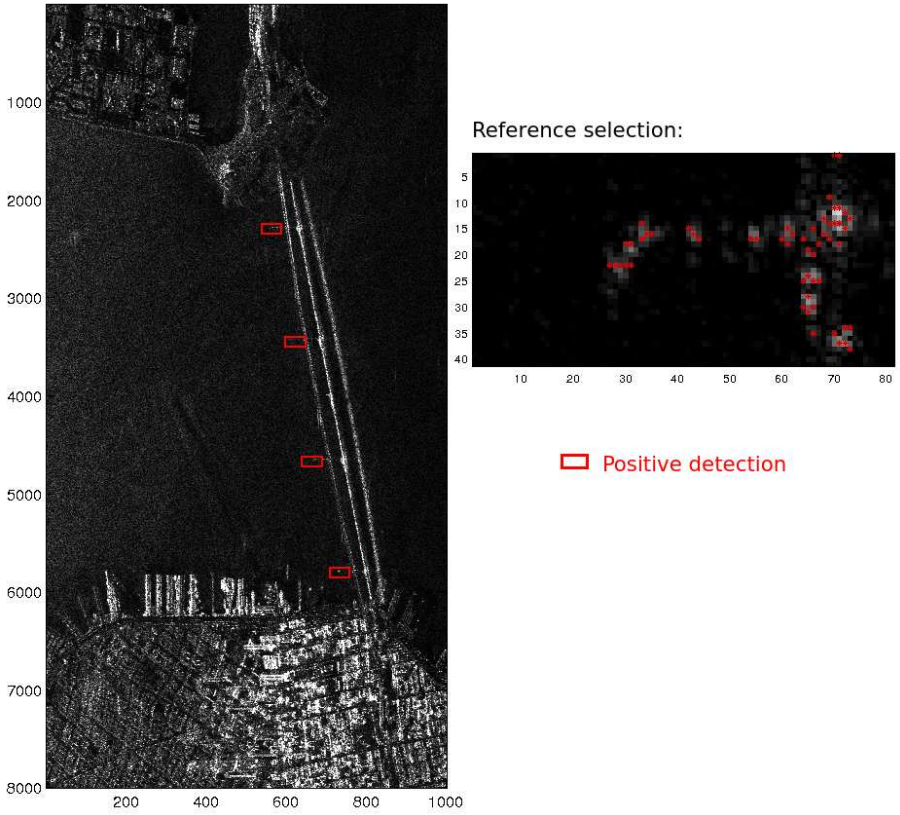

Figure 27: SAR total image on the left, selection of one suspender of the Oakland Bay bridge, and results of the corresponding detection

curves. One example of its efficiency is given by the SAR image of the Oakland Bray Bridge in San Francisco in Fig. 27. We have selected one on the vertical suspenders on the right and determined the spatial distribution of the brightest pixels. The result of a hysteresis threshold on the correlation map is given by the red rectangles in Fig. 27. It gives the good detections of the four vertical suspenders of the bridge exactly.

3 CHANGE DETECTION

In satellite remote sensing, change detection is a functionality of interest for many applications, such as monitoring of urban growth. The objective is to identify and analyze changes in a scene from images acquired on different dates. In this context, radar imaging is emerging as one of the most relevant sensors. In fact, thanks to its ability to observe at any time (day and night), it is an indispensable means of observation in emergency situations when weather conditions are unfavorable for an optical acquisition.

In addition, under some acquisition configurations, it provides very good detection performance, including in complex environments such as in urban areas White (1991).

The most relevant configuration is when the available data is of the same type from the same sensor with the same parameters (incidence, resolution, and frequency).

However, obtaining such data is not always possible in the short term if the revisit time of a single sensor is too large, or if the characteristics (incidence) during its passage are not close enough. In particular, the current situation tends to favor the use of images from different sources (TerrarSAR-X, CSK, RADARSAT, etc.).

Recent works Kempf and Anglberger (2013) showed that change detection can remain effective for different sensors where the resolutions and frequencies differ. It is worth noticing that it concerns the case of low resolution images which means a negligible impact from the differences in the other parameters. However, the resolution of current sensors continues to improve and in this case, the effects of the difference in the other characteristics such as the incidence can greatly complicate the comparison of data, especially in the presence of 3D objects. Therefore, it is necessary to focus on configurations with few or no differences in these features to ensure the detection function. Then, another difficulty always lies in the interpretation of changes detected.

GIven that polarimetric modes that enhance analysis capabilities are nowadays deployed on several satellites, the use of polarimetric analysis to improve the characterization of the change can be considered. However, we have already seen that up to now, polarimetric acquisitions are always done at the expense of a loss in spatial resolution.

Thus, I have been interested in the comparison of images where only the resolution strongly differs, as is the case when the SAR sensors switch in polarimetric mode.

I have investigated several types of data and presented results in (Weissgerber, **Colin-Koeniguer**, and Janez, 2014):

- Satellite images under interferometric conditions: a high resolution SAR image (spotlight mode with a resolution of 1m x 1m and a HH polarization) acquired in October 2011, and a polarimetric SAR image (StripMap mode with a resolution of 2m x 6m) acquired in April 2010, over San Francisco

- Airborne images under non-interferometric conditions: A high resolution SAR image (Stripmap mode with a resolution of 10 cm x 20 cm with a HH polarization) acquired in 2004, and a polarimetric SAR image (StripMap mode with a resolution of 60 cm x 60 cm) acquired in 2005, over Toulouse.

As highlighted in previous works by Kempf and Anglberger (2013), the main difficulty for change detection is to have comparable images. This requires several pre-processing steps. The main difficulty lies in the difference in radiometry. This difference in appearance is due to:

- Differences in radiometric calibration.

- Differences in texture, linked to the difference in resolution.
- Differences in signal-to-noise ratio.

The pre-processing thus consists in bringing the images to a similar geometry and in matching their radiometric levels. This involves the following operations:

- Calculating the images in a common grid and coregistration. We choose to compute the image in the worst resolution of the polarimetric image by selecting the common spectrum portion.
- Making amplitudes and spectra shapes comparable A first step is to adjust the histogram of the high-resolution image on the polarimetric one. At a higher resolution over Toulouse, the differences in radiometry still exist but are less important. Moreover, different spectrum windows have also been applied to the processed data, which must be corrected before their use for a change detection operation: the spotlight HR image is filtered by a Hamming window whereas the polarimetric stripmap mode is not.

Once the pre-processing steps were done, I investigated a new change criteria for detection. Despite pretreatments, it turns out that the comparison of both images is not always perfect. The challenge is to find a criterion that is independent from the changes in texture, and highlights changes in the structure content of the image itself. This is precisely the idea of the Structural Similarity Index: SSIM. This index has been proposed to quantify the quality of an image after a processing operation such as a compression. It may nevertheless be used for change detection Thomas et al. (2012), although this is rarely presented in SAR.

The preprocessing steps previously proposed are essential to improve the efficiency of the change detection process as seen in Fig. 28 about an area with only one change that can be seen in the lower left area.

The last step consists in a hysteresis threshold on the SSIM map. For results that are presented below, the low and high thresholds have been automatically set to $m + \sigma$ and $m + 5\sigma$ respectively where m is the mean of the parameter that is considered, and σ is the standard deviation.

The biggest change that is detected corresponds to a building construction, the City College of San Francisco, constructed between 2009 and 2012. Analysis is possible using the content of the polarimetric information available here before the change. The parameter double-bounce from the Yamaguchi decomposition (Yamaguchi et al., 2006), adapted to the case of urban areas, shows that the observed appearance is an area of bare soil without vegetation or building.

This study has been demonstrated also on airborne images acquired under non-interferometric conditions, over the Toulouse site. Here, the co-registration algorithm previously presented, eFolki, was particularly useful, since it allowed the images to be superimposed with a subpixellic precision, adapting

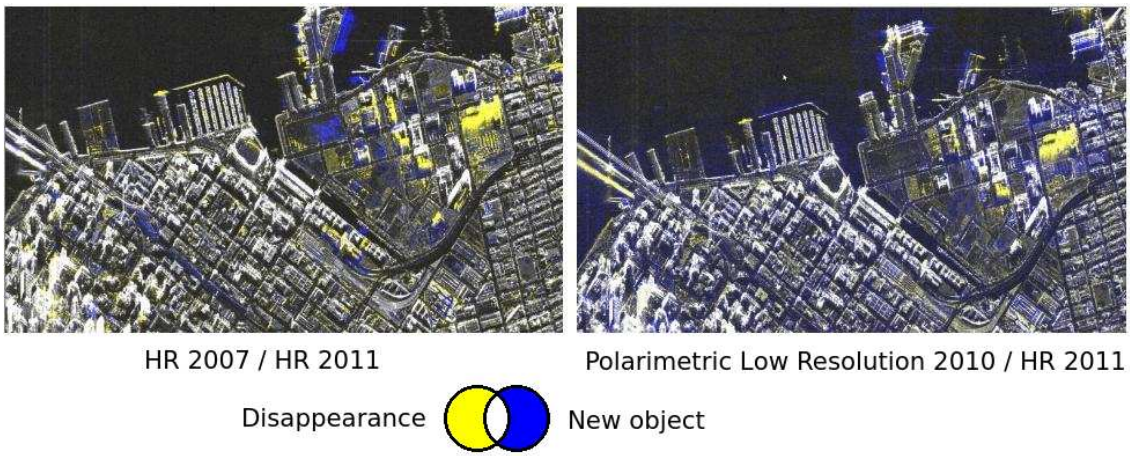

Figure 28: Change detection maps on San Francisco after preprocessing

to terrain elevation. Registration accuracy has allowed the detection of change of car positions. The main changes that have been detected are of three types: one new building, car parks and growth of the trees that are along a canal.

Comparisons between the SSIM and a classical intensity ratio parameter roughly show that:

- SSIM is less sensible to vegetation changes, or homogeneous change in intensity, because SSIM overcomes homogeneous changes of mean intensity or standard deviation. Similarly, the SSIM emphasizes less changes resulting from the presence of the shadow behind the building.
- Both are well able to detect the new presence of the cars on the parking lot.
- Generally, false alarms that appear for both parameters are small. The elastic intensity ratio most often generates false alarms in the low intensity areas, for example, bare soil, while SSIM false alarms appear most often in high intensity pixels, for example some strong echoes of buildings that have not been modified.

The proposed benefit of polarimetry is twofold: polarimetry can help to analyze and characterize detections, and can also be a way of reducing the number of false alarms. For example, false alarms belonging to strong echoes located on the double bounce line can be immediately identified as such: a real change that would be linked to the construction of a building could not give isolated detections. It therefore appears possible to improve the detection performance by eliminating some false alarms through their polarimetric analysis.

4 SPECTRUM RECONSTRUCTION

As we have already seen, the polarimetric mode is often acquired with a degraded resolution. The PhD thesis of Flora Weissgerber concerns the enrichment of a high-resolution image by a polarimetric image with a degraded

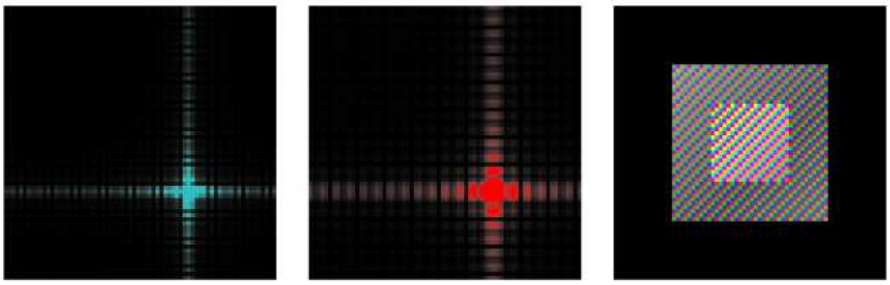

Figure 29: The bright point estimation and complementarity of spectra

spatial resolution. At the beginning of her PhD, Flora Weissgerber designed an algorithm for spectrum reconstruction or resolution enhancement.

She designed a sliding window algorithm that works in two steps:

- In the first step, each sliding window containing N pixels is supposed to contain only one bright point. The ratio of the energy between both windows of the same polarization but different resolutions is estimated using the amplitude ratioof common portions of spectra.

  This estimation is followed by the estimation of the entire polarimetric vector. By inverse Fourier transform, we obtain an estimation of the polarimetric vector for the window, enriched by the high resolution one.

- These estimations are stored until the window has covered the whole image. The mean amplitude and phase values, computed using the circular first moment, are then derived for each pixel.

This algorithm has been tested on an ONERA data set acquired over Toulouse in a full-polarimetric acquisition. In order to obtain a low resolution image and a ground truth, she created a lower resolution image of the given one, using half of the initial resolution spectrum, in range and in azimuth.

The efficiency of the method has been illustrated on an example of two bright scatters that are separated in the HR image but not in the low resolution one. These scatters are separated again in the resulting enriched polarimetric image, as illustrated in Fig.30.

Moreover, the stability of the polarimetric answers has also been checked.

The actual drawback of the algorithm is the polarimetric correlation that appears in clutter. This artifact is due to the initial hypothesis of the algorithm, which considers a one bright point model for each window. The algorithm is being improved by the inclusion of cases where the window contains only clutter, or possibly a segment. This improvement would include the sequential extraction of bright scatters of the image.

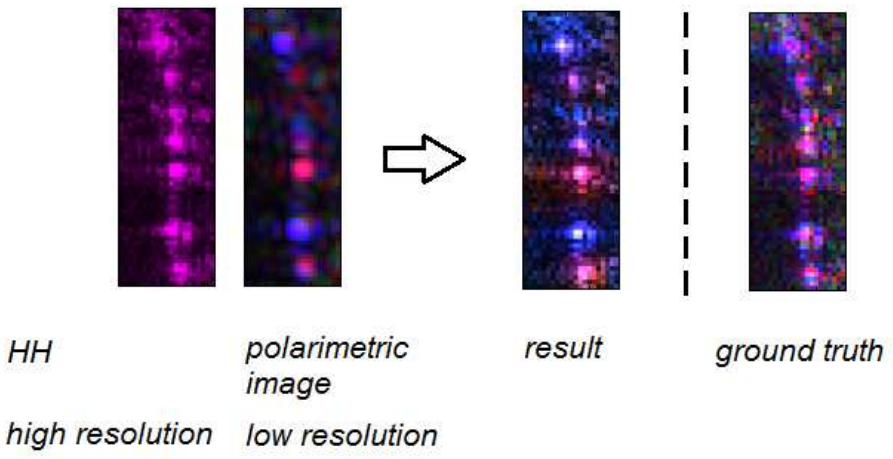

Figure 30: Reconstruction of a polarimetric image using HR image

SUMMARY

This second part concerned all studies relating to the processing of a radar image. Here is a summary of the points that we discussed:

- The first section of this part was about the co-registration of images. The algorithm called eFolki proposed by Aurelien Plyer has been diverted from its original field of work. It was particularly useful for the registration of data under interferometric or non-interferometric conditions and for images in the presence of a very strong temporal decorrelation. Given that it seems very promising when adapted for the radar, this should be the result of future developments for remote sensing imagery and in particular to respond to the issues of big data.
- The following section is focused on the advances made in regard to the statistics of radar signals. It led to three important aspects, developed over three different thesis; respectively those of Nicolas Trouvé, Azza Mokadem and Flora Weissgerber, including:
  - A decline in the use and effectiveness of SIRV to process polarimetric signals, and a study on the matrix distances suitable for polarimetric detection or segmentation.
  - A result concerning coherent addition of radar speckle patterns, different from the addition of speckle patterns in optics: the coherent addition of two speckle patterns following exponential laws always follows an exponential law, instead of a gamma law with shape parameter 2 in optics. New results regarding the statistical behavior of the interferometric coherence are also given.
  - The proposal of circular statistics to address the polarimetric or interferometric phase signals and a study on the relationship between amplitude and phase of a complex statistical correlation.
- Finally, the last section in this part was constituted by works on the detection of targets of interest and change detection. A final application for the enrichment of the spectrum of a polarimetric image using a High Resolution spectrum is being developed by Flora Weissgerber and showed very encouraging results.

Part III

FROM 2D TO 3D

The classic SAR image is projected onto an image plane. However, advanced techniques can provide three-dimensional information: either by the reconstruction of three-dimensional surfaces, or by 3D SAR imaging, i.e a reflectivity map along three spatial axes. In order to obtain a 3D image of the terrain surface, interferometric SAR is typically used. We first try to obtain the same kind of results using only the polarimetric information. Then, polarimetry is considered as a means to improve the result of interferometry. Finally, we discuss how polarimetry can help tomographic SAR, the imaging technique that produces slices of the target at various heights to form a 3D data cube.

7

3D FROM PURE POLARIMETRIC INFORMATION

1 RECONSTITUTION OF A RELIEF BY A POLARIMETRIC IMAGING RADAR

Traditionally, interferometry or formerly radargrammetry techniques have been dedicated to the production of three-dimensional maps. Polarimetry can act as an aid to these techniques. However, as we have already seen, polarimetry is highly dependent on the geometry of the scene, and it can also be investigated alone for the purposes of 3D reconstruction.

In fact, part of my studies have attempted to answer this question: how can we use purely polarimetric information for the volumetric reconstruction of the target?

In the polarimetric vision systems existing for some animals, two main criteria are investigated:

- The depolarization effect, whose orientation can be linked to the polarizing effects in the presence of an oriented flat surface.
- The polarimetric orientation angle.

The orientation angle is well known in polarimetric radar images. Several studies have shown that this angle is related to the azimuth slope of a surface. If the ground is modeled as a set of oriented facets, the polarimetric orientation angle Ψ is related to the azimuthal slope and range slopes according to:

$$\tan\Psi = \frac{-\tan\zeta}{-\sin\theta + \tan\eta\cos\theta} \tag{43}$$

where ζ refers to the azimuthal slope, η to the range slope and θ is the orientation angle, as schematized in Fig.31. However, this data is insufficient to recover both orientations, since there is one relation for two unknowns.

It is possible to compensate for this missing data in several ways:

- Statistically by an iterative method which ensures the continuity of the particular area.
- or with the aid of a flight with a different azimuth, and a clever combination of data from these two flight orientations.

The first solution was successfully performed during my PhD, but for a particular case: it was applied to a P-band image of the dune of Pyla in France, where the slope was considered to not be significant along the azimuth axis, and where the initialization method was particularly facilitated from the horizontal surface of the sea.

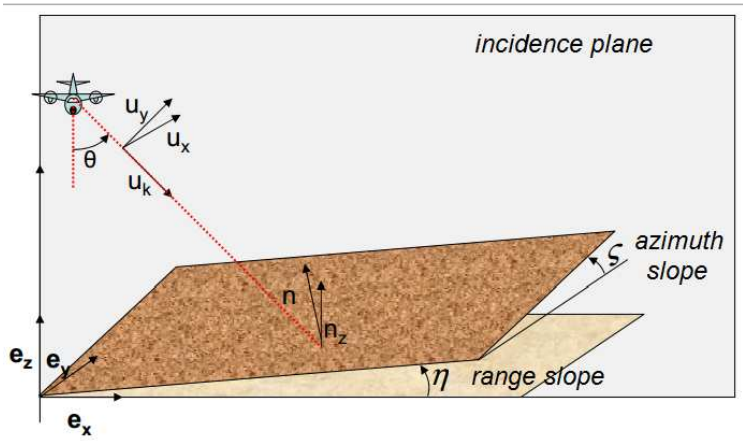

Figure 31: Definition of the orientation of a surface with the radar

Computed on several satellite San Francisco images, the estimate of the orientation angle Ψ was too noisy to be used for direct 3D reconstruction, including at lower frequencies (L-band) where this method is supposed to work best.

In order to study this subject more in depth, I also proposed a method that combines the polarimetric information with that provided by a circular imaging. We saw earlier that the circular imaging alone could theoretically provide a volumetric imaging of the scene. Unfortunately, at X-band in particular, 3D imaging is very difficult if not impossible, due to the fact that scatterers are very anisotropic. The solution that I have proposed to reconstruct the slopes of the terrain from a circular polarimetric image consists in two steps:

- the range directed slopes could be estimated by the look angle which maximizes the response of the ground. The resulting look angle is represented in 32 for a P-band circle SAR image in Sweden. The effectiveness of this estimation has been shown by comparison to ground truth elements.
- Thus, the azimuthal slope could be estimated classically by the polarimetric orientation angles for the trajectory segment whose line of sight is perpendicular to the precedent one. This orientation angle represents a rotation of the antenna about the line-of-sight for which the Sinclair matrix becomes diagonal. Hence this angle is measured in a plane perpendicular to the look-direction.

This solution has unfortunately not had the opportunity to be tested on real data, but could be investigated in a simulation.

2 PROSPECTS FOR 3D NAVIGATION IN OPTICAL POLARIMETRY

In general, issues of 3D space information reminiscent of those that could be used in navigation, for robotics for example.

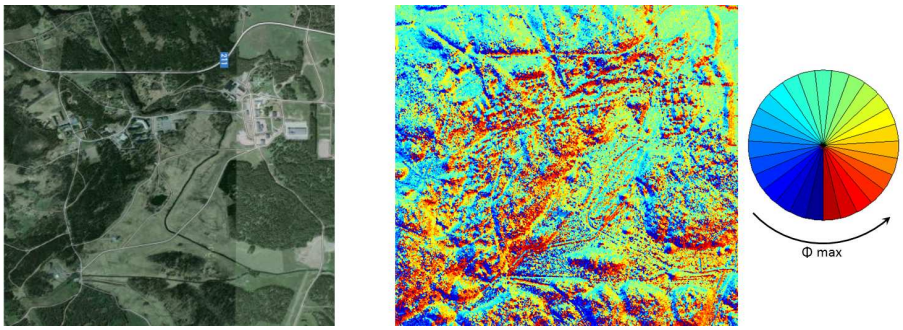

Figure 32: on the right, look angle maximizing the answer on a P-band circle SAR image in Sweden, and on the left the corresponding site

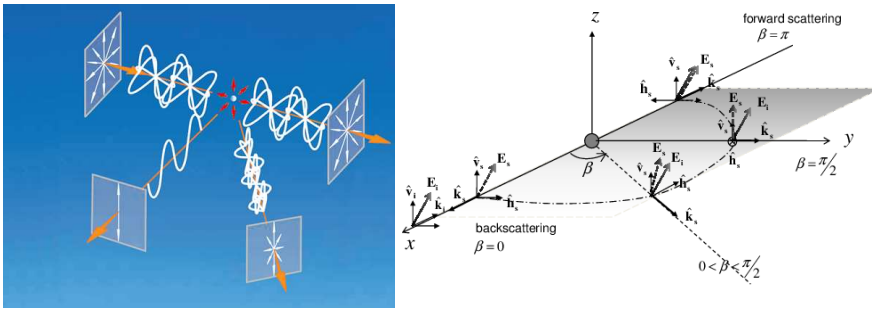

Figure 33: The degree of polarization of light changes with the look angle of the receiver, after diffusion on molecules

Searches can then be guided by the navigation systems that some animals develop using to their polarimetric vision. Polarized light is widely used by some animals, for defense, communications and navigation.

When unpolarized sunlight enters the atmosphere, the air particles cause Rayleigh scattering and the light becomes partially linearly polarized, as is illustrated in Fig.33. The zenith angle of the sun can be estimated from patterns of incident polarization. This analysis of the sky polarization is the navigation technique that honeybees use for orientation.

This change in the polarization degree with the angle of the receiver is the same as in bistatic radar images, as we highlighted in (Trouvé, **Colin-Koeniguer**, Fargette, and De Martino, 2011).

Similarly, the orientation of smooth surfaces such as water surfaces can be detected from the reflection-polarization patterns. Similarly in robotics, these polarimetric techniques could be used to detect surfaces and estimate their positions, whereas other sensors such as stereo-vision cameras fail in the presence of specular returns in particular.

8

3D FROM POLARIMETRIC INTERFEROMETRY

One of the key ideas of PolInSAR data is that it is possible to obtain interferometric coherence from all possible linear combinations of polarization states.

1 DIFFERENT GENERALIZED COHERENCE

Several definitions for this generalized coherence have been successively proposed. In the first one, these linear combinations are described by two vectors called the two generic mechanisms: one for each image of the pair. Using different vectors makes it possible to take into account polarimetric decorrelation between the two scattering mechanisms. The definition of this coherence for the two mechanisms ω_1 and ω_2 is (Cloude and Papathanassiou, 1998):

$$\gamma(\omega_1, \omega_2) = \frac{\omega_1^\dagger T_{12} \omega_2}{\sqrt{\omega_1^\dagger T_{11} \omega_1}\sqrt{\omega_2^\dagger T_{22} \omega_2}} \tag{44}$$

If the same projection vector ω is chosen for both images, the generalized coherence can be written as follows:

$$\gamma = \frac{\omega^\dagger \, \mathbf{T_{12}} \, \omega}{\sqrt{\omega^\dagger \, \mathbf{T_{11}} \, \omega}\sqrt{\omega^\dagger \, \mathbf{T_{22}} \, \omega}}. \tag{45}$$

This generalized coherence is defined using the same polarimetric projection vector for the first and the second antenna. This definition of the coherence set constrained to a unique mechanism is well suited in the case of an interferometric configuration where both antennas as well as the incidence angles are very close. It is even more suitable in a single-pass acquisition since signals are not affected by temporal decorrelation effects.

In practice, matrices $\mathbf{T}_{11}$ and $\mathbf{T}_{22}$ are very similar because they are both coherence matrices of the target viewed under very close incidence angles. Provided that this assumption is valid, the mean average on the denominator is very close to the geometric average. It is then possible to replace the definition of γ by the following:

$$\widetilde{\gamma} = \frac{\omega^\dagger \, \mathbf{T_{12}} \, \omega}{\omega^\dagger \, \mathbf{T} \, \omega}, \tag{46}$$

where matrix $\mathbf{T}$ is defined as $\mathbf{T} = (\mathbf{T_{11}} + \mathbf{T_{22}})/2$. Since the arithmetic mean of non-negative real numbers is greater than or equal to their geometric mean, the modified coherence $|\widetilde{\gamma}|$ is lower than the generalized coherence $|\gamma|$, and

thus always lies between 0 and 1. Moreover, the argument is not modified by this definition change:

$$|\widetilde{\gamma}| \leqslant |\gamma|, \ \arg\gamma = \arg\widetilde{\gamma}. \tag{47}$$

The set of all complex coherences can be plotted in the complex plane. It will be called the *coherence set* and written as $\Gamma(\mathbf{T_{12}}, \mathbf{T})$.

It is mathematically proved in (Flynn et al., 2002) that:

$$\Gamma(\mathbf{T_{12}}, \mathbf{T}) = \Omega(\mathbf{T}^{-\frac{1}{2}}\mathbf{T_{12}}\mathbf{T}^{-\frac{1}{2}}). \tag{48}$$

The set $\Omega(\mathbf{A})$, is also called the *field of values of matrix* $\mathbf{A}$, or *numerical range* of matrix $\mathbf{A}$, and is defined by

$$\Omega(\mathbf{A}) = \left\{\mathbf{x}^\dagger\mathbf{A}\mathbf{x} : \mathbf{x} \in \mathbb{C}^n, \|\mathbf{x}\| = 1\right\} \tag{49}$$

In an attempt to propose a physical interpretation of the linear combination of the generalized coherence, a possibility is to define it as an elliptic state. It is the so-called *polarization subspace method* (PSM) based on finding local maxima of the copolar or crosspolar coherence functions (Pascual et al., 2002). Physically, the mechanisms must be represented as an elliptic polarization transformation. The *polarization state conformation* (PSC) algorithm is very similar: it is based on the knowledge of the polarimetric basis transformation along with the polarization signatures of both interferometric images (Qong, 2005). Finally, we will see in next section that these different definitions can be extended to the multibaseline case, using 3xN complex vectors.

Once the generalized coherence set has been defined, it is possible to model it for different objects of interest: a forest scene, building, bare soil, etc. In the next section I present my contributions to one particular modeling case: the N point scatterer modeling, which is especially useful for deterministic targets.

2 N BRIGHT POINTS WITHOUT INTERACTION

We use the same data model as in the ESPRIT algorithm, but without the thermal noise. This model can be applied for resolution cells containing several point scatterers without taking into account the interactions between scatterers or the volume effects. The signal $\mathbf{k_i}$ acquired by the antenna i in polarization xy consists of a sum of N different elementary scattering contributions or bright points:

$$k_i^{xy} = c_A s_A^{xy} e^{-j4\pi\frac{\rho_{iA}}{\lambda}} + c_B s_B^{xy} e^{-j4\pi\frac{\rho_{iB}}{\lambda}} + \dots \tag{50}$$

c_A is the total power or *span* of point A, ρ_{iA} is the distance between point A and the antenna i, and s_A^{xy} is the complex reflectivity coefficient for polarization xy. Since the span is described by c_A, we can assume that the complex

diffusion vector $\mathbf{s_A} = (s_A^{xx}, s_A^{xy}, s_A^{yy})$ is normalized. All bright points A, B, ... N are in the same resolution cell defined by the first antenna, so that one may assume that $\rho_{1A} = \rho_{1B} = \cdots = \rho_{1N} = \rho$.
Equation 1 can be rewritten in the matrix form:

$$\mathbf{k_1} = \mathbf{Sc}, \quad \mathbf{k_2} = \mathbf{SDc} \tag{51}$$

where $\mathbf{S}$ is a complex $3 \times N$ matrix whose columns contain the normalized polarimetric diffusion vectors for each point, $\mathbf{c}$ is the real column vector of length N containing the span of each point, and $\mathbf{D}$ is the N-diagonal matrix containing the interferometric phases $\Phi_i = 4\pi\frac{\Delta\rho_i}{\lambda}$:

$$\mathbf{D} = \mathrm{diag}(e^{-j\Phi_A} \ldots e^{-j\Phi_M}) \tag{52}$$

The coherence matrices can be computed by means of the matrices $\mathbf{S}$, $\mathbf{D}$ and $\mathbf{c}$ by:

$$\begin{aligned} \mathbf{T}_{12} &= <\mathbf{k_1}\mathbf{k_2}^\dagger> = <\mathbf{Scc}^\dagger\mathbf{D}^*\mathbf{S}^\dagger>, \\ \mathbf{T}_{11} &= <\mathbf{k_1}\mathbf{k_1}^\dagger> = <\mathbf{Scc}^\dagger\mathbf{S}^\dagger>, \\ \mathbf{T}_{22} &= <\mathbf{k_2}\mathbf{k_2}^\dagger> = <\mathbf{SDcc}^\dagger\mathbf{D}^*\mathbf{S}^\dagger> \end{aligned} \tag{53}$$

As shown by (**Colin**, Titin-Schnaider, and Tabbara, 2006b), points having different polarimetric responses represented by a matrix $\mathbf{S}$, will be represented by the mechanisms in the space orthogonal to the space spanned by $\mathbf{S}$, described by the columns of the matrix $\mathbf{M} = \mathbf{S}^{\dagger\,-1}$..

3 OPTIMIZATION

Maximizing coherence means finding polarimetric combinations that maximize the interferometric coherence module. Interferometric coherence optimization can have several goals, as we will develop in the future. More importantly, the optimization methods obviously differ depending on the definition of generalized coherence that we seek to optimize.

During my PhD, I proposed an algorithm to provide a numerical solution for the optimization of coherence defined using a single mechanism, bringing this problem to calculate the numerical radius of a matrix.

Thereafter, I investigated several applications where this optimization could be useful. Coherence optimization is first connected to the following conclusion: in the absence of thermal noise, and under the assumption of Goodman speckle for one type of scatterer, the estimate of the phase coherence is more accurate when the modulus of the coherence is high. Also, the coherence optimization can be envisaged to improve the quality of the phase:

- Either to improve the phase unwrapping algorithms.
- or to improve the estimation of DEM.

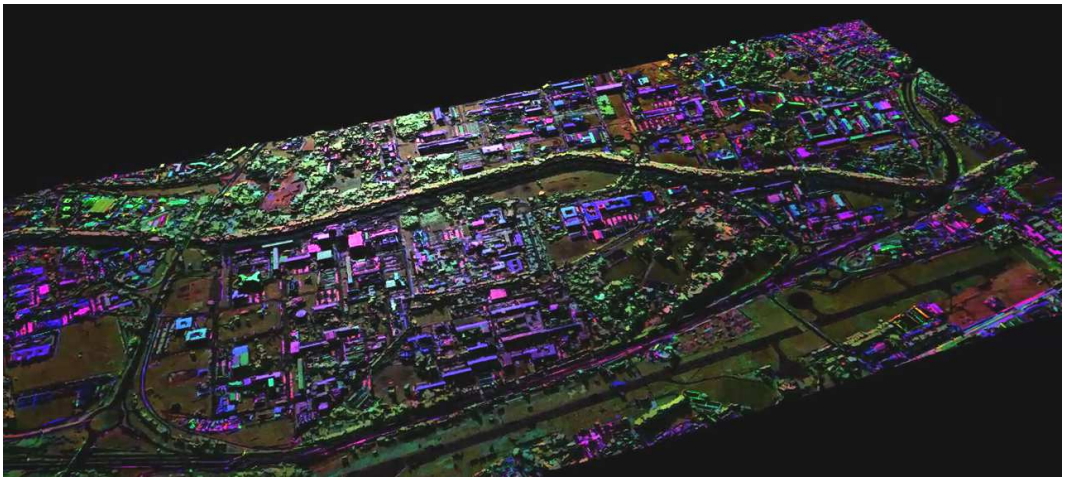

Figure 34: 3D rendering obtained over Toulouse (France), using single pass PolInSAR data acquired by RAMSES (Onera)

As regards the improvement of 3D estimation, the coherence optimization has been interfaced with the segmentation method discussed in Part 2. Results obtained on PolInSAR data acquired by RAMSES (Onera) over Toulouse are shown in Fig. 63. An animation of this reconstruction is given on the web site *http://www.onera.fr/fr/imagedumois/la-ville-en-3d-avec-le-radar*. The precision of estimates was investigated in (**Colin-Koeniguer** and Trouvé, 2014).

However, I have also shown that the coherence optimization can be viewed in various contexts: for example, when using optimized coherence for classification. Several classification algorithms use coherence modules defined in the polarimetric base found by optimization, since they generally offer better contrast than those calculated in the Pauli basis. One parameter has been proposed to see how the coherences of the optimal basis differ (**Colin**, Titin-Schnaider, and Tabbara, 2003). An example of such an application will be shown in the following part.

Finally, in general, the optimization can be used in inversion algorithms based on the modeling of the generalized coherence. This may be the case in the inversion of the Random Volume over Ground model. In particular, I demonstrated in my PhD thesis that under certain assumptions, the extremities of the coherence set determined by proper optimization allowed the separation of different phase scattering centers present in the same resolution cell.

Also, much of my work has involved the study of the geometrical properties of the coherence shape in a particular modeling of the resolution cell, containing a superposition of N mechanisms without interaction. It is the summary of these studies that I present in the next section.

4 GENERALIZED PROPERTIES OF THE COHERENCE SHAPE FOR N BRIGHT POINT MODELING

4.1 *Two mechanisms*

Let us recall the definition of the generalized coherence set for two mechanisms:

$$\gamma(\omega_1, \omega_2) = \frac{\omega_1^\dagger T_{12} \omega_2}{\sqrt{\omega_1^\dagger T_{11} \omega_1}\sqrt{\omega_2^\dagger T_{22} \omega_2}} \tag{54}$$

The results that follow have been proposed in (**Colin**, 2006) Without any mathematical constraint, the coherence set is a disk centered on zero in the complex plane. Indeed, it is invariant by rotation around zero because $\gamma(e^{j\theta}\omega_1, \omega_2) = e^{j\theta}\gamma(\omega_1, \omega_2)$. This means that all interferometric angles can be obtained using a well selected couple of mechanisms.

Let $\mathbf{v_1} = \mathbf{T_{11}^{\frac{1}{2}}}\omega_1$ and $\mathbf{v_2} = \mathbf{T_{22}^{\frac{1}{2}}}\omega_2$. γ is now written as:

$$\gamma(\mathbf{v_1}, \mathbf{v_2}) = \frac{\mathbf{v_1^\dagger T_{11}^{-\frac{1}{2}} T_{12} T_{22}^{-\frac{1}{2}} v_2}}{\|\mathbf{v_1}\|\|\mathbf{v_2}\|} \tag{55}$$

In the case of $\arg(\mathbf{v_1^\dagger v_2}) = 0$, let $\mathbf{u_1} = \frac{1}{\|\mathbf{v_1}\|}\mathbf{v_1}$ and $\mathbf{u_2} = \frac{1}{\|\mathbf{v_2}\|}\mathbf{v_2}$. We still have $\arg(\mathbf{u_1^\dagger u_2}) = 0$, and $q = \mathbf{u_1^\dagger u_2}$ is a real number between 0 and 1. Thus, the 2MC coherence set with the constraint $\arg(\mathbf{v_1^\dagger v_2}) = 0$ is the union of all q-numerical ranges of matrix $\mathbf{A} = \mathbf{T_{11}^{-\frac{1}{2}} T_{12} T_{22}^{-\frac{1}{2}}}$

$$\Gamma = \bigcup_q F_q(\mathbf{A}) \quad q \in [0, 1[$$
$$F_q(\mathbf{A}) = \left\{ \mathbf{u_1^\dagger A u_2}, \|\mathbf{u_1}\| = \|\mathbf{u_2}\| = 1, \mathbf{u_1^\dagger u_2} = q \right\} \tag{56}$$

The q-numerical range of a matrix is a mathematical object whose following properties are already known Li et al. (1994): it is still a compact and convex subset of the complex plane ; the spectrum of $\mathbf{A}$ $\sigma(\mathbf{A})$ satisfies $q\sigma(\mathbf{A}) \subseteq F_q(\mathbf{A})$; F_q is invariant under unitary similarities, and $F_0(\mathbf{A})$ is a disk whose center is at the origin and whose radius is $R_A = \min\{\|\mathbf{A} - \lambda\mathbf{I}\|\}$ where $\|.\|$ denotes the spectral norm. Examples of a q-numerical range for a given matrix are given in Fig. 35.

Once again, and despite the constraint, all interferometric angles can be obtained because $F_0(\mathbf{A})$ lies in Γ. Moreover the boundary $\partial F_q(\mathbf{A})$ is C^1 smooth, which means that the boundary cannot have corners. Thus, the theoretical shape of this set will probably not add useful information regarding the numerical range.

Most generally, the constraint that is most commonly proposed in the literature Cloude and Papathanassiou (1998) to defined the 2 MC coherence is

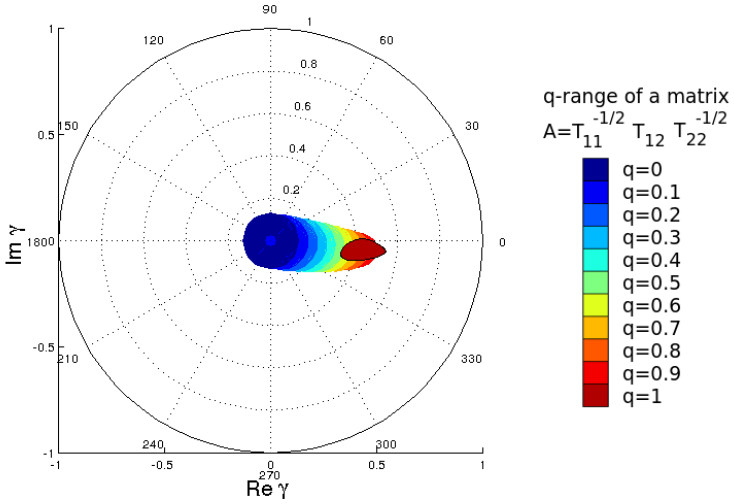

Figure 35: q-numerical ranges of a matrix $\mathbf{A}$

$\arg(\omega_1^\dagger \omega_2) = 0$. This constraint is different from the preceding one. However, it should be noted that the set of $\arg(\gamma(\boldsymbol{\omega_1}, \boldsymbol{\omega_2})$ under the constraint $\arg(\boldsymbol{\omega_1^\dagger \omega_2}) = 0$ is equal to the set of all arguments of $(F_q(\mathbf{T_{12}}))$. Considering $F_0(\mathbf{T_{12}})$, we see that the conclusion about all interferometric angles that can be obtained is still valid.

These conclusions are independent from the type of targets under study or modeling considerations. To our knowledge, they have been drawn for the first time in literature in (**Colin**, 2006).

4.2 *One mechanism, for at least three points, and statistics on amplitudes*

Given that the study of the geometrical properties of generalized coherence seems to not be useful for interferometric height inversion, we now restrict the study to the case of one mechanism.

The first modeling that has been proposed is the case in which statistical variations concern only amplitudes. The following hypotheses are chosen: statistical variables $\mathbf{S}$, $\mathbf{D}$, and $\mathbf{c}$ are independent, and $\mathbf{C} =< \mathbf{cc}^\dagger >$ describes the coherence matrices of the polarimetric powers.

Monostatic configuration: the case of three independent points

The previous mathematical study in (**Colin**, Titin-Schnaider, and Tabbara, 2006b) focuses on the case of a modeling of 3 bright points. It allows the following assertion to be deduced introducing the matrix $\mathbf{A} = \mathbf{T}^{-\frac{1}{2}} \mathbf{T_{12}} \mathbf{T}^{-\frac{1}{2}}$ the local maxima of the numerical range of $\mathbf{A}$ are located on the unit circle and their phases match the interferometric angles of the bright points.

Moreover it is possible to introduce another matrix $\mathbf{B} = \mathbf{T_{11}}^{-\frac{1}{2}} \mathbf{T_{12}} \mathbf{T_{22}}^{-\frac{1}{2}}$. If $\mathbf{C}$ is diagonal, then the numerical range is exactly a triangle whose vertices have phases corresponding to the interferometric angles, as represented in Fig. 36.

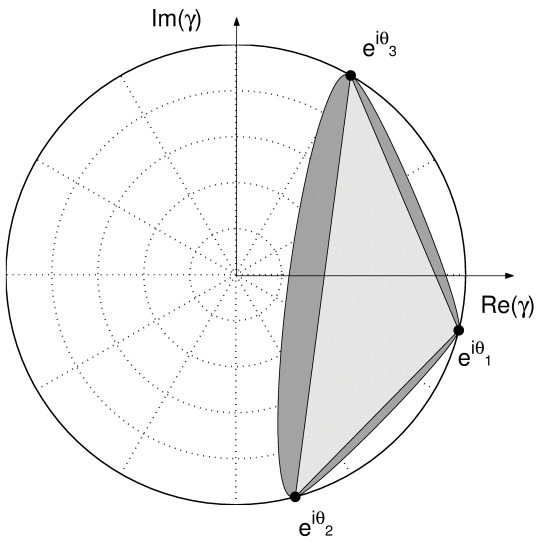

Figure 36: Coherence shape for a model of three types of scatterers

A bias is introduced if non-diagonal elements of **C** are not equal to zero and **S** is not a unitary matrix.

The representation of the coherence set makes it possible to have a mathematical representation of the adequacy of our model. For example, it provides a graphical way to study the consequences of polarimetric changes in the statistical population that is used, or the consequences of additive noise, as shown in Fig. 37.

Moreover, it shows that an optimization procedure is able to separate the different interferometric angles and to retrieve the matrices **S** and **C**. For the thorough treatment of the optimization we refer the reader to (**Colin**, Titin-Schnaider, and Tabbara, 2005b).

Monostatic configuration: the case of four independent points

Here **S** is considered as a 3×4 matrix. We distinguish three sub-cases by the number of points that are orthogonal to the subspace formed by the others. These points will be located on the unit circle.

- No point is orthogonal to the others. It is thus possible in this case to use another property of the numerical field of values, called the *Poncelet property*:

  For any point λ on the unit circle, there is a unique n-gon (polygon with n sides) which circumscribes $\partial W(\mathbf{A})$, is inscribed within the unit circle and has λ as a vertex.

  If $\mathbf{A} \in S_n$ then its numerical range has the n-Poncelet property Gau and Wu (2003). $\mathbf{A} \in S_n$ if and only if **A** is a contraction, it has no eigenvalue of

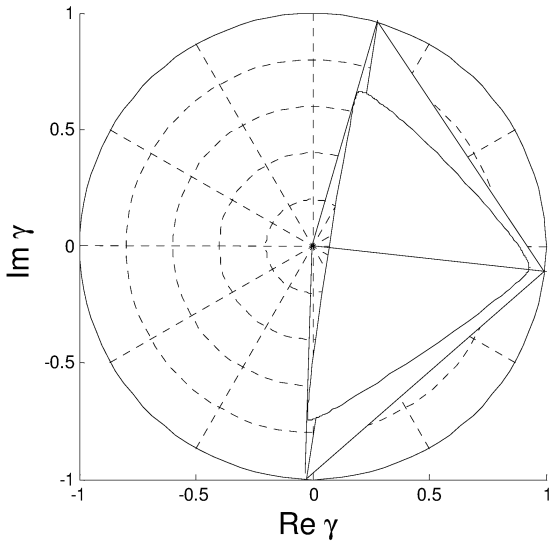

Figure 37: Coherence shape with and without statistical variations on **S**, the polarimetric returns

modulus 1, and $rank(\mathbf{I} - \mathbf{A}\mathbf{A}^{\dagger})^{\frac{1}{2}} = 1$. We can prove that this last property is true if **C** is diagonal (no correlation between polarimetric channels). As a consequence of this property, the numerical range of **A** is inscribed in a quadrilateral whose vertices are exactly on the unit circle, as in the example given in Fig.38.

- one bright point is on the unit circle. Let $\mathbf{s}_1$ be the polarimetric diffusion vector that is orthogonal to the space spanned by the others. We can express all matrices in the basis $(vect(s_1), vect(s_1)^{\perp})$. Matrix **A** will be

$$\mathbf{A} = \begin{bmatrix} \begin{pmatrix} \lambda_1^* & 0 & 0 \\ 0 & & \\ 0 & & \mathbf{A}' \end{pmatrix} \end{bmatrix}, \lambda_1 = e^{-j\Phi_1} \tag{57}$$

  The numerical range of this matrix is the convex hull of an ellipse and the point λ_1. Moreover, the submatrix $\mathbf{A}'$ has the same properties as the matrix **A** ; this means that if **C** is a diagonal matrix, the ellipse will be inscribed in a triangle whose vertices are on the unit circle, as in the representation given in Fig.39.

- If two bright points are on the unit circle, this means that the two last points cannot be independent. It is thus equivalent to the case of three independent points, whose last one has a modulus lower than 1.

In the case of bistatic measurements, we can transfer the above analysis back to 4×4 matrices. The optimization procedure will be able to separate up to

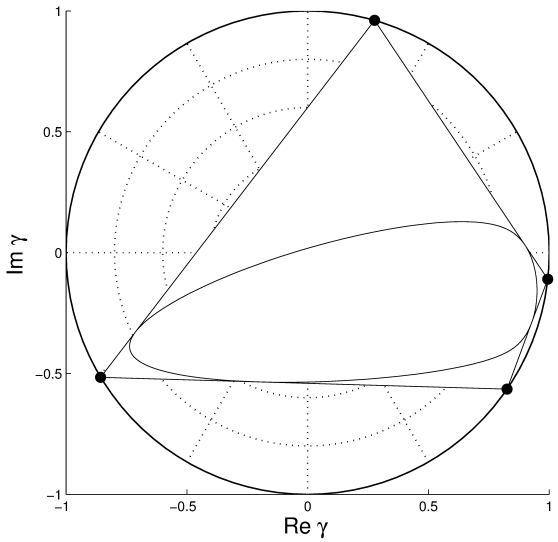

Figure 38: Coherence shapes for a 4 point scatterer mixing model

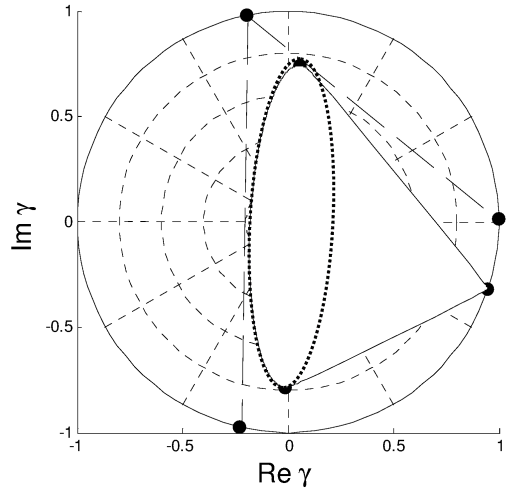

Figure 39: Coherence shapes for a 4 point scatterer mixing model

four independent points, and the Poncelet property can be extended to the case of five independent points.

4.3 *for N<3 points using one mechanism and general noise statistics*

The previous modeling is not satisfactory to simulate resolution cells containing 1 to 2 types of scatterers, or to study the impact of polarimetric decorrelations regardless of power fluctuations. For this reason, we have also considered alternatives to be able to simulate the important cases of the one and two scatterer type.

for one single point

Let us first consider that the statistical population observed concerns only one physical type of targets, denoted by A. This is the case for bare soil. When only one type of bright point exists in the resolution cell, then the polarimetric scattering vector samples are simply written as:

$$\mathbf{k}_1^i = c_A^i \mathbf{s}_\mathbf{A}^i = \mathbf{x}_\mathbf{A}^i, \quad \mathbf{k}_2^j = e^{-j\Phi_A^j} c_A^j \mathbf{s}_\mathbf{A}^j = e^{-j\Phi_A^j} \mathbf{x}_\mathbf{A}^j, \tag{58}$$

where $\mathbf{k}_1^i$ is one sample of scattering vector of the first image population, and $\mathbf{k}_2^j$ is the corresponding sample of the scattering vector of the same population in the second image. In order to account for statistical fluctuation, we can simply assume that:

- vectors $\mathbf{x}_\mathbf{A}^i = c_A^i \mathbf{s}_\mathbf{A}^i$ and $\mathbf{x}_\mathbf{A}^j = c_A^j \mathbf{s}_\mathbf{A}^j$ are two samples of the same population of vector $\mathbf{x}_A$, classically described by the probability density function of a circular Gaussian vector with a zero mean Lee et al. (1994a), Lee et al. (1994b).
- the statistical distribution of the interferometric angle follows a normal distribution. In reality the theoretical distribution for the interferometric phase deduced from a Gaussian speckle pattern is more complicated but it has already been shown that the Gaussian distribution is a good approximation.

Once these variables have been generated, we are able to reconstruct sets of polarimetric scattering vectors $\mathbf{k}_1$ and $\mathbf{k}_2$ and create associated coherence matrices. As an example, three different coherence sets are represented in Fig. 40. They have been generated using different coherence Wishart matrices $\mathbf{M}_A = < \mathbf{x}_A \mathbf{x}_A^\dagger >$. This shows that this simple model allows us to describe coherence sets representing various cases that we encounter in practice on an image.

for N=2 points

Due to the presence of overlays, we can find several cells on urban images that can contain two different types of bright scatterers, with different polarimetric

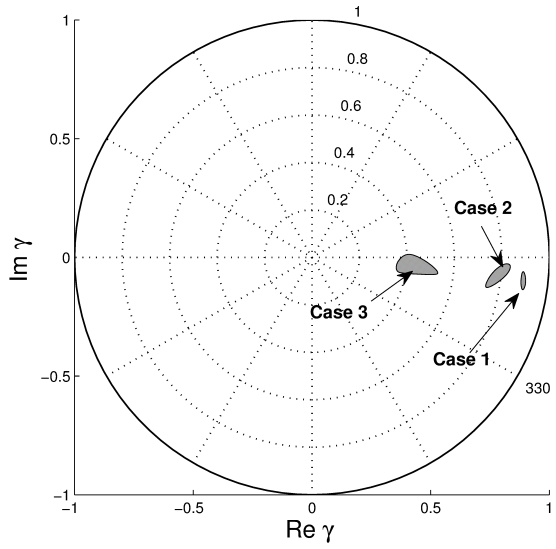

Figure 40: Coherence shapes for a 1 point scatterer model

behaviors and different elevations. The most frequent cases are superposition of the ground and diffraction by the roof, the ground and the scattering by the roof, or the strong double bounce echo and the scattering by the roof.

Now the mathematical modeling of the statistical population becomes:

$$\mathbf{k}_1^i = \begin{bmatrix} \mathbf{s}_A^i & \mathbf{s}_B^i \end{bmatrix} \cdot \begin{bmatrix} c_A^i \\ c_B^i \end{bmatrix}, \tag{59}$$

$$\mathbf{k}_2^j = \begin{bmatrix} \mathbf{s}_A^j & \mathbf{s}_B^j \end{bmatrix} \cdot \begin{bmatrix} e^{-j\phi_A^j} & 0 \\ 0 & e^{-j\phi_B^j} \end{bmatrix} \cdot \begin{bmatrix} c_A^j \\ c_B^j \end{bmatrix}. \tag{60}$$

Given that it seems difficult to envisage the polarimetric statistical fluctuation independently from the total power fluctuation, we can consider here that c_A and c_B are just deterministic parameters quantifying the mixture of two types of scatterers A and B. Thus, they can be viewed as a proportion rather than amplitude, and replaced by p and $1-p$, where $0 < p < 1$, and the model becomes:

$$\mathbf{k}_1^i = p\mathbf{s}_A^i + (1-p)\mathbf{s}_B^i \tag{61}$$

$$\mathbf{k}_2^j = p\mathbf{s}_A^j e^{-j\phi_A^j} + (1-p)\mathbf{s}_B^j e^{-j\phi_B^j} \tag{62}$$

We can still also assume the same distribution for the interferometric phase as in the previous section. Now we just need to define two statistical laws for the distribution of $\mathbf{s}_A$ and $\mathbf{s}_B$ vectors, using two covariance matrices

$$\mathbf{M}_A = < \mathbf{s_A} \mathbf{s_A}^\dagger > \text{ and } \mathbf{M}_B = < \mathbf{s_B} \mathbf{s_B}^\dagger > . \tag{63}$$

Once this modeling has been assumed, it is possible to see that the corresponding coherence shape looks like an ellipse.

Different cases of similarity between $\mathbf{M}_A$ and $\mathbf{M}_B$ can be considered. It is possible to see that the more similar $\mathbf{M}_A$ is to $\mathbf{M}_B$, the less we describe the angular diversity.

To conclude with this section, we have shown empirically that:

- A good way to model coherence shapes is to separately model the statistical laws of the various matrices or vectors used to parameterize our model: interferometric phase, polarimetric coherence matrices and deterministic relative powers.
- Statistical fluctuations on the power only allow the interest of maximizing coherence to be understood, but cannot account for the actual shapes nor model cell resolution containing one or two mechanisms only.
- The coherence shape corresponding to a two-mechanism resolution cell looks like an ellipse whose major axis is parallel to the segment joining the two interferometric phases of the mixture. This result has been used in (Cellier and **Colin**, 2006). In the case where fluctuations in phase are not too large, then the major axis of the ellipse intersects the unit circle on the two interferometric phases involved in the mixture.

Recent studies Cui et al. (2015) make use of this knowledge on coherence shapes. They show that research in this field for POLINSAR applications is still active. These theoretical results are also put to use in an inversion algorithm for building heights, presented in the last part.

9

TOMOGRAPHY

The basic idea of three dimensional imaging algorithms is to form a second synthetic aperture in the direction of the translational movement. This direction, denoted as the normal direction , is perpendicular to the range and azimuth directions. This situation is achieved in the dual domain, by obtaining several slices of the reflectivity spectrum. For the case of airborne SAR, there are especially two kinds of acquisition that make it possible to obtain three dimensional images: the first one is the circular flight path, and the second one is the multibaseline flight path. The second one corresponds to the "tomographic SAR" and is the subject of this section.

The generalization of multibaseline interferometry is the tomography approach, which allows a resolution in the third direction. The resolution in the elevation direction depends on the elevation aperture size, i.e., on the spread of orbit tracks. Tomography or multibaseline Interferometry can be used for layover scatterer elevation separation, to locate different scatterers interfering in the same pixel.

3-D SAR focusing using tomographic processing of multibaseline interferometric data sets, may be considered as a spectral estimation problem. A wide variety of spectral analysis techniques can be used to perform tomography, ranging from classical Fourier-based methods to High-Resolution (HR) approaches.

At the stage of the technique, polarimetry has been investigated only as information *a posteriori* to compare the tomography obtained in the various polarization cases, or to analyze the data after 3D mapping. In this case, a fully polarimetric dual- baseline configuration improves the tomographic accuracy significantly, compared with single-polarization ones, in cases where the estimation in one single polarization is not the most adapted one. Polarimetry also provides additional information, related to scattering mechanisms, which helps building features, such as geometrical shapes, as well as dielectric properties, etc. to be better characterized.

However, polarimetry can also be used in a multibaseline optimization procedure Neumann et al. (2008). Comparisons between the various optimization algorithms are treated as an extension of the studies proposed in the single baseline case.

I followed these developments. Although today tomography is a line research that I have not had time to get involved in, I think that it is a topic of interest that should be considered. Today, the contribution of polarimetry to tomography usually comes after tomographic treatment itself, mainly for analysis purposes. I would advocate a tomography study in urban areas, in relation to any multipath that changes the associated interferometric phases, and which could be detected at the early stage of treatment, using polarimetry.

SUMMARY

This third part has presented the main benefits of polarimetry for tridimensional aspects. It is based on the more in depth knowledge of PolInSAR acquired during my PhD thesis. This work has reinforced my expertise in this field.

- The first section contains more research ideas for the future than actual results. In particular, it offers perspectives on the use of polarimetry for navigation, and more generally on the orientation of surfaces.
- The second part deals with the modeling and mathematical properties of coherence shapes in PolInSAR, particularly for urban areas. From these properties, height inversion algorithms can be proposed.
- The last section opens up opportunities for subsidence and tomography studies.

Part IV

INVERSE PROBLEMS IN POLARIMETRIC IMAGES: FOREST AND URBAN

An inverse problem in remote sensing is aimed at converting observed measurements into information about the physical scene. Inverse problems deal with governing equations that relate the model parameters to the observed data. For radar images, it is related to inverse scattering and involves scattering simulation tools. This last part presents my contribution to research in this field, applied to forest scenes and urban areas.

10

THE USE OF ELECTROMAGNETIC TOOLS FOR INVERSION

SAR data are potentially helpful for a wide variety of human activities, ranging from agriculture to rural and urban planning, disaster monitoring and assessment. However, practical use of these data is often limited by the lack of efficient, possibly unsupervised, tools for the retrieving of effective information. Then, analyzing, interpreting and anticipating SAR images requires support of appropriate electromagnetic modeling.

1 DIFFERENT TYPES OF SCATTERING MODELS. HOW TO CHOOSE ONE?

Modeling takes into consideration the radar geometry and the scene description. The choice of the types of algorithms to solve Maxwell equations and the way of describing the scene are the two important steps to define a simulation tool.

Let us detail the choices concerning the description of the scene. For example, concerning the way of describing forests, trees can be described as cylinders for the trunks and branches. However, it raises the question of how to distribute these cylinders. It can be either fractal, using realistic models of biological growth, or more randomly with statistical distributions. In reality, a model that seems realistic for a given application, for example biological growth, will not necessarily be the most appropriate for another application: the scattering of the electromagnetic wave. In other cases, some simplifying choices for scene description can be justified under certain assumptions that must be assessed. For example, a square base cylinder observed by a radar gives a mesh that can improve efficiency significantly for exact modeling computation in respect to the circular one, and is still representative for trunks when they are observed at very low frequency, as demonstrated in (**Colin-Koeniguer** and Thirion-Lefevre, 2010). A fractal distribution is not more effective than a uniform distribution, as has been pointed out by several studies in monostatic configurations, and as has been confirmed in (Thirion, **Colin**, and Dahon, 2006). We have extended this conclusion to the bistatic case in (Everaere, **Colin-Koeniguer**, Thirion Lefevre, and De Martino, 2012). In all cases, it is necessary to control the domain of validity of the approximations that are made in regard to the description of the scene, and to find the best compromise between the simplicity of the calculations and the validity for the application and configuration studied.

Let us now discuss the choices of algorithms to solve Maxwell equations. Simulation models must be sufficiently detailed to ensure high accuracy, but not so detailed as to preclude a numerical solution on real-world computers. Of course, the exact models take into account all scattering mechanisms, but

their computational complexity restricts their application to simple and small scenes.

Furthermore, it is important to determine the type of model outputs: should it be a description of a the complex electric fields, a description of their temporal or frequency variation, or the synthesized SAR image?

2 A WAY OF INVESTIGATING: CROSS UNDERSTANDING AND VALIDATION

Generally, models are supposed to respond to a lack of real data in order to anticipate and predict the performance of post-processing algorithms. Meanwhile, models help to understand the underlying phenomenology in the signal. For example, they allow the different mechanisms present in resolution cells containing vegetation to be distinguished. However, the models themselves involve choices of different types:

- The way to describe the scene (a 3D triangular mesh model, or canonical elements such as cylinders).
- The way to describe materials.
- The way to describe how the sensor and the scene interact: raytrace, or rasterization.
- The type of physical approximations made, neglecting certain mechanisms when beyond the scope of exact modeling, since we want to improve the computation time.

Therefore, how justified are these approximations *a priori*? It is often a vicious circle, because simulators can help us to understand what phenomena are important to take into account. In order to answer to this apparent contradiction, Laetitia Thirion Lefevre from SONDRA and myself have developed a research line using a modeling approach that simultaneously leads to the physical understanding and the validation of the model. This approach appears in several applications such as forest (**Colin**, Thirion, Titin-Schnaider, and Tabbara, 2004a), (Thirion-Lefevre and **Colin-Koeniguer**, 2008) and urban areas.

For the forest for example, we know that the exact models are constrained by the extent of the scene that they are able to simulate. Also, we used a coherent scattering modeling (COSMO) of vegetation developed by Laetitia Thirion Lefevre during her PhD thesis. This simulation tool describes the forest by means of a set of dielectric cylinders organized in several layers above a rough dielectric ground, representative of trunks and branches. For each cylinder it computes the direct scattering, the double-bounces implying the ground, and the triple bounce. It also takes into account the attenuation effects. However, this is an approximate tool that neglects the direct contribution of the ground, and neglects the multiple interactions between cylinders. This type of model has allowed us to go further in our understanding of the scattering by a forest than the more simplified models, such as that called Random Volume over Ground. In particular, it meks it possible to understand that:

- Most false alarms in forests are due to strong double bounce echoes between the trunks and the ground (Thirion and **Colin**, 2005).
- At P-band, the Random Volume over Ground model is insufficient to represent the influence of the layer of trunks. Also, the RVoG model was extended to an additional layer of trunks and associated FOPEN detection methods were developed (**Colin**, Cantalloube, and Dupuis, 2006a).
- The COSMO model allowed us to deduce the relationship between the height of the phase center of a forest measured by an interferometric radar, the attenuation coefficient, and the total height (Thirion-Lefevre and **Colin-Koeniguer**, 2007).
- In bistatic polarimetry, it has been shown that the contribution of trunks was predominant in the backscattering configuration, while the branches contributed mostly via simple diffusion in the specular direction.
- This type of model has also allowed us to understand that horizontal polarization is favored in the double bounce mechanism, because of the asymmetry of the Fresnel coefficients on the ground. Meanwhile, successive validations of the code were made from measurements in an anechoic chamber, first on an isolated cylinder, then on a group of up to six cylinders. As often as possible, comparisons were made between simulation results and actual SAR measurements.

Concerning urban areas, the collaboration continued between electromagnetic modeling and intended application, including target detection from multipath. This collaboration has been extended by the joint supervision of the PhD thesis of Azza Mokadem. In this thesis, the idea was to achieve the state of the art on all of the types of simulators that can be used, in order to choose the best one able to give us a way of:

- better understanding the mechanisms in this type of environment,
- anticipating configurations suitable for detection,
- both justifying or denying the approximations made by the considered model.

This thesis led to the following research approach: we chose to make scaled controlled measurements in an anechoic chamber. The first difficulty that we faced in the experimental part was that we cannot conduct an experiment with both a valid scale factor and far-field condition. Also, we conducted experiments without respecting the scale ratio to validate experimentally the exact codes, representative of all of the phenomena encountered. The frequency of application of these codes has been taken to the maximum computational capacity. Thus, at this limit scale, approximate codes such as MOCEM or Fermat could also be compared, and their ability to account for predominant full-scale phenomena could be proved.

In both application cases, forest and urban areas, the research approach was the same:

- Use exact modeling to understand the phenomenology of essential representative blocks for the representation of the scene (cylinder over ground for the forest, urban canyons for urban areas).
- Transition to higher frequencies.
- Propose faster simulators making approximations to the real frequencies for inversion purposes: a *Trunk and Volume over ground* for a forest, our own geometrical code *Urban Canyon* for the urban areas, or an extension of MOCEM to canyons.

In the following sections, the results for these two application frameworks, forest and urban, are detailed, with both experimental the approach and simulation studies.

11

POLARIMETRY FOR FOREST IMAGES

Understanding the terrestrial carbon cycle and predicting future climate changes are important topics in climate research. One of the major uncertainties in the current carbon cycle models lies in terrestrial ecosystems, mainly forests. Rather than estimating forest carbon directly, biomass can be used instead since about half of biomass is carbon.

The forest being a dense object, the radar is an ideal tool for analysis, because of its penetration capabilities. Polarimetry has immediately been shown to be of interest for this type of environment, due to the presence of several orientation and geometric effects. Later the forest was the first medium studied with PolInSAR data.

1 POLINSAR FOREST INVERSION

The canopy height is a key parameter for describing forests since many studies have tried to link it to biomass. Also, interferometry allows the height of the scattering phase center of a forest to calculated. However, this height is not directly the total height of the vegetation, because the wave penetrates the medium. Moreover, the elevation of this scattering phase center depends on the height found by polarimetry, and this is the key idea of PolInSAR.

In an attempt to model this dependence between the height of the vegetation, and the interferometric height found for the different polarizations, the model most used in the literature is the Random Volume over Ground model. During my PhD thesis, using the traditional methods of inversion for this model of forests at P-band, it turned out that the penetration at this frequency made the presence of trunks prevailing. Thus, I proposed to take into account a layer of trunks in the model in (**Colin**, Titin-Schnaider, and Tabbara, 2005c).

This kind of modeling is also used for FOPEN. Foliage Penetration Radar is a technical approach to find and characterize man-made targets under dense foliage, as well as characterizing the foliage itself. The algorithm proposed by S. Cloude for the detection of targets behind the forest, using a filtering of the RvoG model, has been adapted to our model of random volume and trunks successfully.

However, some questions have remained open. In particular, new measurement campaigns led in Sweden have shown that the detection of vehicles hidden in the forest was much more complex in this new area, particularly because of the density of the forest, and perhaps also the wet conditions. Moreover, it appears that the attenuation of the forest is the most difficult parameter to obtain by inverting a model. For this reason, we continued to explore the possibilities of these attenuation values with Laetitia Thirion Lefevre. We proposed a study on the link between extinction and height of the phase centers.

Figure 41: Scale equivalence principle illustrated to study forest scattering

We also have led a study about the statistical behavior of attenuation by simulation in (Thirion, **Colin**, and Dahon, 2006).

2 INVERSION OF BISTATIC POLARIMETRY IN FORESTS

The bistatic configuration has recently renewed the studies concerning forests, both for civilian and military aspects. For civilian aspects, the bistatic configuration leads to an additional degree of freedom by breaking the assumption of reciprocity. Also, the additional measured cross-polarization coefficient allows to a more promising inversion to be considered. For military applications, the idea is to choose a better acquisition geometry for detection, finding the one for which the ratio between forest and target signals is maximized.

The lack of real data is the main difficulty to conduct these studies. Concerning bistatic SAR data, there are only a few stationary measurements with parallel trajectories, which therefore offer a limited potential in terms of geometry cases. Bistatic acquisition performed at X-band is not the band of interest for penetration capabilities. Finally, bistatic SAR data conducted over a forest between ONERA and FOI are not polarimetric.

Also, my studies have mainly relied on two types of data:

- data at the scale of anechoic chambers,
- data at the optical scale.

This last point, initiated during the PhD thesis of Nicolas Trouvé, is the subject of the PhD thesis of Etienne Everaere. This original principle of scale equivalence between nanotube forests and real forests is illustrated in Fig. 41.

Meanwhile, the simulation tool COBISMO, an extension of COSMO suitable for a bistatic situation continues to be used in the process discussed previously:

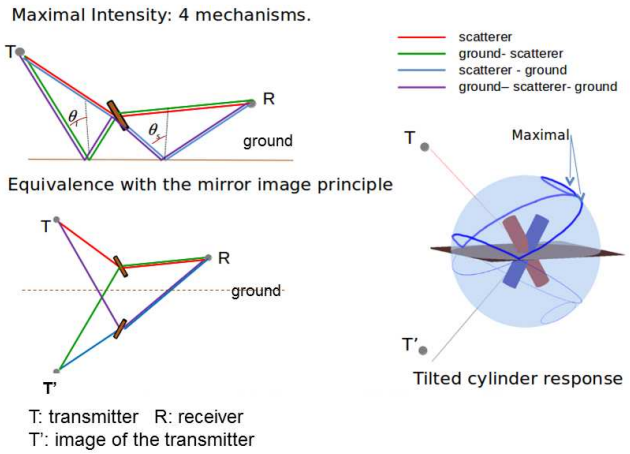

Figure 42: The maxima of intensities in the forest are explained by the cylinder return and the mirror principle

it is a tool both to develop our understanding of the forest, and to deepen the validation of the tool.

A first validation phase was conducted in parallel to the LORAMBIS campaign on simple and controlled elements measured in an anechoic chamber. Groups of metallic cylinders have been measured, as military vehicles scaled from their CAD.

During this contract, I was able to show that when we consider only the trunks over ground without interaction between them, the optimal geometric configuration for detection is a configuration with a bistatic angle lying in the incidence plane. The value of the optimal angle depends both on the wavelength, and on the ratio of the heights of the target and the height of trunks. For the low frequency at 250 MHz, and a classical trunk height of 10 meters, this optimal bistatic angle is around twenty degrees. At 400 MHz, the optimal angle decreases to about ten degrees. These configurations are found using simulations of forests with the COBISMO tool, and bistatic indoor measurements for the military vehicles.

Meanwhile, these simulations have helped us to understand the bistatic scattering of the main components of forest, and cylinders, and the type of mechanisms involved: simple scattering, and bounces involving the ground. In the bistatic configuration, double bounces mechanisms differ according to the order of the impact of the element itself and the impact on the ground. Using simulations on cylinders, we are able to predict the receiver positions where the returned energy will be maximum. For a single cylinder, the maximum energy is located on a cone whose aperture angle is the angular difference between the incidence direction and the cylinder axis. The mirror principle enables us to understand the maximum return as a superposition of single mechanisms. The maximum power for one cylinder above the ground is repre-

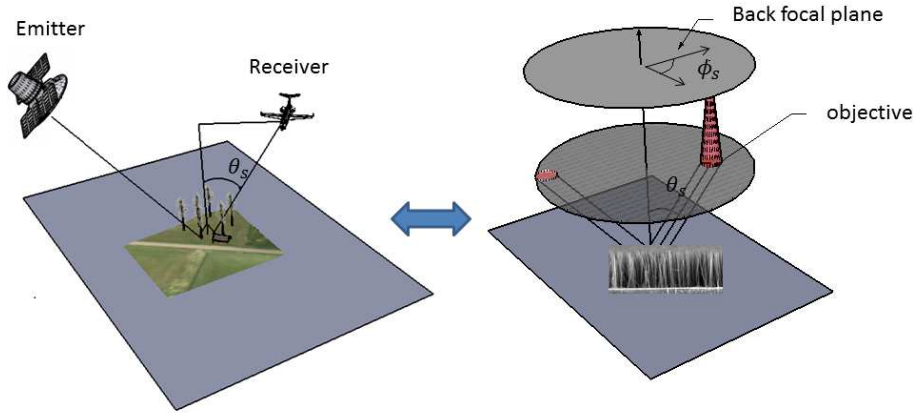

Figure 43: Convergence between a bistatic radar measurement and an optical device to study forest scattering

sented on the half reception sphere, in Fig. 42. The pattern comprises a set of circular rings, each corresponding to a particular mechanism.

In order to improve the search for an optimal configuration, we have also taken into consideration the effects of attenuation according to the bistatic angle. In this context, the COBISMO tool may be insufficient because it neglects the interaction between branches. While this approximation was shown to be realistic enough to reproduce many cases of monostatic measurement, we cannot be sure that it remains valid in the bistatic configuration. Also, realizing sufficiently dense scaled targets in an anechoic chamber is tricky. Nicolas Trouvé initiated an attempt to do so, with a forest of nails measured in an anechoic chamber, as presented in (Trouvé and **Colin-Koeniguer**, 2009). However, to go further, the complexity related to the increase in the number of elements is binding.

In order to answer this issue, the use of an optical device has led to significant advances. The measurement tool used and developed in collaboration in the LPCIM has the following advantages:

- it enables rapid use and lower cost, compared to radar measurements
- it offers a variety of bistatic geometries: for a given position of the emitter, the signal is collected for all receiver positions, as represented in Fig. 43.
- Various scenes, performed using nanotube forests, can be varied in their descriptive parameters. For example, several nanotubes forests used for our study are pictured in Fig. 44.

These measurements have led to a better understanding of a number of points:

- Deterministic polarimetric parameters are well reproduced by simulation by COBISMO, for sparse forests, corresponding to standard forests of trunks, as presented in (Thirion, **Colin**, and Dahon, 2006).

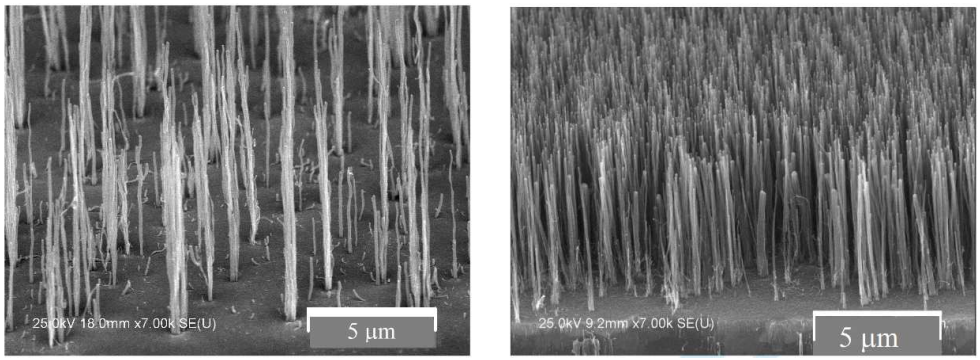

Figure 44: Pictures of two Carbon Nanotube samples measured for analysis. On the left, the so called sparse forest and on the right the so called dense forest. The length of the CNT is around $l = 7.5\ \mu m$ and the ratio is $l/\lambda = 12$

- Some behaviors that we had already predicted by the simulation of the forest are well reproduced:
  - The intensity has a local maximum for the monostatic configuration, and an overall maximum for the specular configuration, as already predicted in (Thirion-Lefevre, **Colin-Koeniguer**, and Dahon, 2010).
  - The double bounce effect predominates in the monostatic configuration and the simple scattering effect is dominant in the specular direction.
- For very dense forests, corresponding to densities of branches, the comparison becomes more difficult. We have recently understood with the help of Antonello de Martino (LPICM) that non-deterministic effects are due to the angular integration of the various multipaths between elements of the scene. If we consider the angular variation of the receiver only for the simple scattering of a set of vertical cylinders on a horizontal surface, it is thus not sufficient to cause depolarization. This is why COBISMO is not able to find the level of measured depolarization. On the contrary, it appears that while the angular diversity and multipath are now included, in this case we would obtain a significant depolarization. Multiple interactions have the effect of creating disorder in the directions of the resulting mechanisms.

This leads to probably one of the important findings of this research: the consideration of interaction effects between cylinder scatterers is probably a key step to be able to predict levels of depolarization in bistatic geometries.

Moreover, this line of research still offers many opportunities for the future:

- The actual determination of the appropriate geometry for FOPEN or inversion purposes.
- The measurement of scenes of nanotubes that are more representative of whole trees, with branches. Recent developments for the growth of

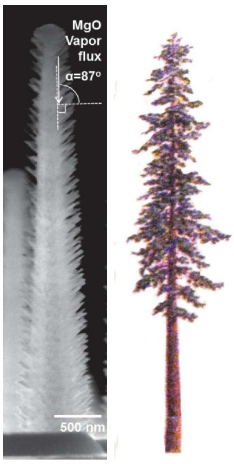

Figure 45: nanotube forest for sequoia

vertically arrays of nanotubes could be used for more complex targets, as proposed by Costel Sorin Cojocaru in LPICM, and as pictured in Fig. 45

- The encoding of multiple interactions in order to be able to predict depolarization effects. This depolarization parameter seems a very promising one for the inversion of parameters such as density of the forest.

12

URBAN IMAGES

In the context of rapid global urbanization, urban environments represent one of the most dynamic regions on earth. Even in developed countries the yearly conversion of natural or agricultural space into residential, industrial or transport areas frequently exceeds 100 ha. The current increase in population has resulted in widespread spatial changes, particularly rapid development of built-up areas, in the city and the surrounding area. Due to these rapid changes, up-to-date spatial information is requisite for the effective management and mitigation of the effects of built-up dynamics. Various studies have shown the potential of high resolution optical satellite data for the detection and classification of urban area. Nevertheless optical satellite imagery is characterized by a high dependency on weather conditions and daytime. Thus, particularly in case of regional and national surveys within a short period of time, disaster management, or when data must be acquired on specific dates, radar systems are more valuable.

Thus, the new generation of civil space borne Synthetic Aperture Radar (SAR)-Systems with short revisit times can serve as a valuable instrument. Promising approaches towards the classification of urban areas include the analysis of multipolarized image analysis.

Unfortunately, we have already seen that SAR sensors using the polarimetric mode often have degraded resolution. However, to ensure detailed mapping of urban structures, we need high ground resolution. Therefore, the emergence and recognition of urban remote sensing appears to be linked to the continuous improvement of the spatial resolution offered by generation sensors. This is why, on order to evaluate the benefits of polarimetry in the urban areas, we have tried to use the satellite data with the best achievable resolution for urban environment, which is often achieved today by X-band systems.

The polarimetric analysis of urban images in this band is still almost unexplored. Over the past years of research, the first data analysis showed that at this small wavelength, polarimetric analysis of urban environment starts to be particularly complicated. Indeed, urban areas are a spatially complex mixture of many scatterers whose electromagnetic and geometric properties are varied, and have to be understood at the wavelength scale.

During my research, and more specifically since 2011, I have studied polarimetric SAR images of urban scenes for at least three different applications: the first one concerns the detection of built-up areas, the second one concerns building elevation, and the final one concerns the study of urban canyons and the potential of multipath for detecting targets not in the line of sight of the radar.

1 DETECTION OF BUILT-UP AREAS

The contribution of urban polarimetry can be justified by the diversity and complexity of the interpretation of the different mechanisms involved. Briefly, the recorded observations are summed up by the scatterings from the targets on the same wave front. For example, the layover areas contain the scatterings from the roof, wall and ground. A mixture of volume scattering by vegetation and double-bounce scattering from buildings can also be observed in low density areas. The total scattering is strongly influenced by the looking directions and the alignment of structures: man-made structures that are arranged perpendicularly to the illumination direction increase the oriented double bounce contribution. In order to use polarimetric parameters within the framework of built-up area detection, four main features of polarimetric analysis in the context of urban areas can be used:

- The first one is that polarimetry is able to distinguish between deterministic or man-made targets and non-deterministic or natural targets.
- The second one is that built-up areas contain a lot of orientation effects that induce a non-zero polarization orientation angle. This polarization orientation angle is defined by the angle of rotation about the line of sight. It has been shown that the polarization orientation angle shifts are induced either by dihedral effects between the ground and a vertical wall not aligned in the along-track direction, or by tilted roofs.
- The third one is that double bounce effects between vertical walls and the ground often produce very strong echoes in the SAR image. On the UAVSAR polarimetric image in Fig. 46, these double-bounce echoes are visible. Due to the worse resolution on TerraSAR-X, they cannot be distinguished. However, we can hope to separate these double bounce effects from the others, by using physical decompositions, such as Freeman-Durden or Yamaguchi decompositions.
- The last one is the lack of azimuthal symmetry. This implies that correlation coefficients between cross-polarization and co-polarization are not equal to zero, contrary to flat surfaces or vegetated areas.

Tested over the TerraSAR-X images of San Francisco, all of these features have failed to correctly detect built-up areas, for several reasons.

- At X-band, the conventional polarimetric parameters of second order (entropy, depolarization) do not behave in the same way as in the previous images acquired at lower frequencies: AIRSAR at L-band, RADARSAT-2 at C-band. More precisely, it appears that entropy remains very high on all of the pixels considered.
- All physical decompositions such as Yamaguchi and Freeman-Durden, fail as soon as the disorientation effects increase, as in the SOMA district,

Figure 46: Double bounce echoes visible on UAVSAR polarimetric images

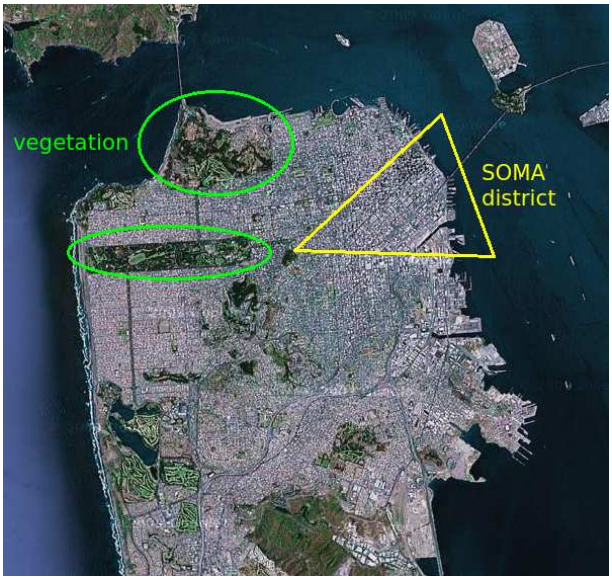

Figure 47: Optical image of the San Francisco test site. The SOMA district is indicated in the yellow triangle.

Figure 48: Entropy in the first polarimetric image of San Francisco: AIRSAR

indicated in Fig. 47. In this case, the medium becomes random and decompositions are not able to separate the different effects. In the same way, polarization orientation angle shifts induced by surfaces with buildings that are not aligned in the along-track direction are very noisy and their estimation becomes irrelevant.

Conventional polarimetric parameters, such as double bounce powers, have all failed to provide a correct classification in a specific area, for all of the images viewed from different sensors. This area is called the SOMA district in San Francisco, and contains many sky scrapers. Moreover, entropy of the image is very high over the whole image.

Looking more carefully at the classification results previously published on San Francisco with other sensors ALOS, AIRSAR and RADARDAT, it turned out that all polarimetric classifications in this area fail. For example, in Fig. 48 we see that the triangle corresponding to the SOMA district has the same entropy as the vegetated areas.

Orientation effects related to this area on the polarimetric response have been identified. Given that this area has an orientation far from the axis of the sensor, it was subsequently shown that the level of HV return is high. It is thus necessary to perform a disorientation in an attempt to reassess these canonical mechanisms in a way that removes the orientation effect. However, this operation is rendered ineffective, mainly because this area has very high entropy, therefore it becomes impossible to make a reliable assessment of the orientation angle and an effective correction.

Also, we summarize our approach to confirm our answers to two different questions:

- Why is the level of entropy high over our entire TerraSAR-X image?
- Why is the level of entropy high in this particular SOMA district?

Several assumptions can be made to answer these questions. For the first one: high entropy in TerraSAR-X images is due to the relative noise of the sensor, or it is due to the degree of complexity of the scene, compared to resolutions, to pixel sizes, and/or to wavelengths.

For the second one: the high entropy of SOMA relates to the complexity of the area which contains many buildings and possibly multipaths, or the high entropy of SOMA mainly relates to the orientation of the streets.

We managed to invalidate the initial assumptions and to confirm the second ones, by using:

- electromagnetic simulations on urban canyons and the influence of multipath, within the framework of the PhD thesis of Azza Mokadem,
- statistics simulations on resolutions and pixel size, within the framework of the PhD thesis of Flora Weissgerber,
- analysis of available images and search for new ones (UAVSAR).

A comparison of all entropy maps thus obtained is given in Fig.49.
This comprehensive study allows us to reach the following conclusions:

- Entropy is obviously affected by the thermal noise of the sensor. However, this influence is less compared to the following two other influences: building orientation and cell size resolution.
- Disorientation in urban areas is not only accompanied by an increase in the cross pol signal, but also an increase in entropy. This means that disorientation leads to mixing the mechanisms randomly, and it is impossible or at least very difficult to correct the effect of disorientation in order to isolate the double bounce component: even if we are able to highlight the presence of this effect, other mechanisms involved remain mixed in the resolution cell. This leads to common misclassification results, even with disorientation algorithms.
- High entropy in urban areas is strongly linked to cell resolution size. For a given wavelength, at L-band, entropy remains low when resolution is poor. Entropy increases with improved resolutions, probably because the spatial variability of polarimetric behavior is more important. For large resolution cells on the contrary, the behavior is more stable from one cell to another.

Once the difficulty linked to the TerraSAR-X polarimetric parameters is better understood, we turn to the initial problem of the best approach to detect built-up areas in this image. Special care has been given to the quantitative performances of the various parameters used for detection. In order to quantify the contribution of polarimetry for building detection, we plotted ROC

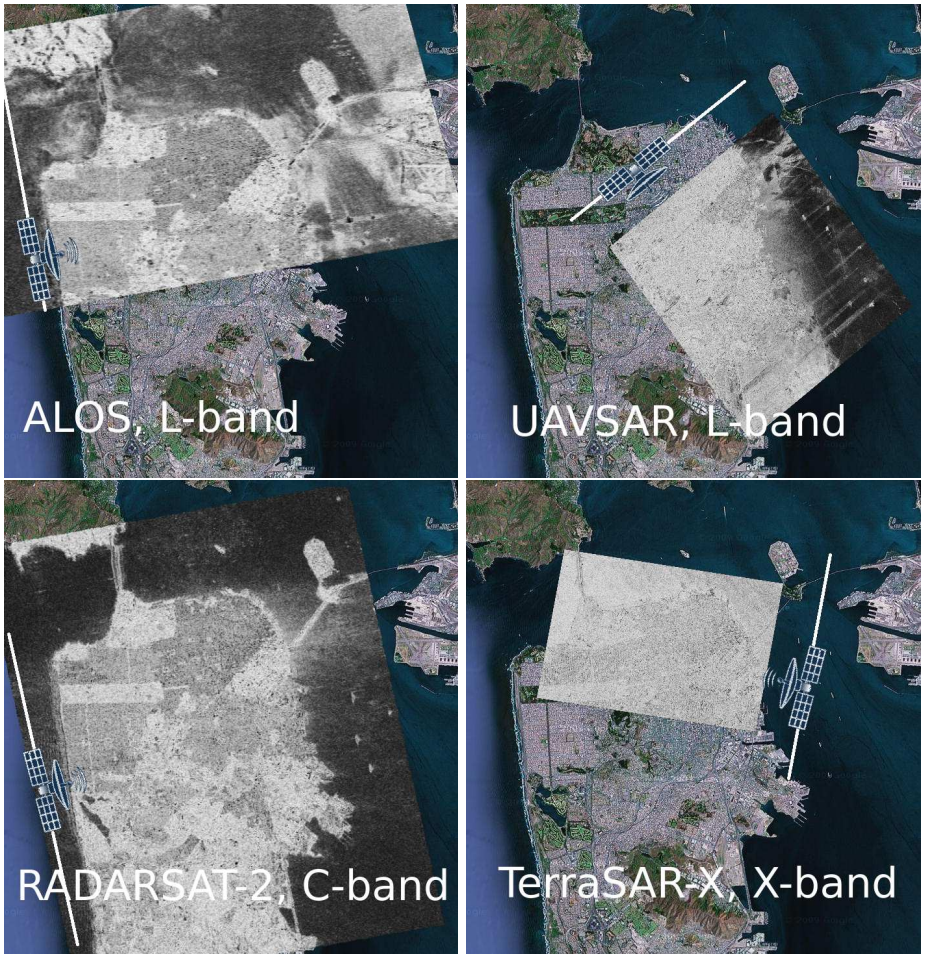

Figure 49: Comparison between the Entropy of various polarimetric images

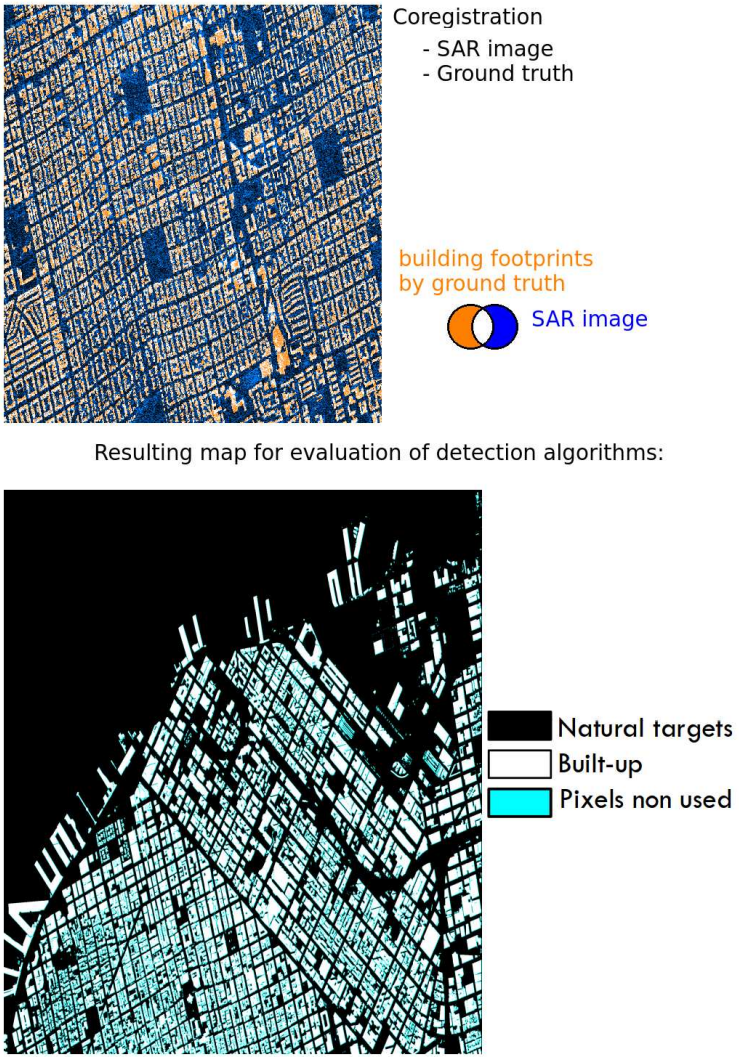

Figure 50: Constitution of a ground truth for classification performance evaluation

(Receiver Operating Characteristic curve) curves that are a plot of the true positive rate against the false positive rate for the different possible cut points of a diagnostic test.

These curves analyze the efficiency of using various input parameters and various distances between the two classes defined by the ground truth, built-up and natural areas. The closer the curve follows the left-hand border and then the top border of the ROC space, the more accurate the test is. Distances between the two classes have been calculated using different parameters: entropy, Yamaguchi double bounce components and the various polarimetric correlations existing in case of non-symmetry. Concerning the ground truth required for this evaluation, a dedicated one has been produced, using a shapefile describing building footprints and their elevation. In order to use this file ground truth to evaluate the performance of different classifications, the coordinates of the buildings were converted into TerraSAR-X longitude-latitude, the height of buildings was taken into account, and each of the masks was recalculated in

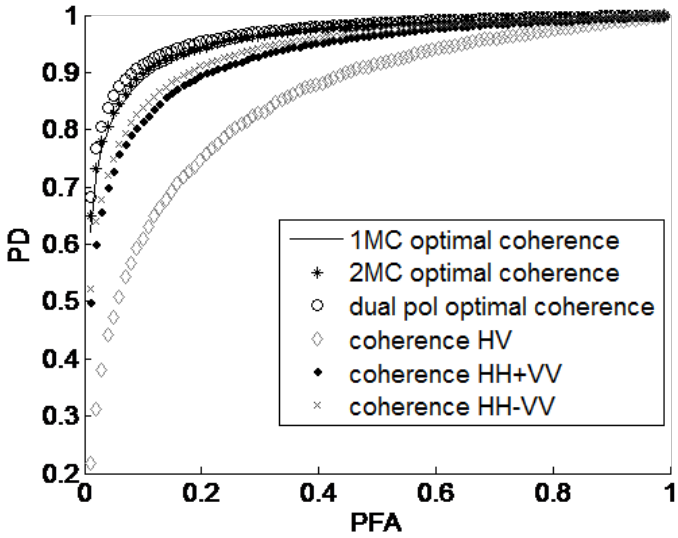

Figure 51: ROC curves for the performance of various interferometric coherences for detection.

the repository sampling of the image. As a precaution, the pixels on the edges of the buildings were not taken into account. Others allow us to define two classes: buildings and outdoor environment. An extract of the Ground Truth thus generated is given in Fig. 50.

These curves clearly show that the best discriminating parameter among those tested is the Yamaguchi double bounce component. However, we must keep in mind that the Yamaguchi parameter does not only depend on the polarimetric content, but also on the powers. When we compare this parameter to the polarimetric intensity channels, we see that it is always less efficient than the polarimetric amplitudes. This proves that polarimetric parameters that are independent from the span (entropy, correlation) do not improve the results found by intensity alone to identify built-up areas.

Since at X-band, the traditional polarimetric parameter fails to identify man-made targets, we propose to use polarimetry contribution to a repeat pass interferometric mode. Indeed, the temporal decorrelation will be very high in this frequency band, because it will be sensitive to displacements of the order of a few centimeters. Thus, the interferometric correlation image exhibits a much better contrast than the intensity image between natural and artificial targets. Again, ROC curves clearly show the benefit of using interferometric coherence for discriminating buildings, at least with HH and VV polarization. Thus, the benefit of polarimetry has been considered through the use of a coherence optimization. The ROC curves shown in Fig.51 also show that the contribution of polarimetry to optimization allows the detection performance to be improved regardless of the type of coherence optimization.

The solution proposed is therefore to use optimized repeat-pass coherent polarimetry as an essential criterion for an unsupervised 2-class classification that will eventually be improved by shape criteria extracted from the span

image. Detection results of this parameter are represented as a binary map in Fig.52.

2 3D RECONSTRUCTION

3D rendering is a logical extension to the classification of buildings proposed in the previous section, to enrich the data necessary to monitor the growth of the urban extension. However, it can also be considered as part of the diagnosis of urban areas after natural disasters such as tsunamis or earthquakes. Natural disaster monitoring and the evaluation of their effects is a complex problem in urban areas, because a lot of parameters can be investigated. Areas of significant changes can be detected making use of high-resolution satellite data, areas where a 3D model can be established on a large scale by interferometry. In this context, the contribution of radar is its immediate use regardless of weather or smoking out due to fires.

The interferometric phase is related to the elevation of the scatters. The quality of its estimation depends mainly on the conditions of acquisition:

- The ambiguity height, corresponding to a phase variation equal to 2π. Phase is defined only for modulo 2π radians, so the resulting elevation map is wrapped with respect to some modulus or ambiguity. If the ambiguity height is too high, as for UAVSAR images over San Francisco, then the precision on height is not sufficient to estimate building elevation. If the ambiguity height is on the order of 50m, as for TerraSAR-X images, then the precision in regard to the height becomes sufficient. For example, in 53 we can see that the double-bounce echo has a different elevation than the roof. However, it is necessary to perform phase unwrapping: for high variations of the relief, or for high buildings, several wrappings of the phase are clearly visible, as shown on the right.

- Temporal decorrelation: the loss of coherence depends strongly on the wavelength and becomes critical at X-band. Thus, still on repeat-pass TerraSAR-X images, coherence is too low on the ground to be able to estimate the ground elevation.

We have already seen that polarimetry combined with interferometry, can improve the product of the latter, either by separation of scattering phase centers, or by improving the interferometric correlation map, by enhancing its value and reducing the noise level of the interferometric phase. I have investigated these two aspects.

For the separation of phase centers, the goal in urban areas can be to obtain the ground height jointly with the elevation of the roof. Within this framework, the benefits of polarimetry are often compared with the benefits of pure technical image processing. The results of techniques for phase separation will obviously depend on three factors:

- The resolution of the images. This is even the essential criterion. Indeed, if the resolution is low, a vertical wall will be found synthesized into

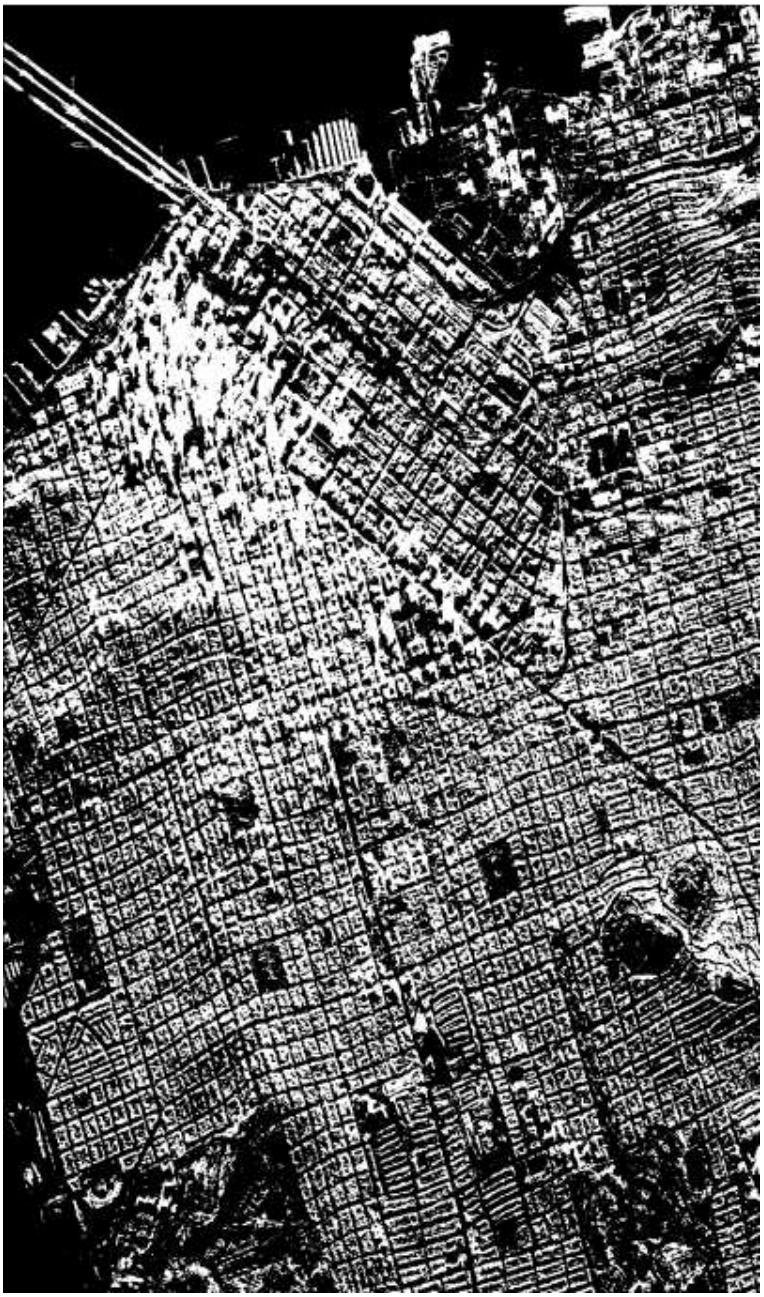

Figure 52: Built up area detection

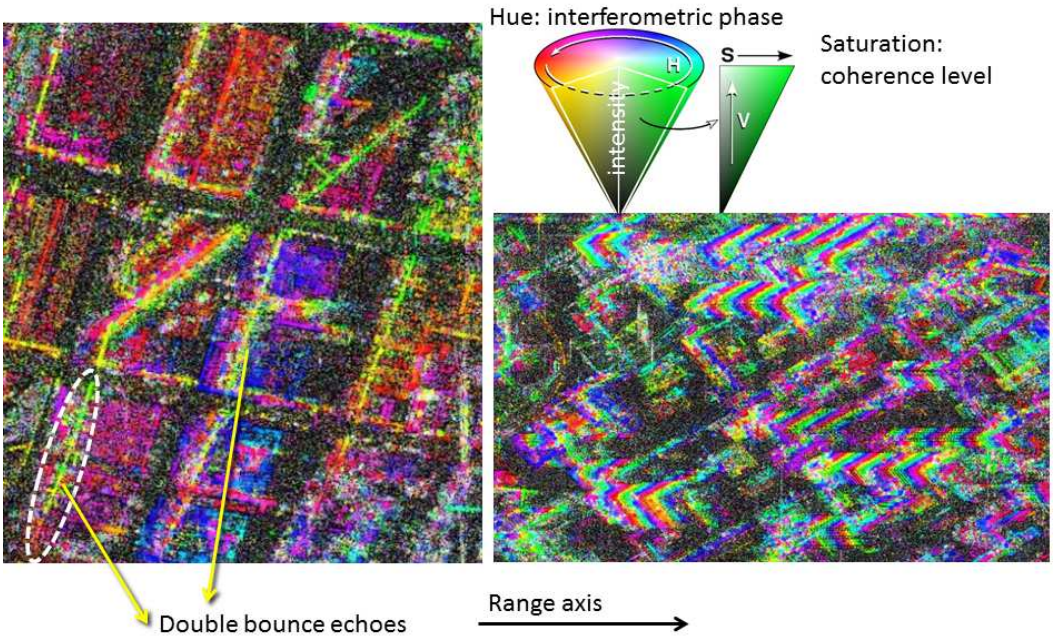

Figure 53: Two extracts of a repeat-pass HR interferogram of TerraSAR-X

a single resolution cell. This wall will include several scattering centers, and potentially different polarimetric returns with different heights will therefore be mixed.

- The frequency. At low frequencies, the wave will not necessarily be sensitive to details. Thus, even a large resolution cell will see a limited number of mechanisms.
- The ambiguity height for the interferometric process, as already pointed before. The distribution of heights observed depends on this parameter: if the ambiguity height is small, then the angular diversity of the generalized coherence will be very important.
- The temporal decorrelation. We have seen that at X-band, the temporal decorrelation of the images is very fast. Particularly in the resolution cells of the San Francisco images containing layover phenomenon, it is clear that the phase of the roof is mixed with the ground phase. However the ground seems to induce a high decorrelation in the mixture and therefore its elevation cannot be estimated satisfactorily.

Thus, concerning the TerraSAR-X images of San Francisco, if the estimate of the height of the roof is possible, at present we have no satisfactory estimate of the height of the associated ground. Our conclusion is that at X-band, it is necessary to have single pass data or very small temporal baselines to be able to provide a 3D rendering over the entire image.

Still at X-band but using single pass POLINSAR images, we have proposed an algorithm to recover the respective heights of the roof and ground from

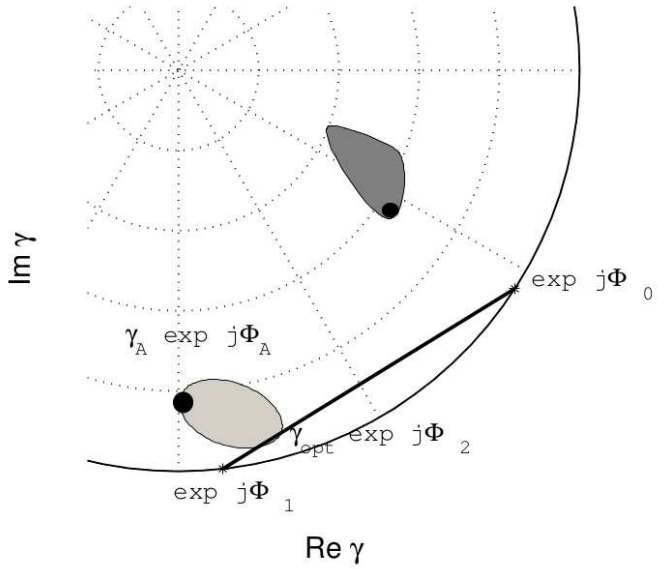

Figure 54: Algorithm to inverse building heights through the coherence shape

their coherence shapes. We have seen in Chapter 3 that in layover areas, the coherence set corresponding to the top of the roof mixed with the ground is a narrow ellipse. If the noise of the interferometric phase is low, then the major axis of this ellipse will intersect the unit circle in the interferometric phase of the roof and the interferometric phase of the ground. However, most of the time, the ground alone is not necessarily visible, or its interferometric phase can be noisy. Thus, the extension of major axis of the ellipse is not always sufficient to ensure a robust regression. Another issue is that it is not uncommon, even in layover areas, for the polarization diversity in the roof pixels to be insufficient to estimate the relevant information on the ground. Moreover, we were also interested in solutions that remain robust even when the pixels selected are not located in the layover area. This is why it seems more appropriate to use the information of both coherence shapes: that associated with the bare ground pixels, and that associated with the roof pixels. In order to estimate the interferometric phase of the ground, the solution of the optimized coherence seems relevant, since it has already been demonstrated that it is a good way to estimate the elevation of one resolution cell containing only one type of scatterer by reducing the noise level. This optimization enables us to find the point $\exp(j\phi_0)$ where ϕ_0 corresponds to the interferometric phase of the ground. This point is represented in Fig. 54.

The optimal coherence linked to the ground alone is also used to make a more robust linear regression of the ellipse in the layover area, especially in the case where the angular range observed is rather limited. Practically, we superimpose the two representations: the first coherence set related to the ground, and the second one related to the roof of the building. Then a line is drawn between two points. The first point is on the unit circle and its phase is the phase of the optimal coherence of the ground. The second point is the

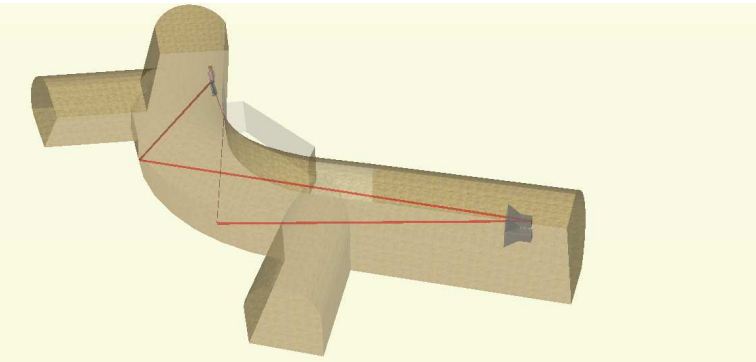

Figure 55: Caponier corridor

optimal coherence of the roof. The intersection of the line joining these points with the unit circle corresponds to $\exp(j\phi_1)$. The total height is deduced from ϕ_1-ϕ_0.

This solution has been shown to be effective in many cases encountered. It has been tested on 140 buildings of a Toulouse POLINSAR image. It it the subject of the paper (**Colin-Koeniguer** and Trouvé, 2014).

3 URBAN CANYONS

In our analysis of entropy effects, probably related to the presence of complex multipaths in urban areas, we discussed the modeling of urban canyons. It was the central point of the PhD thesis of Azza Mokadem, the aim of which was to know whether vehicles or other types of targets placed in the shadow of buildings could be detected by multipath. Note that this detection problem in urban canyons, is not unconnected with the general problem of detecting a vehicle by means of a radar behind a crossroads. I have been able to address this issue by participating in an experiment set up in an underground corridor, for detecting a pedestrian by multipath returns induced by the vertical walls, as shown in Fig. 55.

In order to address the problem of detecting a target in urban areas in a SAR image, we had recourse to experiments, but also simulation tools. Many tools relating to electromagnetic propagation through an urban area exist already. Thus, the aim of the thesis was not to develop one of these simulators, but to determine which could help us to answer the question regarding detection.

Meanwhile, the same approach as for the forest was implemented: cross validation of the codes, and parallel understanding of the urban environment.

Various codes have been considered:

- A code dedicated to the propagation for Telecommunications: Wireless Insite, developed by Remcom.

- A modeling code of SAR images, dedicated to vehicles: MOCEM developed by Alyotech and led by the DGA.

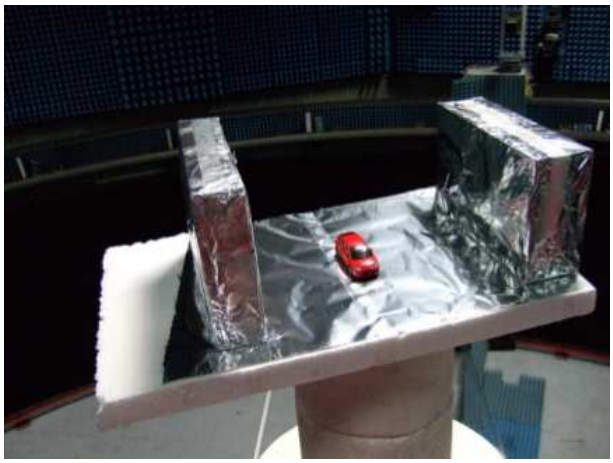

Figure 56: Picture of the scaled measurement performed in the anechoic chamber BABI at Onera

- Exact modeling EM codes: ELSEM 3D at Onera and FEKO, a commercial code.
- An asymptotic model: Fermat, an Onera-Oktale code.

Conducted in collaboration with SONDRA, this PhD thesis has resulted in several measures of PEC urban canyons in an anechoic chamber. The first measurement was carried out full-scale but under near-field conditions, at the NTU (Singapore). A second measurement, pictured in Fig. 56 was performed under far-field conditions, but without complying with the scale ratio in the BABI anechoic chamber at Onera.

This measurement confrontation places us directly before the first validation problem: it is impossible, given the dimensions of existing chambers, to ensure both the scale ratio and the far-field condition.

Near-field range profiles of a canyon were theoretically analyzed, especially during the internship of Nicolas Sar. This complex range profile consists of several equally spaced peaks, associated with different responses, all explained by specular multipath involving the vertical plates or the ground, and arising for different numbers of bounces permitted by all incidence angles covering the opening of the canyon. One example of such a range profile measured in an anechoic chamber is given in Fig. 57. The presence of target results, according to geometrical conditions, in additional peaks.

A first set of simulations with FEKO conducted by Sophie Langlet at the DEMR showed that, even under far-field conditions, although the angle of incidence can be considered unique, a large number of peaks can always be found in the range profiles for certain scale ratios of the canyon. This fact has been confirmed by measurements in the BABI anechoic chamber. Once again, the different peaks present in range profiles are explained by the different paths involving different numbers of bounces, but these different numbers of bounces are achieved by considering the scattering of the plates outside the specular direction. In this case it is not the diversity of incidence angles that

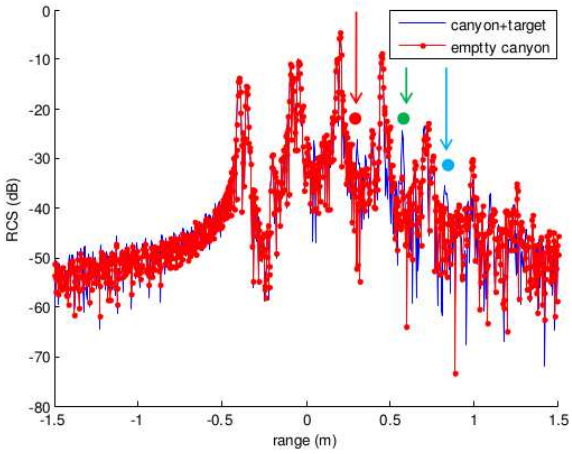

Figure 57: Measurement of the empty canyon range profile

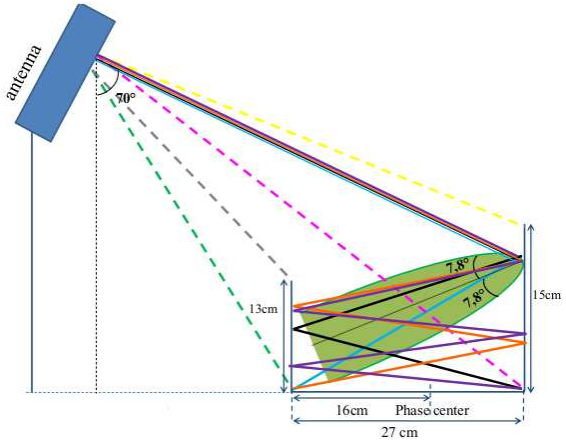

Figure 58: The various peaks present in a range profiles are explained by different paths involving different numbers of bounces

explains many peaks, but rather the widening of the main specular lobe of the return of a plate, when the dimensions of the latter are not large enough in comparison to the wavelength. This is represented in Fig. 58.

Thus, we find the same difficulties for validating a simulation tool in a real case, with the scale ratio, and the far-field condition.

The computation time of the exact codes becomes much too long when the frequency is increased. Therefore, during the PhD thesis of Azza Mokadem, this type of code was used to validate the experimental measurements scaled at a low frequency. As an example, in Fig. 59, two different simulation methods, the temporal one and the Methods of Moments, are able to reproduce the indoor measurement.

Then, the frequency was increased to observe the gradual decrease of the amplitudes of the secondary peaks, approaching a predicted range profile by a very simplified simulation tool.

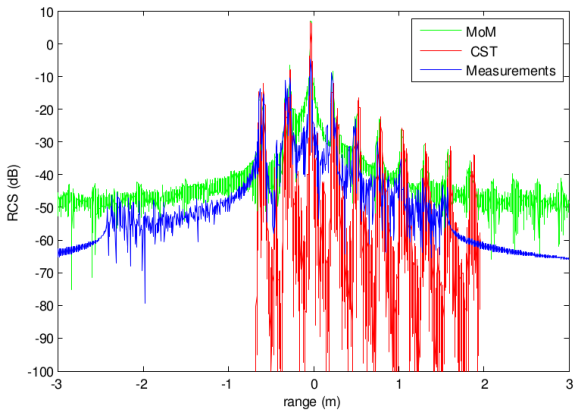

Figure 59: Comparison of different simulation tools and the indoor measurement

This simulation tool, called V3 Urban Canyon, was developed to simulate the range profiles of a canyon by taking into account specular reflections. It is also able to predict the area where a target can be detected by multipath. Meanwhile, it is now undergoing new developments, including:

- The calculation of exact amplitudes involving the areas of surfaces that are involved in multipath.
- The transition of the PEC case to the dielectric case.
- The determination of shadow range positions and the range positions of several key diffuse scattering zones: the ground seen in the Line of Sight of the radar, the roof in the Line of Sight of the radar and the scattering of the ground reflected by the vertical walls.

This last point is illustrated on a realistic example. We chose an existing neighborhood of San Francisco, Japantown, whose 3D modeling is given in Fig. 60 and we show in a given incidence plane how the different returns are synthesized along the range axis.

This representation along the range axis is given in Fig. 61. The point returns coming from specular multipath are given by the various peaks. Colored marks indicate the corresponding rays drawn in the same color. Above the range profile, the varous scattering areas located along the range axis are indicated:

- the green areas correspond to direct backscattering of the ground, in direct line of sight of the radar.
- the blue areas correspond to the direct backscattering of the vertical walls.
- the read areas correspond to the direct backscattering of the roofs
- the magenta areas correspond to backscattering of the ground viewed after a reflection on the vertical wall.

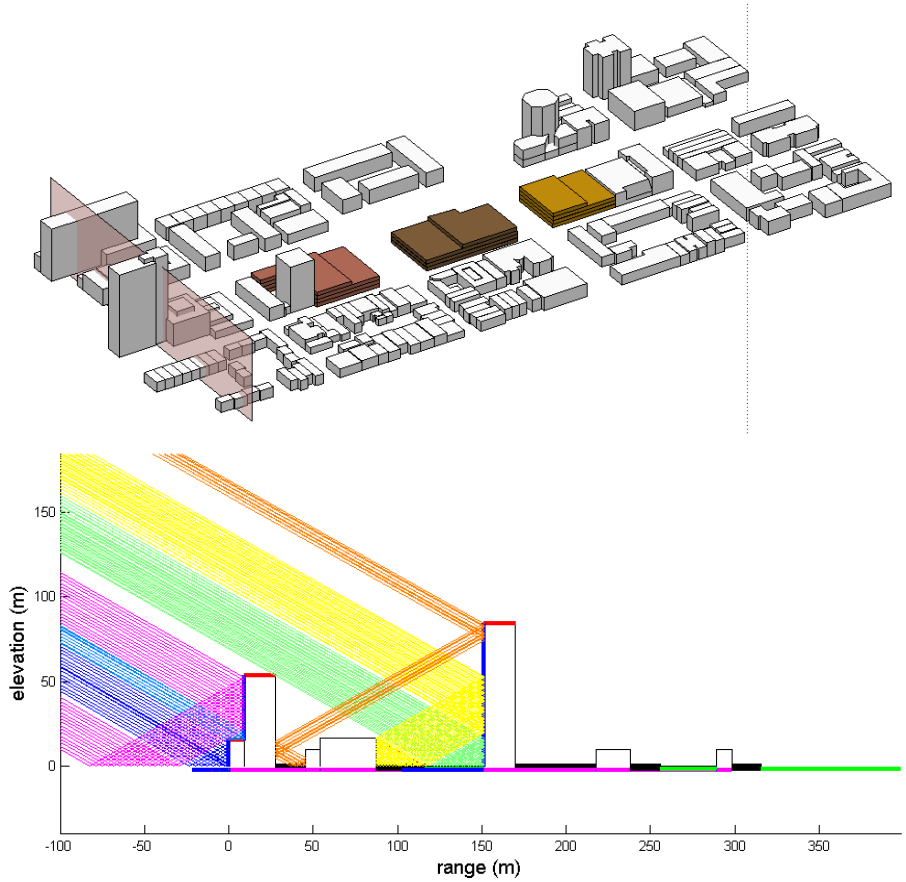

Figure 60: 3D model of Japantown in San Francisco and raytracing of specular scattering according to a section plane

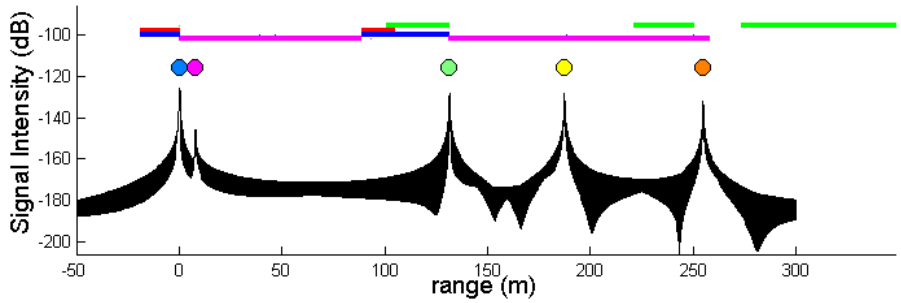

Figure 61: Range profile and diffusion area range positions predicted by URBANcanyon

Such simulations are able to predict the superposition of different mechanisms within the same resolution, whose statistical return in terms of powers and interferometric coherence have already been discussed in Part 2. In this example, we see that up to three mechanisms can be mixed. Moreover, this simulation tool illustrates the importance of geometric effects in the interpretation of the image. Our feeling is that an algorithm dedicated to urban areas could be proposed. This algorithm would not make the assumption of a set of isotropic and white bright scatters, but rather a superposition of point responses associated with multipath and some diffuse returns whose positioning would result from a specific simplified 3D geometry.

Along with such a development of a tool based on the geometry, other urban area simulators have been evaluated. The Wireless Insite code was rejected because it failed to account for waveforms of large bandwidths as used by radar systems. Furthermore, its interface was not flexible enough to work on the definition of these waveforms ourselves. Finally, both MOCEM and Fermat codes continue to be investigated today at two different scales: MOCEM is used to report statistical detection performance and to be validated for urban areas; Fermat is used to account for the physical mechanisms on a real scale, such as the importance of diffraction effects.

These research perspectives within this context are therefore many as unprecedented in the open literature. Moreover, the detection problem in urban areas remains connected, as we have seen above in regard to entropy, to the understanding of electromagnetic phenomena and of the signal obtained.

SUMMARY

This last part deals with processing tools for advanced applications.
The first section proposes the use of simulation tools, based on a long-standing collaboration with Laetitia Thirion-Lefevre (SONDRA). A general discussion on the use of simulation models has been proposed, as well as the presentation of our common research approach. This includes

- the development of simulation codes
- their validation, and a joint greater understanding of the scattering mechanisms present in a scene.

The second section outlines the achievements in the field of forestry. They include:

- Understanding the interconnection between canopy height, the phase center interferometric height, and attenuation.
- Understanding of the physical origin of the depolarization, in connection with the bistatic geometry, namely through the thesis of Etienne Everaere.
- Predictions of the most advantageous configurations for detection under forest cover.

The last section outlines the progress made in the field of urban areas, including

- Detection of built-up areas, developed in collaboration with Nicolas Trouvé at Onera.
- A better understanding of entropy in urban scenes. This work will remain ongoing throughout the PhD thesis of Flora Weissgerber.
- Estimation of building heights, through inversion of PolInSAR coherence shape.
- Detection of targets in urban environments. The latter work, more ambitious since we can find no precedent in the literature, is also a larger scale collaborative work, involving simulation and advanced processing.

CONCLUSION

My areas of research on polarimetric imaging radar have been at the interface between physics and mathematical tools. They are now shifting towards image processing algorithms.

The combination of three aspects confers originality to my research:

- The first aspect is a recognized expertise in PolInSAR coherence shape modeling.
- The second aspect is the joint use of optical and radar theories for the development of a polarimetric theory. It includes the use of an optical device to anticipate radar measurements.
- The last aspect is the combination of electromagnetic modeling and signal processing, to meet specific applications.

My contributions in polarimetric imaging performed at Onera are:

- A bistatic polarimetric method that gave rise to a filed patent.
- The recommendation of a bistatic polarimetric coordinate system, suitable for target analysis, and the way to calculate it from the acquisition basis.
- An alternative to conventional bistatic polarimetry theory development, both
  - in terms of the ways of measurement, with the use of an optical device for cheap and quick measurement, and for a wide variety of scenes.
  - in terms of polarimetric decompositions, trough the transfer of optics decompositions to the radar community.
- Alternatives to entropy and alpha polarimetric parameters, with reduced computation costs and with physical meaning. These alternatives are implemented in the PolSARpro software, a Polarimetric SAR Data Processing and Educational Tool from ESA.
- A hierarchical segmentation method for polarimetric images, coupled to an elevation estimation algorithm. It constitutes a proprietary software tool developed under the name of PAPIRUS (Polarimetry and Polarimetric Interferometry Rendering over Urban Scenes).
- Innovative mathematical techniques to study the geometrical properties of PolInSAR coherence shapes. They have also demonstrated in this context the inherent limitations of the two-mechanism coherence.

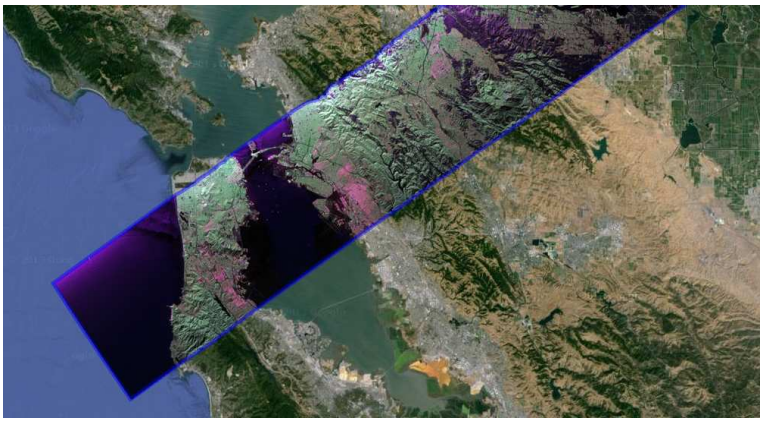

Figure 62: New polarimetric data: UAVSAR. The SAR polarimetric image appears in the blue rectangle

- An algorithm for building height estimation, adapted to the presence of layover, and based on the geometric properties of the coherence shape.
- A deep understanding of the cylinder bistatic polarimetric scattering, and a greater understanding of the forest bistatic polarimetric scattering.
- The prediction of the optimal configurations for target detection through the forest canopy.
- The prediction and understanding of urban canyon range profiles, under far-field or near-field conditions, at different scales.
- The demonstration of the causal link between urban canyon orientations and entropy.
- The demonstration of the causal link between improved resolutions, and the increase in polarimetric entropy in urban areas.
- A methodology for the performance assessment of a detection algorithm for built-up areas in a radar image, by comparison with a topographical database.

Radar polarimetry continues to grow and to raise issues, particularly relating to the diversification of sensors. Access to the data, which was scarce and expensive a few years ago, is increasingly easy. The Sentinel mission and the related approach of ESA in terms of distribution and data access testify to this. Another example are the UAVSAR polarimetric images distributed freely by NASA.

Images are huge, like the one given in Fig. 62: more than 200 000 x 10000 pixels. The revisit times are becoming shorter and the resolutions are improving. In short, we have increasingly more data from different sensors obtained in various configurations and with different characteristics. Due to this changing context, we have to adapt and anticipate future challenges.

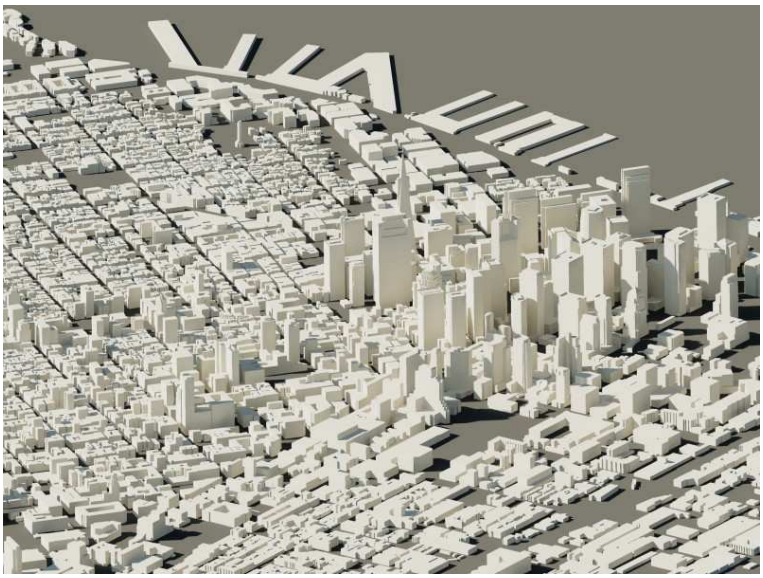

Figure 63: Example of a 3D data base that exists and could be enriched by a radar acquisition

Another point that seems important is the major role that the radar images can play in modern problems, particularly in the urban context. Indeed, radar has two major advantages:

- its responsiveness in a crisis situation, in case of poor visibility condition due to smoke or bad weather, and at night.
- its very good change detection performance, making it suitable for maintaining an up-to-date information.

While in comparison to optical tools (stereo, LIDAR), the maturity of radar processing methods is to date insufficient to consider SAR images for 3D reconstruction in dense urban areas, radar is nevertheless appropriate to promote two lines of research:

- updating data from an existing 3D database.
- quantifying human activity.

In Fig. 63, a 3D data base available on internet sites is an example of information that could be used and updated from remote sensing images, or used for vehicle detection by change detection. Another example of such a 3D modeling with more details, created at Onera, and used for change detection studies, is given in Fig. 64.

Other perspectives offered by the multi-temporal data explosion are:

- subsidence, i.e., measuring the rates of land displacements and the deformation of structures.
- tomography, i.e., the reconstruction of volumetric responses.

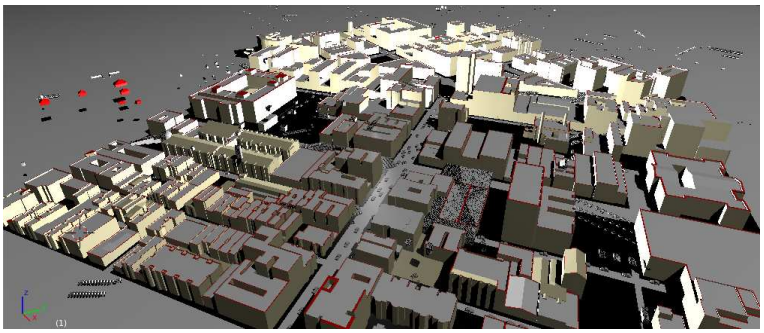

Figure 64: 3D model of San Francisco, created at Onera and used for the prediction of change detection performance by simulators

The contribution of polarimetry to subsidence has been recently evaluated in the ESA study PolSARAp. Up to now, benefit of polarimetry is mainly confined to an improved selection of permanent scatterers, on which the motion is estimated. However, I think that the contribution of polarimetry is not confined to this. Other contributions of polarimetry, such as the characterization of movements by the analysis of mechanisms, could be investigated.

Finally, I would like to express a final thought on future prospects about image processing of multi-temporal remote sensing images. The idea for this is to draw inspiration from the techniques developed in the area of video processing. Video processing also takes advantage of the temporal correlation between images. This temporal correlation offers the capacity to easily capture motion information or gradual changes in time. The processing of remotely sensed images could take advantage of the ideas already developed within the context of video processing, whether for compression, quality improvement, detection or tracking.

Similarly, the joint use of optics and radar polarimetry has been successful to better understand forest measurements. I believe that we should continue on this path, sharing the best algorithms in the fields of remote sensing images and biomedical images. This would include gains in terms of detection, learning and segmentation, supported by a study of the statistical behavior of the images encountered in polarimetric biomedical imaging applications.

BIBLIOGRAPHY

L. Bombrun, S.N. Anfinsen, O. Harant, et al. A complete coverage of log-cumulant space in terms of distributions for Polarimetric SAR data. *ESA special publication SP-695*, pages 1–8, 2011.

H. Cantalloube and **E. Colin**. POLINSAR for FOPEN using flashlight mode images along circular trajectories. In *IGARSS*, 2007.

H. Cantalloube and **E. Colin-Koeniguer**. Assessment of physical limitations of high resolution on targets at X-band from circular SAR experiments. In *Synthetic Aperture Radar (EUSAR), 2008 7th European Conference on*, pages 1–4. VDE, 2008.

H. Cantalloube, **E. Colin**, and H. Oriot. High resolution SAR imaging along circular trajectories. In *IGARSS*, 2007.

H. Cantalloube, H. Oriot, and **E. Colin-Koeniguer**. Physic and experimental issues on high resolution SAR imaging of urban area. In *Geoscience and Remote Sensing Symposium, 2008. IGARSS 2008. IEEE International*, volume 1, pages I–70–I–73. IEEE, 2008.

F. Cellier and **E. Colin**. Building height estimation using fine analysis of altimetric mixtures in layover areas on polarimetric interferometric X-band SAR images. In *IGARSS*, 2006.

F Champagnat, A Plyer, G Le Besnerais, B Leclaire, S Davoust, and Y Le Sant. Fast and accurate PIV computation using highly parallel iterative correlation maximization. *Experiments in fluids*, 50(4):1169–1182, 2011.

R.A. Chipman. Depolarization index and the average degree of polarization. *Appl. Opt.*, 44(13):2490–2495, May 2005.

S.R. Cloude and K.P. Papathanassiou. Polarimetric optimisation in radar interferometry. *Electronics Letters*, 33(13):1176–1178, 1997.

S.R. Cloude and K.P. Papathanassiou. Polarimetric SAR interferometry. *Geoscience and Remote Sensing, IEEE Transactions on*, 36(5):1551–1565, 1998.

Y. Cui, Y. Yamaguchi, H. Yamada, and S. Park. PolInSAR Coherence Region Modeling and Inversion: The Best Normal Matrix Approximation Solution. *Geoscience and Remote Sensing, IEEE Transactions on*, 53(2), Feb 2015. ISSN 0196-2892.

E. Everaere, **E. Colin-Koeniguer**, L. Thirion Lefevre, and A. De Martino. Influence of bistatic angle and forest structure description on classical polarimetric parameters. In *Geoscience and Remote Sensing Symposium (IGARSS), 2012 IEEE International*, pages 6531–6534. IEEE, 2012.

T. Flynn, M. Tabb, and R. Carande. Coherence region shape extraction for vegetation parameter estimation in polarimetric SAR interferometry. In *Geoscience and Remote Sensing Symposium, 2002. IGARSS'02. 2002 IEEE International*, volume 5, pages 2596–2598. IEEE, 2002.

P. Formont, N. Trouvé, J-P Ovarlez, F. Pascal, G. Vasile, and **E. Colin-Koeniguer**. PolSAR classification based on the SIRV model with a region growing initialization. In *POLINSAR*, 2011.

A. Freeman. On ambiguities in SAR design. In *EUSAR*, 2006.

A. Freeman. On the design of spaceborne polarimetric SARs. In *Radar Conference, 2009 IEEE*, pages 1–4, May 2009.

H-L. Gau and PY. Wu. Numerical range and Poncelet property. *Taiwanese journal of mathematics*, 7(2):pp–173, 2003.

A-L. Germond. *Théorie de la polarimétrie radar bistatique*. PhD thesis, Université de Nantes, 1999.

J.J. Gil. Characteristic properties of mueller matrices. *J. Opt. Soc. Am. A*, 17(2): 328–334, Feb 2000.

P. Goy. *Détection d'obstacles et de cibles de collision par un radar FMCW aéroporté*. PhD thesis, University of Toulouse, 2012.

J-R. Huynen. *Phenomenological theory of radar targets*. PhD thesis, University of Technology, Delft, The Netherlands, 1970.

T. Kempf and H. Anglberger. Image fusion of different spaceborne SAR sensors for change detection. In *Radar Conference (RADAR), 2013 IEEE*, pages 1–6. IEEE, 2013.

J-S. Lee, K.W. Hoppel, S.A. Mango, and A.R. Miller. Intensity and phase statistics of multilook polarimetric and interferometric SAR imagery. *Geoscience and Remote Sensing, IEEE Transactions on*, 32(5):1017–1028, 1994a.

J-S. Lee, A.R. Miller, and K.W. Hoppel. Statistics of phase difference and product magnitude of multi-look processed Gaussian signals. *Waves in random media*, 4(3):307–320, 1994b.

C-K. Li, P.P. Mehta, and L. Rodman. A generalized numerical range: the range of a constrained sesquilinear form. *Linear and Multilinear Algebra*, 37(1-3): 25–49, 1994.

Z. Li and J. Bethel. Image coregistration in SAR interferometry. *Proc. Int. Arch. Photogramm., Remote Sens. Spatial Inf. Sci*, pages 433–438, 2008.

KV. Mardia. Directional statistics and shape analysis. *Journal of applied Statistics*, 26(8):949–957, 1999.

SW. McCandless and Christopher R. Jackson. Principles of Synthetic Aperture Radar. *SAR Marine User's Manual*, pages 1–23, 2004.

M. Neumann, L. Ferro-Famil, and A. Reigber. Multibaseline polarimetric SAR interferometry coherence optimization. *Geoscience and Remote Sensing Letters, IEEE*, 5(1):93–97, 2008.

C. Pascual, E. Gimeno, and JM Lopez-Sanchez. The equivalence between the polarization subspace method (PSM) and the coherence optimisation in polarimetric radar interferometry. In *Proc. of the 4th European Conference on Synthetic Aperture Radar (EUSAR)*, pages 589–592, 2002.

A. Plyer, G. Le Besnerais, and F. Champagnat. Massively parallel Lucas Kanade optical flow for real-time video processing applications. *Journal of Real-Time Image Processing*, pages 1–18, 2014.

J. Praks and M. Hallikainen. A novel approach in polarimetric covariance matrix eigendecomposition. In *Geoscience and Remote Sensing Symposium, 2000. Proceedings. IGARSS 2000. IEEE 2000 International*, volume 3, pages 1119–1121 vol.3, 2000a.

J. Praks and M. Hallikainen. A novel approach in polarimetric covariance matrix eigendecomposition. In *Geoscience and Remote Sensing Symposium, 2000. Proceedings. IGARSS 2000. IEEE 2000 International*, volume 3, pages 1119–1121, 2000b.

J. Praks, **E. Colin-Koeniguer**, and M. Hallikainen. Alternatives to Target Entropy and Alpha angle in SAR Polarimetry. *IEEE Trans. Geosc. Remote Sensing*, 47(7):2262–2274, July 2009.

J. Praks, M. Hallikainen, and **E. Colin-Koeniguer**. Polarimetric SAR image visualization and interpretation with covariance matrix invariants. In *Geoscience and Remote Sensing Symposium (IGARSS), 2010 IEEE International*, pages 2035–2038. IEEE, 2010.

M. Qong. Coherence optimization using the polarization state conformation in polinsar. *Geoscience and Remote Sensing Letters, IEEE*, 2(3):301–305, 2005.

J-C. Souyris and C. Tison. Polarimetric analysis of bistatic SAR images from polar decomposition: A quaternion approach. *Geoscience and Remote Sensing, IEEE Transactions on*, 45(9):2701–2714, 2007.

C-T. Tai. Complementary reciprocity theorems in electromagnetic theory. *IEEE Transactions on Antennas and Propagation*, 40(6):675–681, 1992.

E. Colin. A mathematical study about the coherence set in polarimetric interferometry. In *EUSAR*, 2006.

E. Colin. Polarimetric optical tools and decompositions applied to SAR images. In *IGARSS*, 2007.

E. Colin, C. Titin-Schnaider, and W. Tabbara. A new parameter for IFPOL coherence optimization methods. In *IGARSS*, 2003.

E. Colin, L. Thirion, C. Titin-Schnaider, and W. Tabbara. Comparison between simulations and interferometric polarimatric SAR P-band data on a pine-trees forest. In *IGARSS*, 2004a.

E. Colin, M. Tria, C. Titin-Schnaider, W. Tabbara, and M. Benidir. SAR imaging using multidimensional continuous wavelet transform and applications to polarimetry and interferometry. *Int.J. of Imaging Systems*, 14(5):181–221, 2004b.

E. Colin, C.Titin-Schnaider, and W. Tabbara. Polarimetric interferometry and time-frequency analysis applied to an Urban area at X-band. In *IGARSS*, 2005a. presented by A. Reigber.

E. Colin, C. Titin-Schnaider, and W. Tabbara. Coherence optimization methods for scattering centers separation in polarimetric interferometry. *JEMWA*, 19 (9):1237–1250, 2005b.

E. Colin, C. Titin-Schnaider, and W. Tabbara. FOPEN with polarimetric interferometry: validations with experimental data at P-band. In *POLINSAR*, 2005c.

E. Colin, H. Cantalloube, and X. Dupuis. FOPEN and change detection using POLINSAR data at P-band. In *EUSAR*, 2006a.

E. Colin, C. Titin-Schnaider, and W. Tabbara. An Interferometric Coherence Optimization Method in Radar Polarimetry for High-Resolution Imagery. *IEEE Trans. Geosc. Remote Sensing*, 44(1), January 2006b.

E. Colin-Koeniguer and L. Thirion-Lefevre. Bistatic scattering from forest components. Part 2: First validation of a bistatic polarimetric forest model at VHF-UHF band [225-475 MHz] using indoor measurements. *Waves in Random and Complex Media*, 20(1):62–85, February 2010.

E. Colin-Koeniguer and N. Trouvé. Coherence Optimization for Estimation of Building Heights on a Segmented High Resolution PolInSAR Urban Area. In *POLINSAR*, 2011.

E. Colin-Koeniguer and N. Trouvé. A review about alternatives to classical polarimetric SAR parameters. In *SONDRA workshop*, 2013.

E. Colin-Koeniguer and N. Trouvé. Performance of buildings height estimation using High Resolution PolInSAR images. *IEEE Trans. Geosc. Remote Sensing*, 52(9):5870–5879, 2014.

E. Colin-Koeniguer, N. Trouvé, and J. Praks. A review about alternatives to classical Polarimetric SAR parameters. In *Synthetic Aperture Radar (EUSAR), 2010 8th European Conference on*, pages 1–4. VDE, 2010.

E. Colin-Koeniguer, N. Trouvé, E. Everaere, and A. DeMartino. Bistatic polarimetric decompositions applied to depolarizing targets. In *IGARSS*, 2012.

L. Thirion and **E. Colin**. On the use of a coherent scattering model to determine the origin of artificial signatures of a target hidden in a forest. In *POLINSAR*, volume 586, page 33, 2005.

L. Thirion, **E. Colin**, and C. Dahon. Capabilities of a forest coherent scattering model applied to radiometry, interferometry, and polarimetry at P- and L-band. *IEEE Trans. Geosc. Remote Sensing*, 44(4):849–862, April 2006.

L. Thirion-Lefevre and **E. Colin-Koeniguer**. Investigating attenuation, scattering phase center, and total height using simulated interferometric SAR images of forested areas. *Geoscience and Remote Sensing, IEEE Transactions on*, 45(10):3172–3179, 2007.

L. Thirion-Lefevre and **E. Colin-Koeniguer**. First polarimetric validation and results on the bistatic scattering by a set of cylinders using a forest scattering model. *Synthetic Aperture Radar (EUSAR), 2008 7th European Conference on*, pages 1–4, June 2008.

L. Thirion-Lefevre, **E. Colin-Koeniguer**, and C. Dahon. Bistatic scattering from forest components. Part 1: Coherent polarimetric modelling and analysis of simulated results. *Waves in Random and Complex media*, 20(1):36–61, February 2010.

J. Thomas, K. W Bowyer, and A. Kareem. Color balancing for change detection in multitemporal images. In *Applications of Computer Vision (WACV), 2012 IEEE Workshop on*, pages 385–390. IEEE, 2012.

C. Titin-Schnaider. Polarimetric characterization of bistatic coherent mechanisms. *IEEE transactions on geoscience and remote sensing*, 46(5):1535–1546, 2008.

C. Titin-Schnaider. Physical meaning of bistatic polarimetric parameters. *IEEE transactions on geoscience and remote sensing*, 48(5):2349–2356, 2010.

K. Tomiyasu. Tutorial review of synthetic-aperture radar (sar) with applications to imaging of the ocean surface. *Proceedings of the IEEE*, 66(5):563–583, May 1978.

N. Trouvé and **E. Colin-Koeniguer**. Polarimetric study of an anisotropic cloud of cylinders in a bistatic configuration. In *POLINSAR*, 2009.

N. Trouvé and **E. Colin-Koeniguer**. SIRV based distance for polarimetric SAR images hierarchical segmentation. In *EUSAR*, 2010.

N. Trouvé and **E. Colin-Koeniguer**. Shape Constraint Region Growing process and application to 3D Rendering of High Resolution Urban Images. In *POLINSAR*, 2011.

N. Trouvé and **E. Colin-Koeniguer**. Hybrid PolInSAR: High resolution and Polarimetry Applied to Urban. In *POLINSAR*. ESA, 2013. URL https://earth.esa.int/web/guest/polinsar-2013/workshop-programme.

N. Trouvé, **E. Colin-Koeniguer**, P. Fargette, and A. De Martino. Influence of geometrical configurations and polarization basis definitions on the analysis of bistatic polarimetric measurements. *IEEE Trans. Geosc. Remote Sensing*, 49 (6):2238–2250, June 2011.

N. Trouvé, M. Sangnier, and **E. Colin-Koeniguer**. Statistics on High Resolution urban polarimetric images: Application to segmentation and classification. In *Synthetic Aperture Radar, 2012. EUSAR. 9th European Conference on*, pages 26–29. VDE, 2012.

L. Tsang and Q. Li. Microwave remote sensing theory. *Wiley Encyclopedia of Electrical and Electronics Engineering*, 1985.

F. Weissgerber, **E. Colin-Koeniguer**, and F. Janez. Urban change detection by comparing SAR images at different resolutions and polarimetric modes. In *10th European Conference on Synthetic Aperture Radar (EUSAR 2014)*, Berlin, Germany, June 2014.

R.G. White. Change detection in SAR imagery. *International Journal of remote sensing*, 12(2):339–360, 1991.

Y. Yamaguchi, Y. Yajima, and H. Yamada. A four-component decomposition of POLSAR images based on the coherency matrix. *Geoscience and Remote Sensing Letters, IEEE*, 3(3):292–296, 2006.

Polarimetric radar images: from acquisition to inversion

This manuscript provides a summary of my research work conducted in ONERA about polarimetric radar images for remote sensing applications. A polarimetric radar system can measure a larger number of parameters than a single channel radar by discriminating between the polarizations of the electromagnetic wave that the system is able to transmit and receive.

My research in this area includes:
- The technological constraints about the polarimetric sensor design, the image formation process, and the statistical estimates of the variables of interest,
- The image processing algorithms such as co-registration, segmentation and detection,
- The three-dimensional information,
- The electromagnetic model inversion for target detection in environments such as forest and urban areas.

Keywords : SAR ; RADAR ; POLARIMETRY

Images polarimétriques radar: de l'acquisition à l'inversion

Ce manuscrit concerne une synthèse de mes travaux de recherches menés au sein de l'Onera sur les images polarimétriques radar de télédétection. Un radar polarimétrique permet de mesurer un plus grand nombre de paramètres qu'un radar monocanal en exploitant la nature vectorielle de l'onde électromagnétique.

Mes recherches dans ce domaine couvrent :
- La mise en place du mode d'acquisition polarimétrique dès la conception des capteurs, la formation de l'image, et les estimations statistiques des variables d'intérêt,
- Les algorithmes de traitements d'images tels que le recalage, la segmentation et la détection,
- L'obtention d'informations tridimensionnelles,
- Et l'inversion de modèles électromagnétiques fins pour des applications dans des environnements ciblés tels que le milieu forestier et l'environnement urbain.

Mots-clés : RADAR ; SAR ; POLARIMETRIE

Office National d'Études et de Recherches Aérospatiales
Chemin de la Hunière – BP 80100
91123 PALAISEAU Cedex
Tél. : +33 1 80 38 60 60 - Fax : +33 1 80 38 65 10
http://www.onera.fr